

THESIS

BAFFLE-POST STRUCTURES FOR FLOW CONTROL IN OPEN CHANNELS

Submitted by

Caroline Ubing

Department of Civil & Environmental Engineering

In partial fulfillment of the requirements

For the Degree of Master of Science

Colorado State University

Fort Collins, Colorado

Spring 2015

Master's Committee:

Advisors: Christopher Thornton

Co-Advisor: Robert Ettema

Brian Bledsoe

Ellen Wohl

Copyright by Caroline U. Ubing 2015

All Rights Reserved

ABSTRACT

BAFFLE-POST STRUCTURES FOR FLOW CONTROL IN OPEN CHANNELS

This thesis presents theory and laboratory findings regarding the hydraulic performance of baffle-post structures used as a means for controlling flow in open channels. Such structures comprise one to two parallel rows of posts that extend slightly higher than the anticipated depth of flow, and offer a useful means for retarding flow in various channel situations where there is a need to reduce flow energy, possibly to reduce flow capacity to transport bed sediment and manage channel morphology. Observations and data regarding headloss and discharge coefficients and backwater flow profiles associated with varying structure geometry were obtained so as to determine the extent to which a baffle-post structure will retard an approach flow and reduces its capacity to convey bed sediment.

The creation of a M_1 gradually varied flow profile in the upstream reach complicates the use of headloss to characterize hydraulic performance of the baffle-post structures. Instead, the parameter, y_1/y_0 , offers a practical means for describing such performance; y_1 = flow depth at the upstream face of the structure, and y_0 = the depth of uniform flow prior to use of a structure. The most influential geometric variable was influencing structure performance was the lateral spacing between posts, s ; it is expressed non-dimensionally as s/D , where D = post diameter. Qualitative results regarding sediment transport confirm a reduction in bed-sediment transport rate upstream of the structure. However, the turbulent flow structures at the baffle-post structures promote local scour at the base of such structures. Due to the flow acceleration between posts, baffle-posts structures could potentially obstruct fish and other aquatic life passage along the channel.

TABLE OF CONTENTS

ABSTRACT.....	ii
TABLE OF CONTENTS.....	iii
LIST OF TABLES.....	vii
LIST OF FIGURES.....	ix
1.0 Introduction	1
1.1. Scope and Objectives	4
1.2. Background	5
2.0 Theory	8
2.1. Introduction	8
2.2. Hydraulic Performance	8
2.3. Dimensional Analysis	16
2.4. Bed Sediment Transport to and at a Baffle-Post Structure	18
2.4.1. Sediment Trapping Upstream of the Structure	19
2.4.2. Bedforms.....	20
2.4.3. Local Scour at the Structure.....	20
3.0 Experimental Set-up.....	21
3.1. Introduction	21
3.2. Facilities and Materials	22

3.3.	Single-Row Baffle-Post Structure	24
3.3.1.	Schedule of Experiments.....	25
3.3.2.	Procedures	26
3.4.	Double-Row Baffle-Post Structure	27
3.4.1.	Schedule	28
3.4.2.	Procedures	30
3.5.	Sediment Transport Experiments	30
3.5.1.	Set-up	30
3.5.2.	Experiment Procedure	31
3.6.	Study Limitations	32
4.0	Data Analysis and Results	33
4.1.	Introduction	33
4.2.	Water-Surface Profile.....	35
4.3.	Turbulence Structures at a Baffle Post	37
4.4.	Single-Row of Baffle Posts	38
4.4.1.	Influence of Froude Number, Fr_0	38
4.4.2.	Influence of Lateral Spacing, s/D	39
4.4.3.	Influence of Relative Depth, y_0/D	39
4.4.4.	Depth Increase Parameter, y_1/y_0	40
4.4.5.	Choked Flow Conditions	41

4.5.	Double-Row of Baffle Posts	42
4.5.1.	Analysis Approach	42
4.5.2.	Influence of Froude Number, Fr_0	42
4.5.3.	Influence of Lateral Spacing, s/D	43
4.5.4.	Influence of Streamwise Spacing, l/D	44
4.5.5.	Influence of Baffle Post Diameter, D	45
4.5.6.	Influence of Relative Depth, y_0/D	46
4.5.7.	Depth Increase Parameter, y_1/y_0	47
4.5.8.	Choked Flow Conditions	47
4.6.	Bed Sediment Transport to and at a Baffle-Post Structure	49
4.6.1.	Free Flow Conditions	49
4.6.2.	Retarded Flow Conditions with no Armoring	49
4.6.3.	Retarded Flow Conditions with Armoring	50
4.7.	Environmental Impacts	50
4.7.1.	Fish Passage	51
4.7.2.	Aquatic Habitat	52
4.8.	Tables and Figures	53
5.0	Conclusions & Recommendations	95
5.1.	Overview	95
5.2.	Conclusions	96

5.2.1.	General Conclusions.....	96
5.2.2.	Single-Row Baffle-Post Structures	97
5.2.3.	Double-Row Baffle-Post Structures	98
5.3.	Recommendations for Future Research	99
5.3.1.	Future Research in Hydraulic Performance	99
5.3.2.	Future Research in Sediment Transport	100
5.3.3.	Future Research for Scaling	101
6.0	References	102
	Appendix A – Measured Data	105

LIST OF TABLES

Table 3-1: Configurations used for the single-row baffle-post structure experiments, varying lateral spacing. $D = 15.875$ mm for all configurations.	25
Table 3-2: Configurations for experiments, varying lateral and streamwise spacing, as well as baffle post diameter.....	30
Table 4-1: Hydraulic experiment results for single-row baffle-post structures for $Fr_0 = 0.15$ at three different y_0/D values, varying l/D spacing.	53
Table 4-2: Hydraulic experiment results for single-row baffle-post structures at $Fr_0 = 0.45$. Four different y_0/D were tested, varying the sD spacing at each depth.	54
Table 4-3: Hydraulic experimental results for single-row baffle-post structures, varying Fr_0 , y_0 , and s/D spacing.....	55
Table 4-4: B_c values for single-row baffle-post structure experiments.....	56
Table 4-5: Hydraulic experiment results for double-row baffle-post structures at three different y_0/D values, varying post s/D spacing with $D = 16$ mm over a range of subcritical Fr_0 values. Graphical results are presented in the upper graph of Figure 4-25, Figure 4-28, and Figure 4-29. Experiment photographs for $y_0/D = 5.0$ are presented in Figure 4-26.	57
Table 4-6: Hydraulic experiment results for the double-row baffle-post structures at three different y_0/D values, varying s/D post spacing, maintaining $D = 8$ mm, over a range of subcritical Fr_0 values. Graphical results are presented in the lower graph of Figure 4-25, Figure 4-28, and Figure 4-29. Experiment photographs for $y_0/D = 9.9$ are presented in Figure 4-27.	58
Table 4-7: Hydraulic experiment results for double-row baffle-post structures at three different y_0/D , varying l/D post spacing over a range of subcritical Fr_0 values. Graphical results are presented in Figure 4-30, Figure 4-32, and Figure 4-33. Experiment photographs for $y_0/D = 5.0$ are presented in Figure 4-31.	59
Table 4-8: Hydraulic experiment results for the double-row baffle-post structures at three different y_0/D values, varying D over a range of subcritical Fr_0 values, maintaining the same relative s/D and l/D spacing. Graphical results are presented in Figure 4-34, Figure 4-36, and Figure 4-37. Experiment photographs for $y_0/D = 9.9$ are presented in Figure 4-27.	60
Table 4-9: B_c results for flow conditions for the double-row post structure experiments when $y_0/D = 5.0$	61
Table A-1: Measured data for hydraulic performance experiments for single-row baffle-post structures at $Fr_0 = 0.15$	105
Table A-2: Measured data for hydraulic performance experiments for single-row baffle-post structures at $Fr_0 = 0.45$	106
Table A-3: Measured data for hydraulic performance experiments for single-row baffle-post structures at $y_0 = 0.08$ m.....	107
Table A-4: Measured data for hydraulic performance experiments for single-row baffle-post structures at $y_0 = 0.15$ m.....	108
Table A-5: Measured data for hydraulic performance experiments for single-row baffle-post structures at $y_0 = 0.20$ m.....	108

Table A-6: Measured data for hydraulic performance experiments for double-row baffle-post structures at $y_0 = 0.08$ m.....	109
Table A-7: Measured data for hydraulic performance experiments for double-row baffle-post structures at $y_0 = 0.08$ m.....	110
Table A-8: Measured data for hydraulic performance experiments for double-row baffle-post structures at $y_0 = 0.15$ m.....	111
Table A-9: Measured data for hydraulic performance experiments for double-row baffle-post structures at $y_0 = 0.15$ m.....	112
Table A-10: Measured data for hydraulic performance experiments for double-row baffle-post structures at $y_0 = 0.20$ m.....	113
Table A-11: Measured data for hydraulic performance experiments for double-row baffle-post structures at $y_0 = 0.20$ m.....	114
Table A-12: Measured flow and sand depth data for sediment transport experiments for free-flow conditions.....	115
Table A-13: Measured ripple amplitude, A , and wavelength, λ , for sediment transport experiments for free-flow conditions.....	115
Table A-14: Measured flow data for sediment transport experiments for retarded flow due to double-row baffle-post structures without armoring.....	116
Table A-14: Measured sand depth and ripple amplitude, A , data for sediment transport experiments for retarded flow due to double-row baffle-post structures without armoring.....	116
Table A-15: Measured flow and sand depth data for sediment transport experiments for retarded flow due to double-row baffle-post structures with armoring.....	117
Table A-16: Measured ripple amplitude, A , and wavelength, λ , data for sediment transport experiments for retarded flow due to double-row baffle-post structures with armoring.....	117

LIST OF FIGURES

Figure 1-1: A baffle-post structure in a sediment-laden flow.....	2
Figure 1-2: This forested floodplain on the Baraboo River, Columbia County, Wisconsin has features analogous to a baffle-post structure, notably the row of tree trunks are like rows of posts (Photo source: Wisconsin Department of Natural Resources).....	3
Figure 1-3: Flow through the closely spaced bridge piers of this bridge on the River Suír, Ireland, exhibits similar behavior as choked flow through a baffle-post structure. This view shows rapid flow through the bridge opening and the formation of small hydraulic jumps at the downstream side of the bridge. (Photo source: Dr. Donal Ryan, University of Ulster, N. Ireland).	4
Figure 1-4: Willow trestle retards and groynes slow an approach flow and thereby act to retain bed sediment in the Wairau River (Acheson, 1968)	7
Figure 2-1: Three flow sections referenced for formulation of flow through a baffle-post structure.....	9
Figure 2-2: Specific energy diagram for flow in a rectangular channel.	11
Figure 2-3: The maximum value of the unit discharge, q_{max} , before a contraction chokes	12
Figure 2-4: The increase in specific energy and upstream water level needed to pass the choked flow.	13
Figure 3-1: General layout of the baffle-post structure.....	22
Figure 3-2: Re-circulating 8" Plexiglas flume used for experiment.....	23
Figure 3-3: Horizontal baffles installed at the flume inlet to ensure fully developed flow within the flume.....	23
Figure 3-4: Single-row baffle-post structure.....	24
Figure 3-5: Flow depth measurement locations.....	27
Figure 3-6: Plan views of post configurations experiments, varying lateral spacing and baffle post diameter, keeping streamwise spacing constant.....	28
Figure 3-7: Plan view of post configurations for experiments, varying streamwise spacing, keeping diameter and lateral spacing constant, and post configurations for hydraulic performance tests, varying diameter, keeping both lateral and streamwise spacing constant.	29
Figure 3-8: Gradation curve for the silica sand used.	31
Figure 3-9: Flow and sand depth measurement locations along the flume for the mobile bed tests. Note that some of the support structure has been removed to simplify the drawing.	32
Figure 4-1: Flow between the baffle posts is slightly contracted.	35
Figure 4-2: Example shape of water surface profile, with pertinent flow depths indicated ; $y_1 = 0.13$ m; $y_0 = 0.10$ m; $y_{c1} = 0.10$ m; and, $y_{c0} = 0.067$ m. Experiment conditions: $Fr_0 = 0.45, y_0/D = 6.4, \text{ and } s/D = 2.$	36
Figure 4-3: Flow field around a pier is marked by numerous vortices that influence energy loss and pier scour	37
Figure 4-4: General trends for C'_L and C'_D for single-row structures.....	38
Figure 4-5: General trends for C'_L and C'_D over a range of Fr_0 values.....	42
Figure 4-6: General trends for C'_L and C'_D over a range of Fr_0 values, varying s/D spacing.....	43
Figure 4-7: General trends for C'_L and C'_D over a range of Fr_0 , varying l/D spacing.....	44

Figure 4-8: General trends for C'_L and C'_D over a range of Fr_0 , varying D , expressed as y_0/D	46
Figure 4-9: C'_L results for single-row baffle-post structures for $y_0 = 0.08$ m, over a range of Fr_0 values.	61
Figure 4-10: C'_L results for single-row baffle-post structures for $y_0 = 0.15$ m, over a range of Fr_0 values.	62
Figure 4-11: C'_L results for single-row baffle-post structures for $y_0 = 0.20$ m, over a range of Fr_0 values.	62
Figure 4-12: C'_L results over a range of s/D spacing values for $Fr_0 = 0.15$ and three y_0/D values. Results show that the lowest flow depth ($y_0/D = 2.1$) resulted in the highest C'_L values over the range of s/D spacing.	63
Figure 4-13: Result photographs single-row baffle-post structure performance tests at $Fr_0 = 0.15$, corresponding to the letters in Figure 4-12. As anticipated, the magnitude and extent of the downstream wake decreases with an increasing s/D ratio and y_0/D ratio.	64
Figure 4-14: C'_L results over a range of s/D spacing values at $Fr_0 = 0.45$ and four y_0/D values.	65
Figure 4-15: Result photographs for single-row baffle-post structure performance experiments at $Fr_0 = 0.45$, corresponding to the letters in Figure 4-13. As anticipated, the magnitude and extent of the downstream wake decreases with an increasing s/D ; however, y_0/D values appear to have little impact on C'_L , particularly in comparison to the $Fr_0 = 0.15$ results.	66
Figure 4-16: C'_L results, comparing Fr_0 for the same y_0/D . Notice that as y_0/D increases, the discrepancy between the two C'_L becomes larger, especially at lower s/D ratios.	67
Figure 4-17: Result photographs for single-row baffle-post structures experiments corresponding to the letters in Figure 4-16.	68
Figure 4-18: Depth increase parameter for a single-row of baffle posts at $y_0 = 0.08$ m, varying Fr_0 and s/D spacing.	69
Figure 4-19: Depth increase parameter for a single-row of baffle posts at $y_0 = 0.15$ m, varying Fr_0 and s/D spacing.	69
Figure 4-20: Depth increase parameter for a single-row of baffle posts at $y_0 = 0.20$ m, varying Fr_0 and s/D spacing.	70
Figure 4-21: Depth increase parameter, y_1/y_0 , for a single-row of baffle posts at $Fr_0 = 0.15$	71
Figure 4-22: Depth increase parameter, y_1/y_0 , for a single-row of baffle posts at $Fr_0 = 0.45$	72
Figure 4-23: Specific energy diagram for baffle-post structure at various spacings.	73
Figure 4-24: Experimental results on the specific energy diagram for free-flow and choked flow conditions at $Fr_0 = 0.45$	74
Figure 4-25: C'_L results for a depth of 0.08m, over a range of Fr_0 values, varying s/D spacing for two D values. The letters in the graphs correspond to experiment photographs presented in Figure 4-26 and Figure 4-27 below.	75
Figure 4-26: Photographs of s/D spacing results for $y_0/D = 5.0$. The letters correspond to the data points given in Figure 4-25. Notice that ΔE through the structure increases with an increasing Fr_0 , even though C'_L decreases with the Fr_0 . On the other hand, ΔE through the structure, and corresponding C'_L , decreases as s/D spacing of the structure increases.	76
Figure 4-27: Photographs of lateral spacing results for $y_0/D = 9.9$. The letters correspond to the data points given in Figure 4-25. Notice that ΔE through the structure increases with an increasing Fr_0 , even though the C'_L decreases with the Fr_0 . On the other hand, the ΔE through the structure, and corresponding C'_L , decreases as s/D spacing of the structure increases.	77

Figure 4-28: C'_L results for $y_0 = 0.15$ m, over a range of Fr_0 , varying s/D spacing for two different D values. (a) $y_0/D = 9.5$; $l/D = 2$ and (b) $y_0/D = 18.4$; $l/D = 4$	78
Figure 4-29: C'_L results for $y_0 = 0.20$ m, over a range of Fr_0 values, varying s/D spacing for two different D values. Note: the datum point in Figure 4-29 (b) at $s/D = 6$ and at $Fr_0 = 0.1$, in which $C'_L \approx 6.8$ is an outlier.....	79
Figure 4-30: C'_L results for $y_0 = 0.08$ m, over a range of Fr_0 , varying l/D spacing for $D = 16$ mm. The letters correspond to experiment photographs presented in Figure 4-31.....	80
Figure 4-31: Photographs of l/D spacing results for $y_0/D = 5.0$. The letters correspond to the data points given in Figure 4-30. The ΔE value through the structure, and corresponding C'_L , is not significantly different for the varying l/D spacing configurations.	81
Figure 4-32: C'_L results for $y_0 = 0.15$ m, over a range of Fr_0 , varying l/D spacing for $D = 16$ mm	82
Figure 4-33: C'_L results for $y_0 = 0.20$ m, over a range of Fr_0 , varying l/D spacing for $D = 16$ mm	82
Figure 4-34: C'_L results for $y_0 = 0.08$ m, over a range of Fr_0 , varying D for the same s/D and l/D spacing. The letters correspond to experiment photographs presented in Figure 4-35.	83
Figure 4-35: Experiment photographs results showing varying D over a range of Fr_0 values for consistent s/D and l/D spacing. The letters correspond to the C'_L values presented in Figure 4-34.....	84
Figure 4-36: C'_L results for $y_0 = 0.15$ m, over a range of Fr_0 values, varying D , expressed as y_0/D for the same relative s/D and l/D spacing.....	85
Figure 4-37: C'_L results for $y_0 = 0.20$ m, over a range of Fr_0 values, varying D for the same s/D and l/D spacing.	85
Figure 4-38: Experiment results comparing the 16-2-2 configuration at three different y_0 values, expressed by the dimensionless term, y_0/D	86
Figure 4-39: C'_L results comparing six y_0/D values for the same single-row structure. Please note that the series presented on the left side of the legend indicate results from the single-row structure experiments, where y_0/D was varied for $Fr_0 = 0.15$ and $Fr_0 = 0.45$. The right side of the legend shows results from the double-row hydraulic performance tests where Fr_0 was varied for three different y_0/D values.	86
Figure 4-40: The variation of flow depth parameter y_1/y_0 for a double-row baffle-post structure with rows spaced at $l/D = 2$. The additional parameter in this figure is y_0/D , which exerts only a very small effect for the range of values investigated.....	87
Figure 4-41: Specific energy diagram for double-row baffle-post structure at various l/D spacing. The y_0/D value, l/D spacing and D remained constant.	89
Figure 4-42: Experimental photographs for free flow conditions	90
Figure 4-43: Experimental photographs for retarded flow conditions with no armoring at the base of the structure.....	91
Figure 4-44: Experimental photographs for retarded flow conditions with armoring at the base of the structure	92
Figure 4-45: u_2/u_0 for double-row structure varying l/D spacing at $y_0 = 0.08$ m.....	93
Figure 4-46: u_2/u_0 for double-row structure at $y_0 = 0.08$ m. The top graph varies l/D spacing. The bottom graph varies D	94

1.0 Introduction

The purpose of the laboratory study this thesis presents was to determine the hydraulic performance of baffle-post structures, simple hydraulic structures of possible use in controlling flow and bed-sediment transport in open channels. Baffle-post geometry influences the headloss and discharge coefficients associated with flow through baffle-post structures and, relatedly, the increase in approach flow depth associated with such structures. For constant rate of approach flow, increased flow depth leads to reduced rate of bed-sediment transport, thereby enabling baffle-post structures to function as a means for promoting bed aggradation.

River-bed control is an age-old activity, as throughout history, humankind has gravitated towards rivers for water, food and transportation. However, rivers have also brought misery through flooding and problems related to bed-sediment transport. To combat these problems, humankind has attempted to control river-beds by means of various types of hydraulic structures. The purposes of these structures are broad, ranging from dams which detain flow and sediment, to levees designed to prevent flooding, to drop-structures which dissipate flow energy. Occasionally, energy dissipation structures have been used to reduce flow energy for the ultimate purpose of detaining bed sediment along a river bed (i.e., grade-control or grade-building structure, GCS and GBS respectively) when the bed profile had to be maintained or raised. Such structures act to retard and spread flow across channels, ultimately build the grade of the existing channel. They do so by locally increasing flow resistance, reducing approach-flow velocities, and dissipating flow energy. This study focuses on the hydraulic performance of one type of grade-control structure – the baffle-post structure, as illustrated in Figure 1-1. The hydraulic performance of these structures has received little attention. In particular, there appear to be no prior studies relating the geometric characteristics of baffle-post structures to hydraulic performance such as

expressed using common indices, notably discharge and headloss coefficients associated with flow through baffle-post structures.

By retarding an approach flow, and locally dissipating flow energy, baffle-post structures offer a way to maintain the grade of a channel, as well as possibly elevate and flatten the grade. This function is accomplished by the posts slowing and deepening the approach flow, letting flow and washload sediment pass, but causing a portion of the approach bedload sediment transport to deposit on the channel bed upstream of the baffle-post structure. When spaced relatively widely apart, local scour at the posts may be relatively minor, but when closely spaced, local scour may be a design concern; this concern presently is unclear.

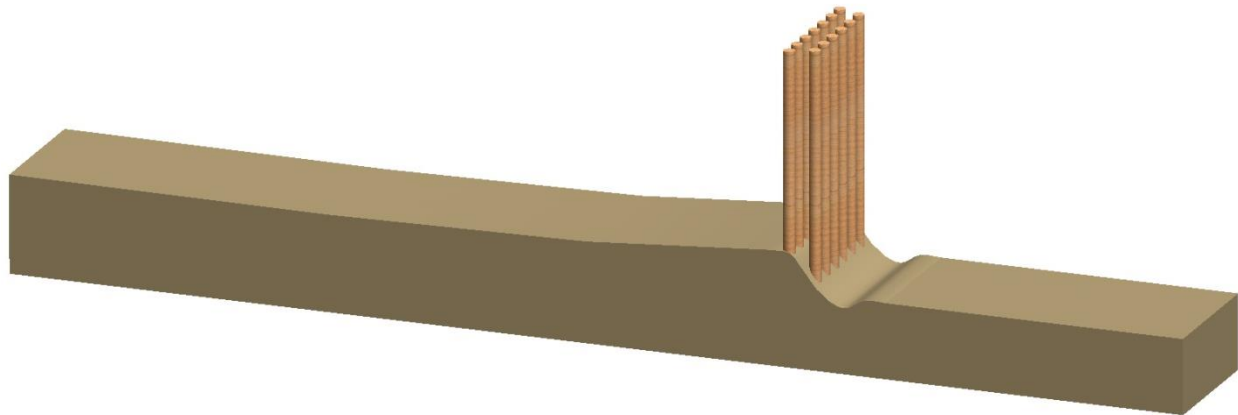


Figure 1-1: A baffle-post structure in a sediment-laden flow

The basic baffle-post structure consists of one to two rows of vertical posts, possibly formed of timber or iron. When used in alluvial channels, posts are typically driven into the channel bed; for certain industrial uses and laboratory flumes, the posts may be fixed to a base plate or cap block. The posts themselves usually are evenly spaced, with a second row staggered so that its posts align between those in the upstream row.

A single row of posts is analogous to several other engineered or natural structures. For instance, a single row of metal posts is commonly used for trashracks at water intakes. These structures are primarily intended to catch floating debris (e.g., woody debris, reeds, trash) so that it does not enter an intake. While there is interest in the headloss associated with flow through trashracks, the prevailing flow velocities normally are quite low so that the local headloss behavior of trashracks is only of moderate concern unless the trashrack becomes severely blocked.

Additionally, a row or series of rows of timber posts can be considered analogous to trees on a floodplain, as illustrated in Figure 1-2. Therefore, the present study has relevance to flow through trees as local resistance elements on floodplains. Fairly numerous studies have been devoted to flow over vegetated floodplains, the literature on this topic is quite extensive, and includes information about roughness and vegetation behavior during floodplain flow, there is a need for information (discharge and headloss coefficients) regarding the hydraulic performance of a row of trees.



Figure 1-2: This forested floodplain on the Baraboo River, Columbia County, Wisconsin has features analogous to a baffle-post structure, notably the row of tree trunks are like rows of posts (Photo source: Wisconsin Department of Natural Resources)

Moreover, the blockage associated with a row of posts can be likened to that caused by closely spaced bridge piers, especially as commonly observed for old arch bridges, such as that illustrated in Figure 1-3. A concern for bridge waterway design is the spacing of piers so as not to choke the approach flow (Yarnell, 1934, El-Alfy, 2009). For old arch bridges, such as in Figure 1-3, the structural constraints of stone or masonry typically result in relatively short spans and thick piers that substantially constrict flow. The findings of this study, therefore, are likely to be relevant for several flow situations, notably flow between trashrack bars, trees on floodplains, and bridge piers.



Figure 1-3: Flow through the closely spaced bridge piers of this bridge on the River Suir, Ireland, exhibits similar behavior as choked flow through a baffle-post structure. This view shows rapid flow through the bridge opening and the formation of small hydraulic jumps at the downstream side of the bridge. (Photo source: Dr. Donal Ryan, University of Ulster, N. Ireland).

1.1. Scope and Objectives

This study addresses the hydraulic performance and the associated sediment trapping ability of the “baffled” flow openings. The hydraulic structure comprises one or two rows of uniformly spaced posts, as shown in Figure 1-1. The objectives of the study are:

1. Formulate the hydraulic performance of “baffled” flow structures in terms of headloss coefficient, C_L , and, relatedly, discharge coefficient, C_D ;
2. Determine the water level rise developed by a baffle-post structure; and,
3. Assess, in a preliminary way, the susceptibility of baffle-post structures to local scour when placed in channels having an alluvial bed.

The formulation of flow through a baffle-post structure is supported with dimensional analysis of the main variables associated with approach flow and flow through the structure. Dimensional analysis is needed as a means for working around complications related to the non-uniform character of the flow field formed by baffle-post structures.

A number of environmental considerations must be taken into account with the use of baffle-post structures in rivers. Especially important are considerations regarding fish and amphibian passage, for which space between posts, velocity magnitudes, and turbulence levels are significant concerns. The present study briefly discusses them.

1.2. Background

This study was motivated by interest in developing concepts for hydraulic structures that would retard flows in alluvial channels, causing such flows to deposit a substantial portion, possibly all, of their bed sediment load. An overall application of this action is to elevate the grade of a channel’s bed; i.e., to promote channel aggradation. For example, this application is being considered for the North Fork of the Toutle River, which drains a watershed on the side of Mount Saint Helens. The eruption of this volcano in 1980 coincides with a large debris avalanche that introduced a large amount of sediment into the upper reaches of the North Fork of the Toutle River. The U.S. Army Corps of Engineers (USACE) wishes to retain a significant quantity of this sediment in the upper reaches of the river. For this

purpose, USACE is interested in several concepts for hydraulic structures that will retain bed sediment in the river.

A baffle-post structure holds promise as one of many potentially useful concepts. The structure would dissipate the kinetic energy upstream, resulting in a decreased bedload sediment carrying capacity. However, the “baffled” flow openings would allow the suspended load to pass. Over time, the deposition of the upstream bedload could increase the stream bed elevation; thus, decreasing the slope of the streambed, promoting sediment deposition. As the literature on baffle-post structures, or flow through similar structures (e.g., closely spaced bridge piers) is sparse, there was a need to conduct the present study to provide the information needed for selecting the geometric aspects of baffle-post structures and to determine their effect on an approach flow, as well as to check their susceptibility to local scour.

While the primary objective of the structure is to retain sediment bedload, other factors to consider include: fish passage, aquatic habitat, and the cost and constructability of the structure. For example, the Toutle River watershed contains suitable habitat for several species of anadromous salmonids such as: steelhead trout, Coho salmon, Chinook salmon, and other wild salmon species. In-stream structures must allow upstream fish passage to provide habitat. Furthermore, the shallow waters in an alluvial depositional plain, like the one on the North Fork of the Toutle River, provide habitat for avian and wildlife populations, which must also be considered should the structures be installed.

Over several decades, hydraulic structures have been used to retain sediment bedload; an example is shown in Figure 1-4. However, no thorough study on the hydraulic performance of a baffle-post structure was available. The results of this study are presented as general values. The hydraulic performance of this structure can be easily extrapolated and applied to most river systems.

Furthermore, the analysis can also be applied to flow through trash racks, a forested floodplain, or closely spaced bridge piers.



Figure 1-4: Willow trestle retards and groynes slow an approach flow and thereby act to retain bed sediment in the Wairau River (Acheson, 1968)

2.0 Theory

2.1. Introduction

A baffle-post structure is a form of flow contraction that acts to choke and thereby retard an approach flow, raising its depth immediately upstream of the structure, and projecting a backwater flow profile upstream. Associated with flow through contractions are headloss and discharge coefficients, and relatedly possible flow depth increases. These hydraulic terms are often used to characterize the hydraulic performance of hydraulic structures that alter and control flow. This chapter outlines the fluid mechanics theory and dimensional analysis considerations relating these parameters to approach flow conditions. It also outlines considerations associated with bed sediment transport toward and through a baffle-post structure placed in an alluvial channel.

2.2. Hydraulic Performance

The essential action of a baffle-post structure is to retard an approach flow, slowing it, spreading it, and dissipating a portion of its energy. The main requirement of application interest for baffle-post structures located in alluvial channels is the increase in water depth immediately upstream of such structures. A depth increase is associated with retarding of the approach flow so as to reduce the flow's capacity to transport bed sediment.

The hydraulic performance of a baffle-post structure can be evaluated using conservation of energy, resistance to flow, and continuity principles applied between the three flow cross-sections indicated in Figure 2-1:

1. Between cross-sections 0 and 1, where 0 indicates uniform approach flow well upstream of the structure, and 1 indicates a cross-section immediately upstream of the structure; and,
2. Between cross-sections 1 and 2, where 2 indicates the contracted cross-section within the structure.

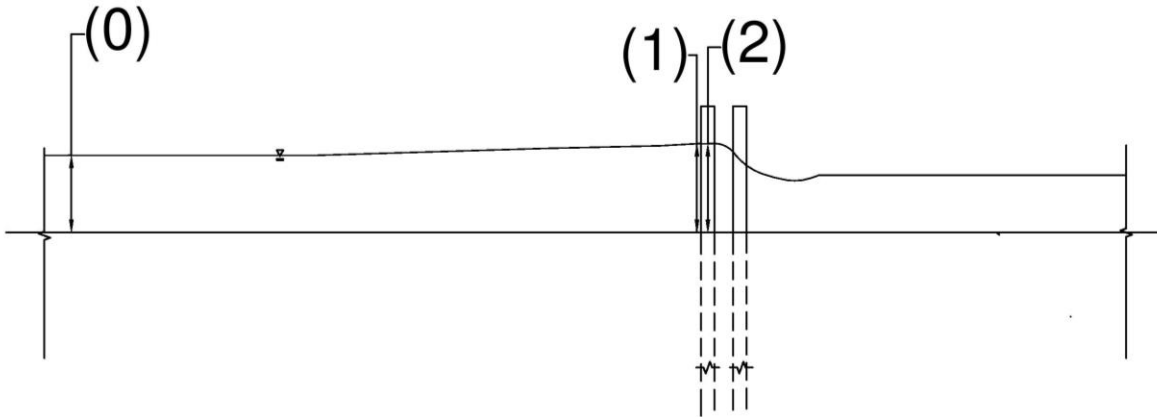


Figure 2-1: Three flow sections referenced for formulation of flow through a baffle-post structure

The three cross-sections usefully characterize the approach flow upstream (section 0) of the flow region influenced by the structure; the cross-section of maximum depth (section 1), and flow passage through critical depth within the structure (section 2).

The specific energy diagram is a useful tool for explaining the hydraulic performance of a baffle-post structure. The specific energy of an open-channel flow is defined as the energy with respect to the channel bottom. Considering a rectangular channel conveying a uniform approach flow, as for this study, E_0 can be written in terms of the unit discharge, q_0 , which is the flow rate per unit width, Eq. (2-1);

$$E_0 = y_0 + \frac{q_0^2}{2gy_0^2} \quad (2-1)$$

For a given channel of constant width, the value of the unit discharge will remain constant along the channel, although the depth, y_0 , may vary. The specific energy diagram, Figure 2-2, depicts this relationship, showing that for a given specific energy above the minimum, there are two physically possible depths, y_0 and y'_0 . These depths are known as alternate depths and represent subcritical and supercritical flows. The minimum specific energy, E_{min} , or critical flow conditions represents the minimum energy needed to support a given flow rate in a given channel. A single depth is possible in critical flow conditions, which is referred to as the critical depth, y_{c_0} . The critical depth can be calculated in terms of the flow's unit discharge, $q_0 = Q/B$;

$$y_{c_0} = \sqrt[3]{\frac{q_0^2}{g}} \quad (2-2)$$

Based on the concepts of specific energy and critical depth, the minimum energy at critical flow depth is

$$E_{min} = y_{c_0} + \frac{q_0^2}{2g(y_{c_0})^2} = \frac{3}{2} \sqrt[3]{\frac{q_0^2}{g}} \quad (2-3)$$

Knowing that $Q = bq_0$ and combining Eqs. (2-2) and (2-3), the minimum specific energy corresponding to q_0 can be expressed as

$$y_{c_0} = \frac{2}{3} E_{min} \quad (2-4)$$

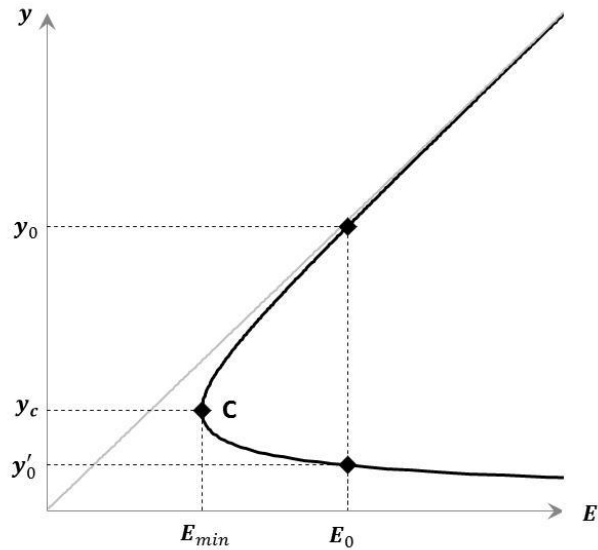


Figure 2-2: Specific energy diagram for flow in a rectangular channel.

When a channel contracts, increasing the unit discharge, $q > q_0$, a set of curves exist, each with increasing value of critical depth, y_c , and E_{min} , as indicated in Figure 2-3. Eventually, the contraction reaches critical width whereby E_{min} coincides with E_0 . Associated with this critical flow depth is a critical width, B_c , defined as the maximum contraction the flow can pass through without becoming choked. In other words, any constrictions narrower than B_c will produce an “overcritical” contraction so that there is not enough energy to maintain the given flow rate through the constriction. According to Jain (2001), the critical width can be calculated as

$$B_c = \left(\frac{3}{2}\right)^{3/2} \frac{Q}{\sqrt{gE_0^3}} \quad (2-5)$$

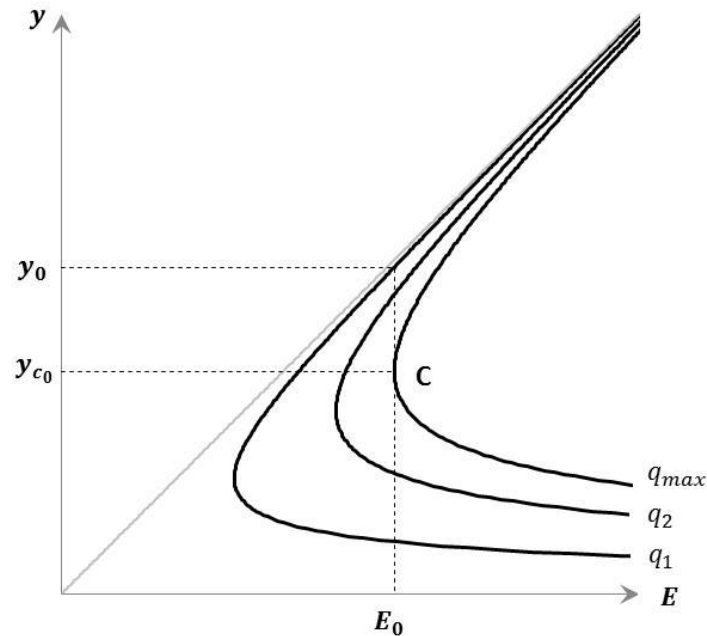


Figure 2-3: The maximum value of the unit discharge, q_{max} , before a contraction chokes

When the effective width of the flow constriction is less than B_c , the contraction acts as a “choke,” as the available specific energy, E_0 , is unable to pass the flow through the contraction. The flow backs up producing an M_1 (backwater), gradually varied flow water surface profile, elevating the magnitude of specific energy required to pass the flow through the contraction. The flow within the contraction stays critical, as the approach flow only backs up to the extent that generates the minimum energy needed to pass the given rate of flow through the contraction, as shown in Figure 2-4. The downstream flow may be supercritical or subcritical depending on the downstream conditions. For example, if there was a downstream control, such as a sluice gate, the flow would tend to be subcritical; however, if there is any doubt about downstream conditions, the tendency is towards supercritical flow downstream of the contraction (Henderson, 1966).

The additional energy necessary to push the flow through the structure, ΔE , becomes evident in the increased flow depth at the contraction.. Figure 2-4 indicates the increase in specific energy and associated water depth upstream of the contraction. The increase in specific energy is dissipated as

flow turbulence when the flow passes through the contraction and in a hydraulic jump formed immediately downstream of the contraction.

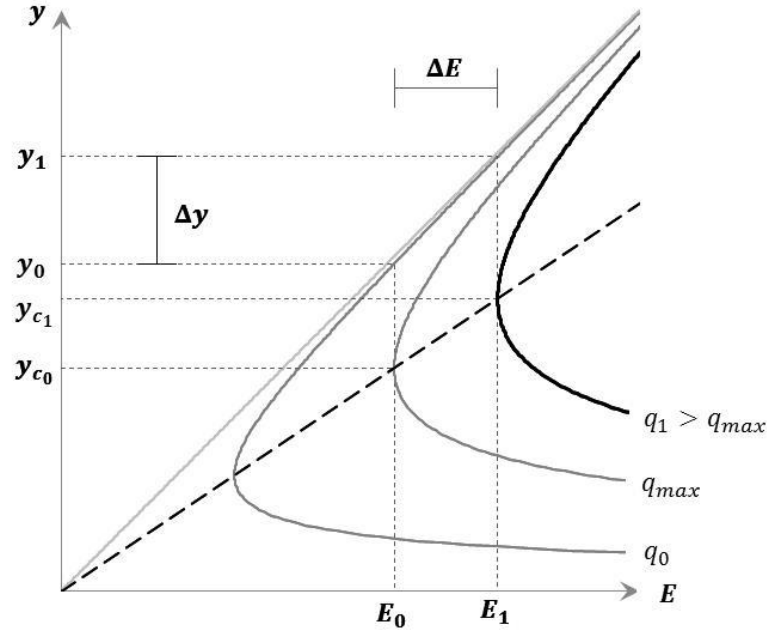


Figure 2-4: The increase in specific energy and upstream water level needed to pass the choked flow.

The additional energy, ΔE , needed to pass a given flow rate through a choked contraction can be evaluated in terms of the specific energy adjustments between sections 0 and 1:

$$\Delta E = E_1 - E_0 = \left(y_1 + \frac{q_1^2}{2gy_1^2} \right) - \left(y_0 + \frac{q_0^2}{2gy_0^2} \right)$$

Or,

$$\Delta E = (y_1 - y_0) + \frac{q_1^2}{2gy_1^2} - \frac{q_0^2}{2gy_0^2} \quad (2-6)$$

Here, y_0 is the normal depth of flow for the uniform section of approach flow well upstream of the structure, and y_1 is flow depth at section 1. The unit flow discharge, q_0 , is constant upstream of the structure, and q_1 is the unit discharge just upstream of the structure.

The additional energy, ΔE , can be expressed in terms of the maximum unit discharge, q_{max} , related to E_0 , and q_1 , related to E_1 ; see Figure 2-4. From Eqs. (2-1) through (2-4);

$$\Delta E = \frac{3}{2} \sqrt[3]{\frac{q_1^2}{g}} - \frac{3}{2} \sqrt[3]{\frac{q_{max}^2}{g}}$$

It is common to express a local headloss, h_L , in terms of a headloss coefficient, C_L , and an average approach velocity, u_0 , such as

$$h_L = C_L \left(\frac{u_0^2}{2g} \right) \quad (2-7)$$

The source of the increased energy, ΔE , at the structure is due to the reduction in flow resistance along the reach of channel impacted by the backwater curve the structure creates. From the Darcy-Weisbach resistance for flow equation, the headloss produced by flow resistance is

$$h_{L0} = \frac{fL}{4R} \left(\frac{u_0^2}{2g} \right) \quad (2-8)$$

Where f is the Darcy-Weisbach friction factor and L is the length of channel encompassed by the backwater curve. The backwater curve produces a reduced magnitude of headloss, h_{L0-1} , which can be approximated as

$$h_{L0-1} = \frac{1}{2} \left[\frac{fL}{4R_0} \left(\frac{u_0^2}{2g} \right) + \frac{fL}{4R_1} \left(\frac{u_1^2}{2g} \right) \right] \quad (2-9)$$

Eq. (2-10) simply approximates h_{L0-1} to the average of h_{L0} and h_{L1} . The difference in headloss equals ΔE ; i.e.,

$$\Delta E = h_{L0-1} - h_{L0} \quad (2-10)$$

The energy increment needed to push flow through the structure is then dissipated as the flow passes through the structure and through the possible hydraulic jump immediately downstream of it.

Therefore, the headloss associated with the structure is:

$$\Delta E = h_{Lbaffle} = h_{L0-1} - h_{L0} \quad (2-11)$$

Invoking the approximations $R_0 \approx y_0$, and $R_1 \approx y_1$, and considering continuity (i.e., $u_1 = u_0(y_0/y_1)$),

leads to

$$\Delta E = h_{Lbaffle} = \frac{1}{2} \left(\frac{fL}{4} \right) \left(\frac{u_0^2}{2g} \right) \left[\frac{1}{y_0} - \frac{y_0^2}{y_1^3} \right] = \left\{ \left(\frac{fL}{8} \right) \left[\frac{(y_1/y_0)^3 - 1}{y_0(y_1/y_0)^3} \right] \right\} \left(\frac{u_0^2}{2g} \right) \quad (2-12)$$

From Eqs. (2-7) and (2-12),

$$C_L \left(\frac{u_0^2}{2g} \right) = \left\{ \left(\frac{fL}{8} \right) \left[\frac{(y_1/y_0)^3 - 1}{y_0(y_1/y_0)^3} \right] \right\} \left(\frac{u_0^2}{2g} \right) \quad (2-13)$$

So that

$$C_L = \left(\frac{fL}{8} \right) \left[\frac{(y_1/y_0)^3 - 1}{y_0(y_1/y_0)^3} \right] \quad (2-14)$$

Eq. (2-14) shows that a unique value for C_L does not exist for a baffle-post structure of given geometry and approach flow Froude number, because the term $(fL/8)$ includes the influence of approach-flow resistance, and varies with the properties of the approach flow.

This variation, explored briefly in Chapter 4, is circumvented by taking a dimensional analysis approach, as described in the next section. Experiments conducted for this study measured values of flow depths y_0 and y_1 . While f can be estimated, the value of L is unknown and was too large to measure within the given flume. Therefore, these values of C_L are better stated as a dimensional headloss coefficient,

C'_L

$$C'_L = \frac{C_L}{\left(\frac{fL}{8} \right)} \quad (2-15)$$

Eq. (2-15) indicates that C_L' is not dimensionless and (as with C_L) likely varies with approach flow velocity and the hydraulic resistance of the channel in which a baffle-post structure is located.

In some situations, it may be of interest to know the discharge coefficient, C_D , associated with a baffle-post structure. Because the head difference associated with a local head loss through flow openings is often used as a means of measuring flow rate, it can be shown (e.g., Daily & Harleman, 1966) that headloss and discharge coefficients often relate as

$$C_D = \frac{1}{\sqrt{C_L}} \quad (2-16)$$

2.3. Dimensional Analysis

To work around the complications introduced by the non-uniform nature of the flow at a baffle-post structure, it is useful to resort to dimensional analysis, which also offers a framework for assessing how approach-flow conditions and baffle-post structure geometry influence the hydraulic performance of baffle-post structures.

The dominant variables influencing flow and energy dissipation through a baffle-post structure can be assembled and stated in the following functional manner:

$$f(N, D, s, l, y_0, q_0, B, g, \nu) = 0 \quad (2-17)$$

Where:

- N is the number of baffle post rows,
- D is the baffle post diameter
- s is the lateral spacing, from center to center, of the baffle posts,
- l is the streamwise spacing, from center to center, of the baffle posts,
- y_0 is the flow depth at section 0,

- q_0 is the unit discharge at section 0,
- B is the width of the channel,
- g is the unit gravity constant, and
- ν is the kinematic viscosity of water.

Eq. (2-17) assumes fully turbulent flow with negligible surface tension effects. Applying the Buckingham Π theory for dimensional analysis, and using D , q_0 , and ν as the repeating variables, the nine variables can be combined as six dimensionless parameters;

$$f' \left(N, \frac{s}{D}, \frac{l}{D}, \frac{y_0}{D}, \frac{q_0/y_0}{\sqrt{gy_0}}, \frac{q_0}{\nu} \right) = 0 \quad (2-18)$$

The first four parameters define geometric properties of the baffle-post structures, including the number of rows, dimensionless lateral and streamwise spacing, and dimensionless flow depth. The last two parameters describe the uniform approach flow conditions, at section 0. The fifth term is the Froude number;

$$Fr_0 = \frac{u_0}{\sqrt{gy_0}} = \frac{q_0/y_0}{\sqrt{gy_0}}$$

The final term is the Reynold's number;

$$Re_0 = \frac{u_0 y_0}{\nu} = \frac{q_0}{\nu}$$

Using the appropriate variables and dimensions, two dimensionless relationships can be formed for headloss and discharge coefficients, C_L and C_D , respectively;

$$C_D = f_D \left(N, \frac{s}{D}, \frac{l}{D}, \frac{y_0}{D}, Fr_0 \right) \quad (2-19)$$

$$C_L = f_L \left(N, \frac{s}{D}, \frac{l}{D}, \frac{y_0}{D}, Fr_0 \right) = C_D^{-2} \quad (2-20)$$

Here, C_D and C_L are dependent parameters whose values depend on the basic set of independent parameters grouped in the parentheses. These two equations assume the flow to be fully turbulent, and thus drop the Reynolds number parameter.

A dependent parameter of practical design interest is the depth increase parameter, y_1/y_0 , as this parameter is usually required to select the geometric layout and dimensions of a baffle-post structure. Therefore, an important functional relationship for design is

$$\frac{y_1}{y_0} = f_y \left(N, \frac{s}{D}, \frac{l}{D}, \frac{y_0}{D}, Fr_0 \right) \quad (2-21)$$

The laboratory experiments conducted for this study explore the relationship between the parameters in this equation. While it is possible to write functional relationships such as Eqs. (2-14) and (2-16) for C_L and C_D , the relationships are likely to be overly complicated for practical use.

2.4. Bed Sediment Transport to and at a Baffle-Post Structure

The presence of a baffle-post structure exerts several influences on the alluvial bed in which it is installed:

- 1) By retarding the approach flow, the structure reduces, or partially traps, bedload sediment transport in the backwater region upstream of the structure; and,
- 2) The turbulence structures generated by flow around the structure's baffle posts enhance bed sediment transport, causing local scour of the bed at the structure.

2.4.1. Sediment Trapping Upstream of the Structure

As discussed in the previous section, a backwater curve develops upstream of the structure, increasing the flow depth and decreasing the flow velocity, thus reducing the sediment discharge. An often used method to quantify sediment discharge is based on the difference between the existing and critical shear stress within the channel, such as the Meyer-Peter and Müller Equation (Wong & Parker, 2006).

$$q_s = 4.93 (\tau_* - 0.0470)^{1.60} \sqrt{(G - 1) g D^3} \quad (2-22)$$

Where q_s is the bedload sediment unit discharge, ρ_s is the sediment density, ρ is water density, g is the acceleration due to gravity, D is the size of the bed material, τ_* is the dimensionless grain shear stress, and τ_{c^*} is the critical dimensionless shear stress where sediment begins to move. This bedload formula estimates the unit sediment discharge by volume. Variation of the complete formulation of Eq. (2-22) can be found in several textbooks dealing with sediment transport, e.g., Simons and Senturk (1977), (Julien, 2010), and (Wohl, 2014).

Assuming that the only varying parameters are the flow depth and flow velocity,

$$q_s \sim (\tau_* - \tau_{c^*})^{3/2} \quad (2-23)$$

Dimensionless shear stress is defined as

$$\tau^* = \frac{\tau}{g(\rho_s - \rho)D} = \frac{\gamma y S_f}{g(\rho_s - \rho)D} \quad (2-24)$$

The two driving factors in the above equation are the flow depth, y , and the friction slope, S_f , which can be defined using the Manning's equation;

$$S_f = \frac{u^2 n^2}{R^3} \quad (2-25)$$

Once the structure induces a backwater flow profile, S_f decreases because u decreases, and R increases. As S_f decreases, τ decreases and the unit sediment discharge also decreases along the length of the backwater influence.

2.4.2. Bedforms

Once sediment particles become mobile, they generate small perturbations on the once smooth channel. These perturbations can grow with time, typically forming into classic configurations, known as bedforms (Julien, 2010). The type and size of these bedforms typically give insight into the magnitude of sediment discharge for a given sediment grain diameter. In alluvial channels with subcritical flow, the following bedforms can develop: plane bed, ripples, dunes, and washed out dunes. In general, as the sediment discharge increases, the sand bed will transition from plane bed, to ripple to dune conditions. Bedforms were used as a metric to qualitatively quantify the sediment trapping ability of the structure. Due to the range of Froude numbers tested, washed out dunes were not expected to form.

2.4.3. Local Scour at the Structure

Local scour is a concern at the baffle-post structure, due to the critical flow conditions at the contraction. At the structure, the flow transitions from a backwater, M_1 , curve to a draw down curve, M_2 . Under draw down flow conditions, the velocity increases as the flow depth decreases. Using the same logic presented in the paragraphs above, the friction slope will increase and the flow depth will decrease, causing the bed shear stress to increase. Therefore, the unit sediment discharge will increase. The need for scour protection at the base of this structure will be explored in this study.

3.0 Experimental Set-up

3.1. Introduction

Experiments were conducted to determine the influences of baffle post geometry (number of rows, post spacing and post diameters) on the hydraulic performance of baffle-post structures. The hydraulic parameters of interest were:

- 1) Headloss coefficient and, relatedly, discharge coefficient;
- 2) Relative increase in water depth at the baffle-post structure; and,
- 3) Sand-bed adjustment upstream of, at, and downstream of a baffle-post structure.

Figure 3-1 shows the general arrangement of the baffle-post structure positioned in the laboratory flume.

The performances of two different post diameters, as well as several configurations of lateral and streamwise spacing, were investigated. These experiments supported the development of a discharge rating curve and an approximate formula to represent the discharge coefficient based on the structure geometry and configuration.

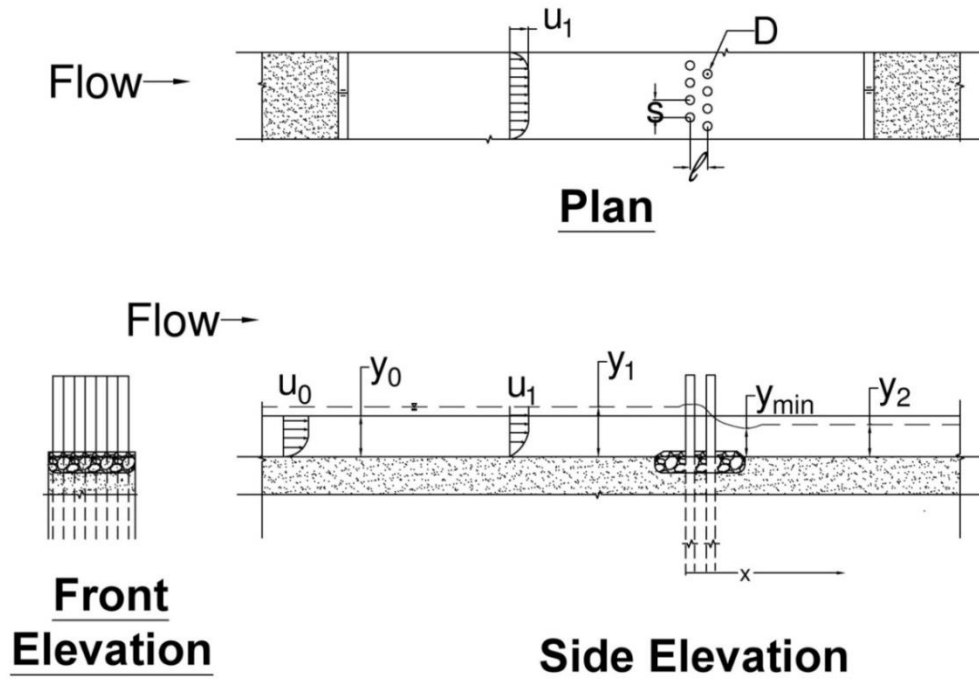


Figure 3-1: General layout of the baffle-post structure

3.2. Facilities and Materials

The experiments were performed at Colorado State University in the Hydraulic Laboratory, and used a re-circulating open channel, Plexiglas flume that was 9.70 m long, 0.20 m wide and 0.36 m deep. Figure 3-2 illustrates the flume. A series of horizontal baffles was installed at the flume's inlet, to ensure the flow entering the flume was uniformly distributed and free of large turbulence structures, as shown in Figure 3-3. The flow entered the flume sufficiently upstream of the location of the model baffle-post structure so that the flow developed the velocity profile typical of fully developed turbulent flow.



Figure 3-2: Re-circulating 8" Plexiglas flume used for experiment

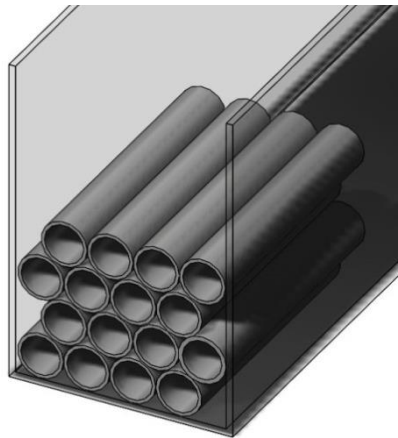


Figure 3-3: Horizontal baffles installed at the flume inlet to ensure fully developed flow within the flume

Flow rate was measured through an orifice plate connected to the pump operation on the flume. The orifice plate measures flow rate by restricting the flow, thus reducing the pressure. Thus, a pressure differential, Δh , can be measured and converted into a discharge using an equation specific to the orifice plate, Eq. (3-1). Average velocity could then be calculated based on the flow area;

$$Q = 0.228 \Delta h^{0.503} \quad (3-1)$$

Where Q is the flow rate in cubic feet per second (cfs) and Δh is the pressure difference in feet. The discharge was then converted into cubic meters per second.

3.3. Single-Row Baffle-Post Structure

The baffle-post models, comprised of cylindrical wooden dowels, were attached to a wooden cap secured to the top of the flume. An example structure is shown in Figure 3-4. The structure was installed to the entire depth of the flume (0.36m), at approximately half of the flume's length, 3.8 m from the inlet. The structure geometry was developed assuming 0.30m (1.0 ft) baffle post diameters for prototype baffle-post structures. In accordance with geometrical similitude, the posts were sized using a width scale of 18. The width scale is defined as the ratio of the prototype width value (1.0 ft) to the model width value. For this study, the width scale was based on a relaxed scaling approach. A 19.2 width ratio was adopted for practical purposes, as dowels are only available in standard sizes. Therefore, the modeled baffle posts diameter, D , was 15.875 mm (0.625 inches). To quantify post spatial density, a blockage ratio was calculated and is defined in Eq. (3-2).

$$p = \frac{\text{Area blocked by structure}}{\text{Total flow area}} \quad (3-2)$$

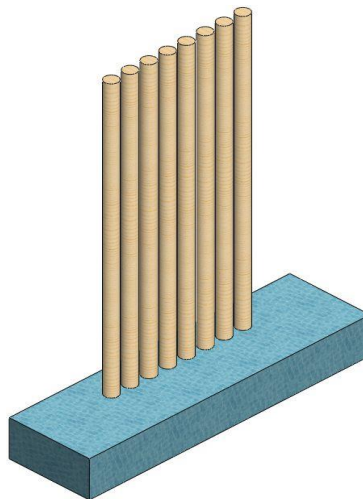


Figure 3-4: Single-row baffle-post structure

The spatial density of posts was also quantified using the effective width of the channel, or the new width of the channel that is not inhibited by baffle posts. The effective width is defined in Eq. (3-3), where B is the width of the flume, k is the contraction coefficient, n , is the number of baffle posts, and D is the baffle post diameter; i.e.,

$$B_{eff} = B - knD \quad (3-3)$$

The contraction coefficient was assumed to be 1.0 and is further discussed in Section 4.0 – Data Analysis and Results.

3.3.1. Schedule of Experiments

Seven different single-row post configurations were investigated, as listed in Table 3-1. Post diameter was fixed at a prototype value of 0.30 m. As discussed in the introduction to this section, a 19.2 width ratio was adopted for practical purposes, which is close to the theoretical geometric ratio of 18. Streamwise spacing of posts can be considered as being infinite (i.e., a single row). Only the relative lateral spacing, s/D , was varied from 1.5 to 6.4; comprising 8 to 1 baffle posts.

Table 3-1: Configurations used for the single-row baffle-post structure experiments, varying lateral spacing. $D = 15.875$ mm for all configurations.

No.	Lateral Spacing, s (mm)	s/D	No. of Posts, n	B_{eff} (m)	p
1	23.813	1.5	8	0.187	63%
2	31.750	2.0	7	0.171	55%
3	47.625	3.0	5	0.156	39%
4	63.500	4.0	4	0.140	31%
5	79.375	5.0	3	0.124	23%
6	95.250	6.0	2	0.092	16%
7	101.600	6.4	1	0.092	8%

3.3.2. Procedures

The single-row baffle-post structures were tested for two different scenarios: flow through a forested floodplain and flow through a GBS. In the context of flow through a forested floodplain, the flow depth is typically relatively shallow. Therefore, flow conditions were selected based on low y_0/D ratios. Two Froude numbers were selected to run these tests: 0.15 and 0.45. These values were selected based on the range of Froude numbers tested in other studies (such as Tsikata et al. 2014) and what was physically possible within the flume. Three y_0/D ratios were selected for Froude number values of 0.15: 2.0, 2.8, and 4.9. Values of Reynolds number ranged from 10,400 to 2,800, decreasing with depth. Using a threshold value of $Re = 2,000$ for turbulent flow (e.g. Jain, 2001), the flow was fully turbulent for all depths. Higher depths were physically possible at a higher Froude number of 0.45; therefore, four y_0/D ratios were selected: 2.1, 3.1, 4.9, and 6.4. Under these flow conditions, the flow was also fully turbulent with Reynold's numbers varying from 46,000 to 8,400.

A second set of experiments was performed on the single-row baffle-post structures, in the context of the hydraulic performance of a GBS. Three of the previous configurations were experimented upon at three relatively deeper flow depths ($y_0/D = 5.0, 9.4, \text{ and } 12.4$) over a range of Froude numbers. Flows were fully turbulent with Reynold's numbers varying from 12,000 to 160,000.

Uniform flow conditions were established by setting the discharge to the appropriate value given the selected flow depth and Froude number. A sluice gate was then adjusted to maintain a relatively uniform and steady flow depth throughout the flume. A difference of 1.0 cm over the flume length of 9.7 m was deemed acceptable. Flow depth measurements were taken at two points along the flume, 0.28 m upstream and directly upstream of the structure, as shown in Figure 3-5. The depth 3.50 m downstream of the flume inlet was then used to calculate the average flow velocity, u_0 , and unit discharge, q_0 within the flume.

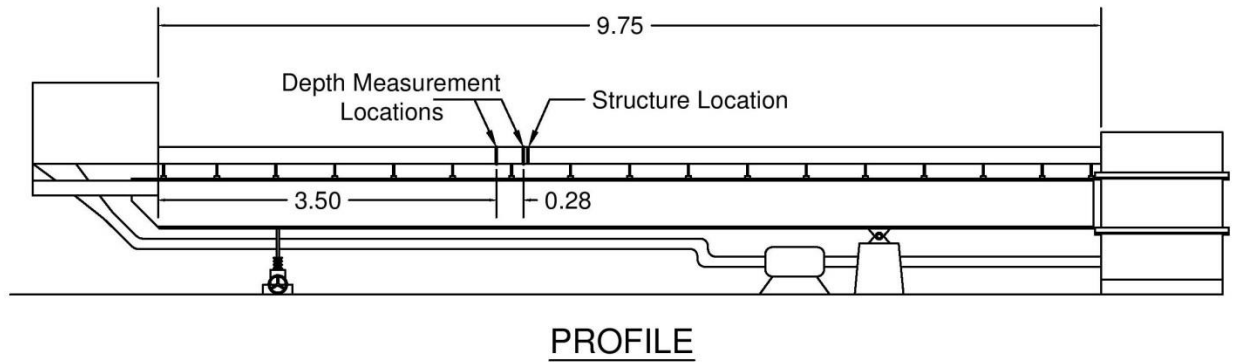


Figure 3-5: Flow depth measurement locations

Once the initial uniform flow conditions were established, the structure was placed 3.8 m downstream from the flume's inlet. Flow depths were measured once again at the same two locations as well as at the minimum depth within the water surface profile. The depth taken immediately upstream of the structure was used to determine the energy dissipation, ΔE , from the structure as well as the new unit discharge, q_1 .

3.4. Double-Row Baffle-Post Structure

The hydraulic performance of a structure formed of two rows of baffle posts was investigated using the re-circulating open channel, Plexiglas flume used to test the single-row baffle-post structures (see Figure 1-2).

The baffle-post structure, comprised of cylindrical wooden dowels, was secured to a wooden cap attached to the top of the flume. The structure was installed to fill the entire depth of the flume, 3.8 m from the inlet. The structure geometry was developed assuming 0.30 m and 0.15 m baffle post diameters for the prototype. Using the same geometric similitude described above, a 19.2 width ratio was adapted. The modeled baffle posts had diameters, D , of 15.875 mm (0.625 inches) and 7.9375 mm (0.3125 inches).

3.4.1. Schedule

To examine the impacts of structure geometry on the hydraulic performance of the two-row structure, the lateral, l , and streamwise, s , distances were varied, along with the post diameter, D . Three lateral distances were tested at two post diameters, as indicated in Figure 3-6. Four streamwise lengths were tested, maintaining a constant lateral spacing and the post diameter, Figure 3-7 (left). Finally, two configurations were investigated to determine the hydraulic performance impact of varying the baffle post diameter, Figure 3-7 (right). Ten configurations were examined, as listed in Table 3-2.

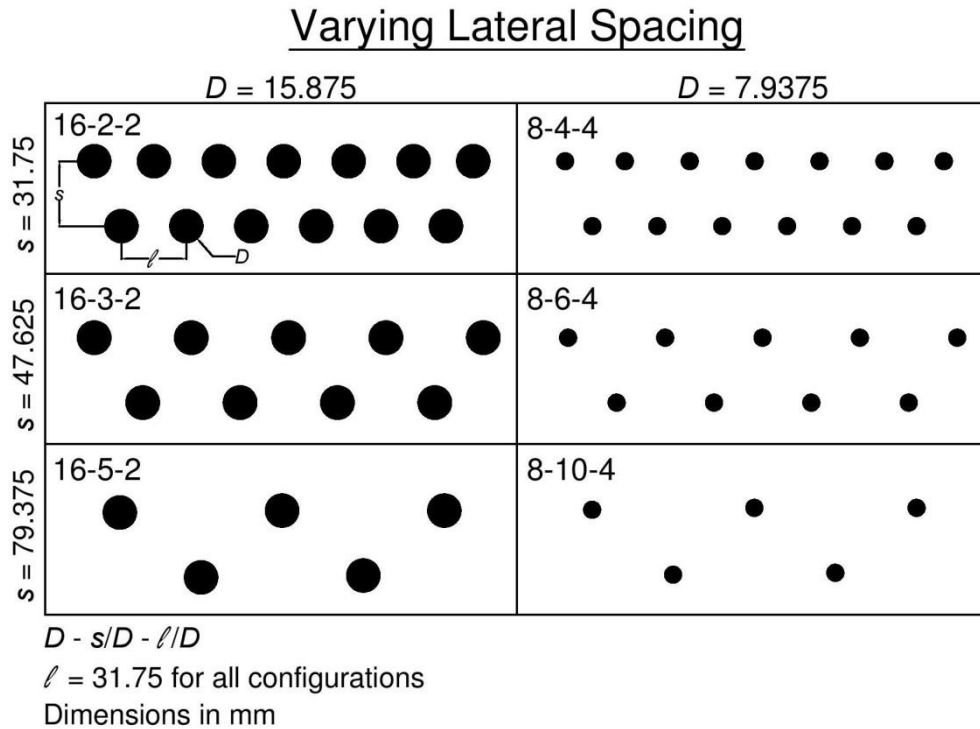
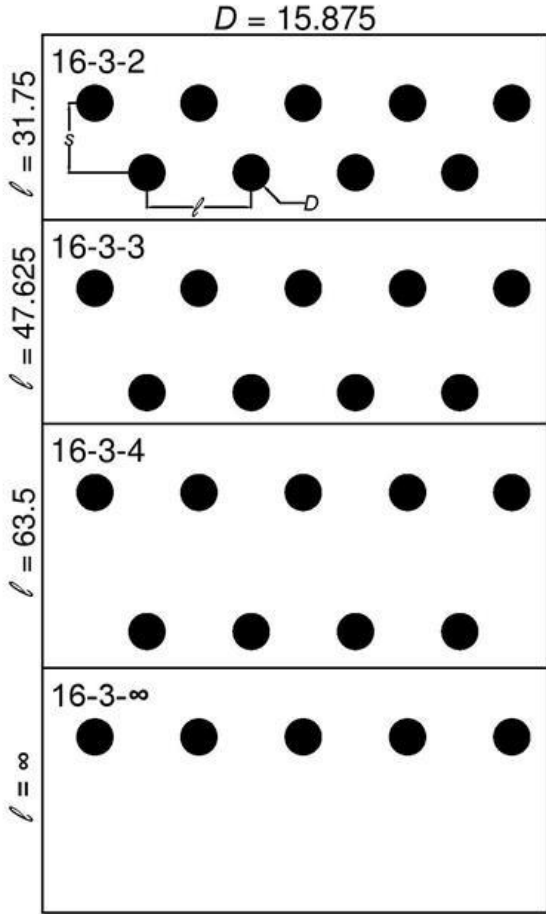


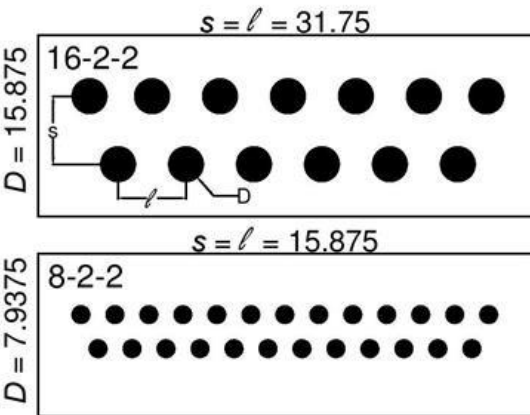
Figure 3-6: Plan views of post configurations experiments, varying lateral spacing and baffle post diameter, keeping streamwise spacing constant.

Varying Streamwise Spacing



$D - s/D - l/D$
 $s = 47.625$ for all configurations
 Dimensions in mm

Varying Bar Diameter



$D - s/D - l/D$
 Dimensions in mm

Figure 3-7: Plan view of post configurations for experiments, varying streamwise spacing, keeping diameter and lateral spacing constant, and post configurations for hydraulic performance tests, varying diameter, keeping both lateral and streamwise spacing constant.

Table 3-2: Configurations for experiments, varying lateral and streamwise spacing, as well as baffle post diameter

No.	Configuration $\left(D - \frac{s}{D} - \frac{l}{D}\right)$	D (mm)	s (mm)	l (mm)	n	B_{eff} (m)	p
1	16-2-2	15.875	31.750	31.750	13	0.092	102%
2	16-3-2	15.875	47.625	31.750	9	0.124	70%
3	16-3-3	15.875	47.625	47.625	9	0.124	70%
4	16-3-4	15.875	47.625	63.500	9	0.124	70%
5	16-3- ∞	15.875	47.625	∞	5	0.124	39%
6	16-5-2	15.875	79.375	31.750	5	0.156	39%
7	8-2-2	7.9375	15.875	15.875	25	0.100	98%
8	8-4-4	7.9375	31.750	31.750	13	0.148	51%
9	8-6-4	7.9375	47.625	31.750	9	0.164	35%
10	8-10-4	7.9375	79.375	31.750	5	0.179	20%

3.4.2. Procedures

Experiment procedure for the double-row baffle-post structures was the same as used for the single-row baffle-post structures. Flow conditions were based on three flow depths, at Froude numbers ranging from 0.10 to 0.58. A typical Froude number found in most rivers is approximately 0.20 (e.g. Julien, 2002 and Wohl, 2014); therefore, the range tested is appropriate. All experiments were run under fully turbulent flow conditions, with Reynold’s number ranging from approximately 8,000 to 114,000. Once uniform conditions were established and the initial flow depths were noted, shown in Figure 3-5, the structure was installed 3.8 m from the flume inlet. Again, the two flow depths and the minimum flow depth were measured.

3.5. Sediment Transport Experiments

3.5.1. Set-up

A further set of experiments was performed to qualitatively analyze the bed-sediment trapping ability of a baffle-post structure. One configuration, 16-2-2, was used. It was selected as it had the tightest

lateral spacing, $s/D = 2$, and the highest resistance due to the second row of baffle posts; thereby, likely producing the greatest degree of choking and slowing of the approach flow.

The same 0.20 m flume was filled with 0.2 mm silica sand to 9.0 cm depth along 7.79 m of the flume. Figure 3-8 shows a gradation curve for the silica sand. The first 0.46 m and last 0.49 m of the flume were filled with pea gravel to hold the sand in place. The structure was installed 5.33 m downstream of the beginning of the sand-bed, to develop sediment transport and bedforms upstream of the structure. Three tests were conducted to analyze the sediment trapping ability of the structure:

- 1) Flow without a structure present;
- 2) Flow with a structure present, but without armoring (rock) at the toe of the structure; and,
- 3) Flow with a structure present and with armoring (rock) at the toe of the structure.

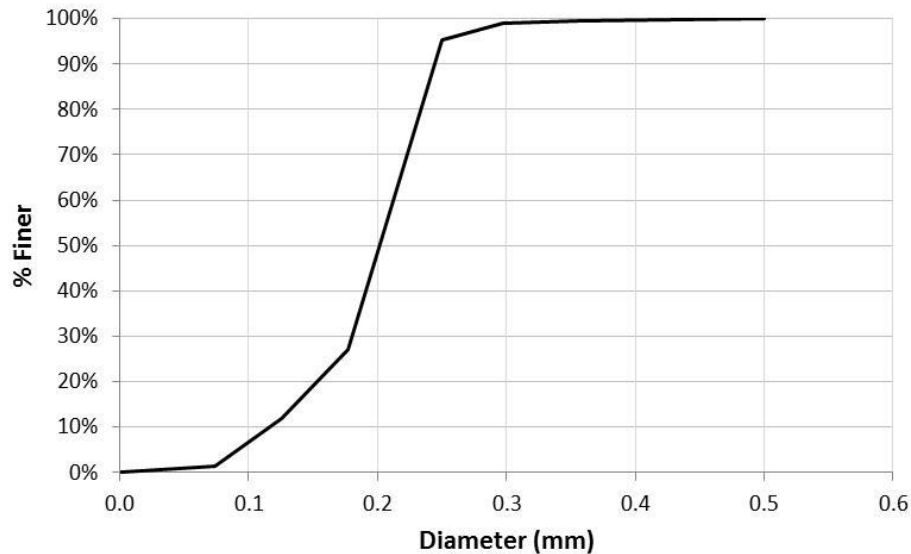


Figure 3-8: Gradation curve for the silica sand used.

3.5.2. Experiment Procedure

The experiments were run with a flow depth of 0.083 m above the initial 0.09 m of sand at a flow rate of $0.005 \text{ m}^2/\text{s}$ and $Fr_0 = 0.35$. The discharge was intended to be high enough to develop bedforms. Once

the hydraulic conditions were established, the experiment was run for 5 hours, periodically measuring flow depth, sand depth, and bedform height. These measurements were made at four locations along the flume, as shown in Figure 3-9.

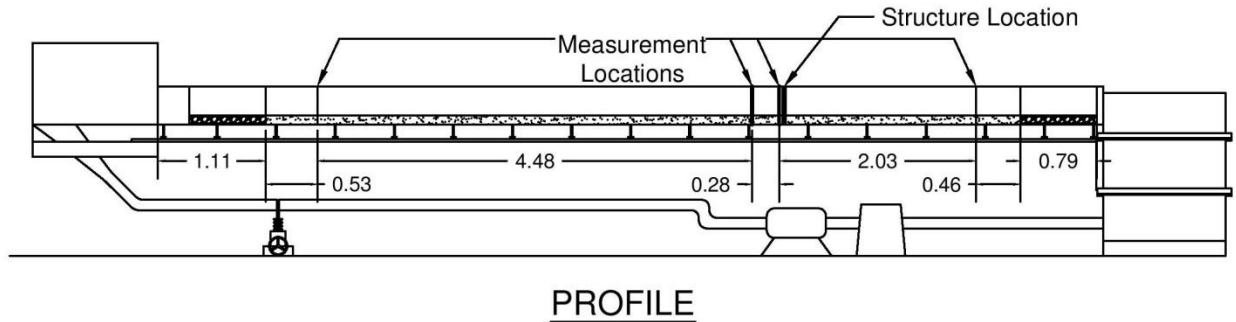


Figure 3-9: Flow and sand depth measurement locations along the flume for the mobile bed tests. Note that some of the support structure has been removed to simplify the drawing.

3.6. Study Limitations

A few limitations should be taken into account when considering the observations and data produced by this study. One limitation concerns the precision of the flow-depth measurements. Depths were measured using a scale whose accuracy was to within 0.5 mm. Further, water flow rates through the flume were measured using an orifice plate, as discussed in Section 3.2. The pressure differential was then converted to a discharge and presented on a digital monitor. The readings were presented to the thousandth decimal places in cubic meters, but results were recorded in 0.00014 m³/s (0.005 cfs) increments.

All experiments were conducted using the 0.20 m flume, and did not take into account side-wall corrections when determining an average approach flow, u_0 . For the purposes of the present study, it was assumed that the flume's plexi-glass side walls exerted a negligible influence on cross-sectional distributions of velocity.

4.0 Data Analysis and Results

4.1. Introduction

This chapter presents measured data investigating relationships for headloss coefficient C'_L (and the related discharge coefficient, C'_D) for flow through the baffle-post structures. This investigation includes analyzing the concept of “overcritical” or “choked flow” that is needed to determine the increase in specific energy needed to pass the flow through the baffle-post structure. Additionally, this chapter presents data expressing the empirical relationship between flow depths, y_1 , at the baffle-post structure and approach flow depth, y_0 . The increase or amplification in flow depth, y_1/y_0 , is of practical importance for determining the likely extent to which a baffle-post structure will retard an approach flow of depth y_0 .

The data trends found for C'_L and C'_D are first presented and discussed for single-row baffle-post structures ($N = 1$), then for double-row baffle-post structures ($N = 2$). For the single-row structures, the data are shown as plots of C'_L versus s/D , with two associated values of Fr_0 . For the double-row structures, the data are presented as plots of C'_L versus Fr_0 , with several associated values of s/D , y_0/D , and l/D . The trends are discussed in general terms that explain the variation of C'_L and C'_D with baffle post geometry and approach flow Froude number, Fr_0 .

Tables in this chapter summarize the data obtained for the baffle-post configurations tested. For the reader’s convenience, all tables and figures containing data are placed at the end of this section. Appendix A contains the measured data for all the experiments.

The equations for choked flow conditions express unit discharge, q_1 , entering the first row of baffle posts as

$$q_1 = \frac{Q}{B_{eff}} = \frac{Q}{B - knD} \quad (4-1)$$

in which k is a contraction coefficient related to flow passage between baffle posts. The present study takes the simplifying, practical step of setting $k = 1.0$, and including variations in k as part of the variations in C'_D and C'_L . Therefore, here

$$q_1 = \frac{Q}{B - nD} \quad (4-2)$$

Figure 4-1 depicts flow between posts in a single row of baffle posts. Although the flow contracts between the posts, and wake eddies are shed, the extent of flow contraction was small enough to justify $k = 1.0$ and the use of Eq. (4-2).

The data tables in this chapter contain estimated values of the critical flow width, B_c , linked to flow choking, as discussed in Section 2.2. These values are compared with the values of $B_{eff} = B - nD$ consequent to the spacing and number of posts in a single row of baffle posts. If $n \approx B/s$, it can be shown that the posts choke an approach flow when

$$\frac{s}{D} \left(1 - \frac{B_c}{B} \right) < 1 \quad (4-3)$$

As the baffle posts are intended to choke an approach flow, Eq. (4-3) is a guide for minimal spacing of posts so that the sum of post openings is less than the choking width, B_c , for an approach flow. Flow contraction at this limit ensures that post spacing will choke an approach flow. Moreover, the presence of a second row of posts introduces additional energy loss that typically ensures flow choking occurs for a double row of posts.

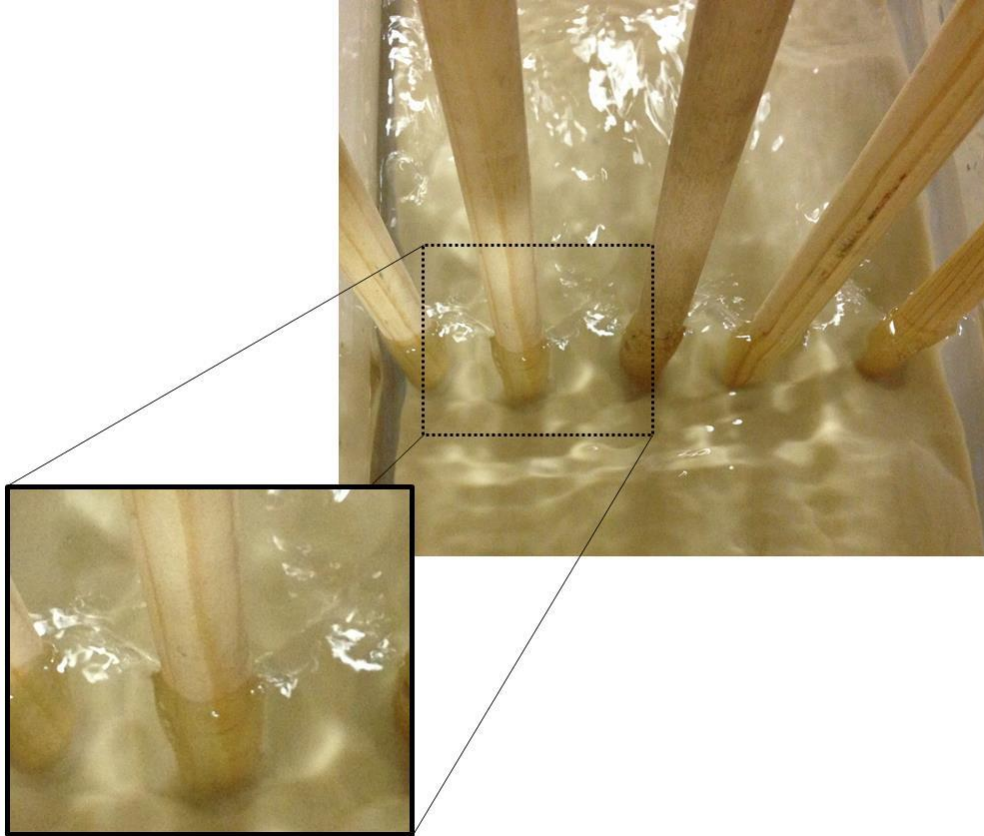


Figure 4-1: Flow between the baffle posts is slightly contracted.

4.2. Water-Surface Profile

The baffle-post structures produced a similar water-surface profile for all post geometries and flow conditions investigated. An example profile is depicted in Figure 4-2, which shows the principal flow features observed for flow up to, through and downstream of a baffle-post structure.



Figure 4-2: Example shape of water surface profile, with pertinent flow depths indicated ; $y_1 = 0.13$ m; $y_0 = 0.10$ m; $y_{c_1} = 0.10$ m; and, $y_{c_0} = 0.067$ m. Experiment conditions: $Fr_0 = 0.45$, $y_0/D = 6.4$, and $s/D = 2$.

Where:

- y_1 is the maximum flow depth at section 1, upstream of the structure;
- y_0 is the flow depth at section 0, uniform flow depth;
- y_{c_1} is the critical flow depth ; and
- y_{c_0} is the supercritical flow depth.

When approaching the baffle-post structure the flow transitioned from uniform flow of depth y_0 into gradually varied flow. The flow depth gradually increased as it approached the posts, forming a M_1 flow profile until it reached the maximum depth, directly upstream of the structure, y_1 . The depth increase relates to the increase in the specific energy needed to pass the flow through the structure. At this point within the control volume, the velocity within the channel had its lowest value. The flow passed through critical depth, y_{c_1} , as it accelerated through the structure, and continued to accelerate, resulting in a rapid decrease in flow depth, reaching the minimum flow depth or maximum flow velocity, which is the original critical flow depth, y_{c_0} . The minimum flow depth varied in magnitude and the streamwise distance from the structure. The flow depth then gradually or rapidly increased, depending

on initial flow conditions and the structure geometry. If the downstream depth drops below critical, it is likely that a hydraulic jump will occur, as shown in Figure 4-2.

4.3. Turbulence Structures at a Baffle Post

The baffle-post structures produce turbulence structures (flow vortices), which increase the turbulence of flow through the baffle-post structure, thus increasing the overall dissipation of flow energy by the structure. Three flow vortices of prominence are shown in Figure 4-3:

- 1) horseshoe vortex at the junction of the post and its base,
- 2) surface roller at the water surface, and
- 3) wake vortex system developed as flow separates from the post.

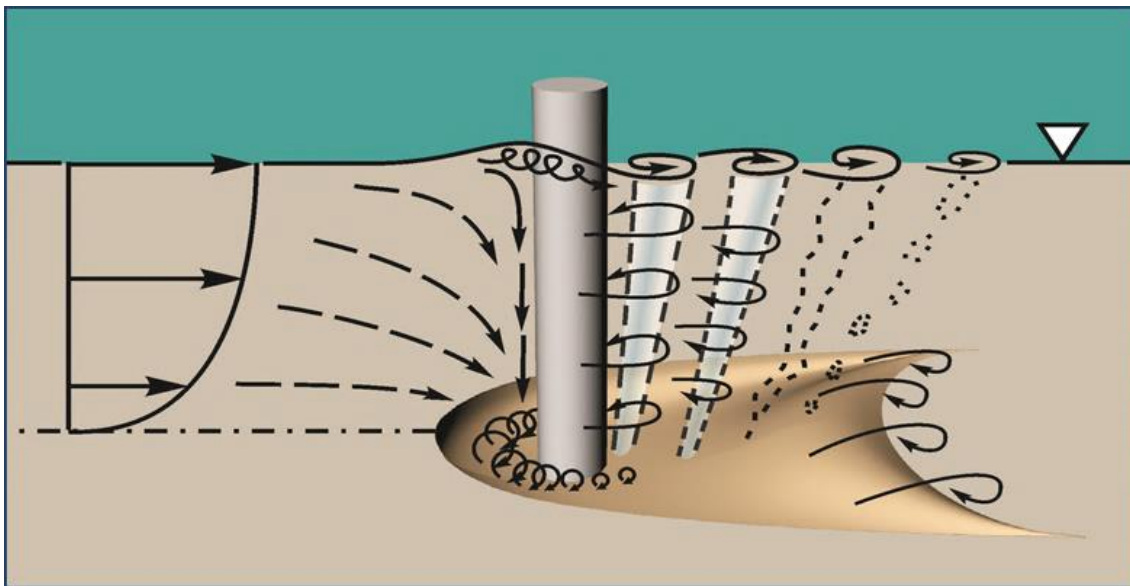


Figure 4-3: Flow field around a pier is marked by numerous vortices that influence energy loss and pier scour

The horseshoe vortex formed at the base of a post from downflows and secondary flows is active in displacing bed material from the foot of the post, and therefore has received much attention in literature, especially regarding bridge piers; e.g. Julien (2002) and Melville & Coleman (2000). The surface-roller vortex occurs just upstream of the baffle post at the top of the water column. Lastly, the

wake vortex develops downstream of the post due to the shear layer surrounding the baffle post (Koumoutsakos & Leonard, 1995).

4.4. Single-Row of Baffle Posts

The hydraulic performance of a single-row of baffle posts was investigated, with the lateral spacing of the posts (i.e., s/D) being the main geometric variable considered, along with a variable Fr_0 of the approach flow. Flow depth data were collected along the flume, as described in Section 3.3.2.

The general trends obtained for C'_L and C'_D are presented in Figure 4-4. The C'_L value decreased as s/D spacing and relative depth, y_0/D , increased, but C'_L increased as Fr_0 increased. However, the corresponding value C'_D increased as s/D , y_0/D , and Fr_0 increased, but at a lesser magnitude. These trends are explained in the following sections.

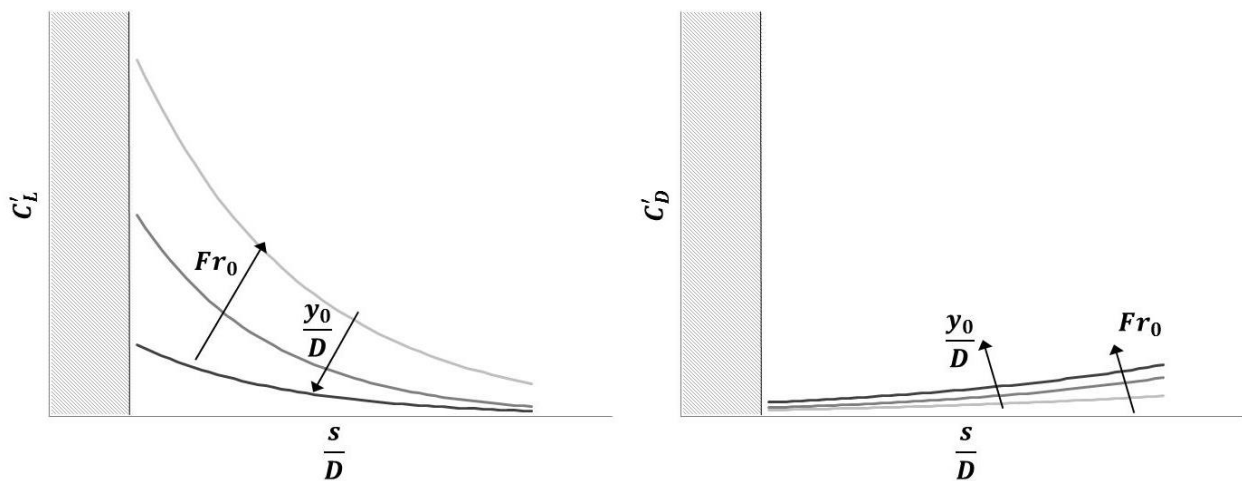


Figure 4-4: General trends for C'_L and C'_D for single-row structures

4.4.1. Influence of Froude Number, Fr_0

The C'_L values increased as the Froude number increased, displaying the influence of the relative difference in flow depth seen in free-flow vs. retarded flow conditions, expressed by the y_1/y_0 term in Eq. (2-14). In physical terms, larger values of Fr_0 result in more turbulence and dissipation of flow

energy due to larger and more interactive flow vortices caused by the baffle posts, as described in Section 4.3. The increase in magnitude and extent of the flow vortices increases ΔE values through the structure, thus increasing the C'_L values. Values of f may slightly decrease as increased Fr_0 is accompanied by large value of Reynolds number, Re . Consequently, Eq. (2-15) shows that increasing Fr_0 leads to larger values of C'_L . The data for the single-row baffle post structures are listed in Table 4-1 through Table 4-3, and displayed in Figure 4-9 through Figure 4-20.

4.4.2. Influence of Lateral Spacing, s/D

The C'_L values had an inverse relationship with s/D spacing; i.e., smaller s/D resulted in a higher C'_L value due to an increase in turbulence caused by the higher roughness through the baffles. When the flow openings were smaller, the flow vortices developed by the baffle posts were closer together and more likely to interfere with each other, which resulted in a more turbulent flow and higher internal energy dissipation, ΔE . Thus, the primary driver of an increase in ΔE was a direct result of a higher density of baffle posts or a higher blockage ratio, p . The additional baffle posts obstructed a larger flow area, which produced higher resistance to flow, thus dissipating more flow energy. This phenomenon has been documented in several other studies, examples include: (Stone, 2002) and (Wilkerson, 2007). Based on the results obtained, C'_L increased with decreasing s/D spacing. Conversely, as the spacing between the baffle posts increased and the effective width increased, more flow can pass through the structure, thus increasing C'_D .

4.4.3. Influence of Relative Depth, y_0/D

At $Fr_0 = 0.15$, C'_L also varied with y_0/D , especially at smaller s/D spacing. For the smallest relative lateral spacing, $s/D = 1.5$, the C'_L ranged from 20.8 at $y_0/D = 2.1$ to 1.6 at $y_0/D = 4.9$, as shown in Figure 4-12. Physically, the decrease in C'_L with an increasing y_0/D can be explained by the magnitude of the various vortices. At small relative depths, the surface roller, downflow and horseshoe vortex impinge on each other, increasing flow turbulence, which further decreased the specific flow energy.

However, as y_0 increased, the horseshoe vortex moved up in the water column, no longer interacting with the channel bottom.

The y_0/D values appeared to have minimal impacts at larger Fr_0 values, Figure 4-14, due to the direct relationship between y_0/D and ΔE . As shown in Figure 4-15, the relative change in water surface elevation through the baffle-post structure increased as y_0/D increased. Furthermore, at a higher Fr_0 both the horseshoe and roller vortices were stronger and larger and possibly interacting at all three y_0/D values. Therefore, the increase in ΔE as a result of the colliding flow paths was likely observed at all three depths, resulting in negligible differences in the C'_L values through the structure.

The same concepts can be applied to explain the C'_D trends. When the flow vortices collided with the channel bottom, the energy upstream pushed a smaller flow volume through the structure. There the ratio of theoretical discharge to actual discharge decreases, thus decreasing C'_D . As the depth increased, the ΔE decreased; thus, the volume of flow that can pass through the structure increased, increasing C'_D .

4.4.4. Depth Increase Parameter, y_1/y_0

As both coefficients for non-uniform flow are complex and impractical, the depth increase parameter, y_1/y_0 , becomes increasingly useful, creating a practical approach to analyzing the water effects of this structure. Figure 4-18 through Figure 4-20 illustrate the influence of s/D spacing over a larger range of Fr_0 values. Figure 4-21 and Figure 4-22 illustrate how s/D spacing influences the depth increase parameter, y_1/y_0 specifically for $Fr_0 = 0.15$ and $Fr_0 = 0.45$, respectively, with relatively shallow flow depths. The figures show that the baffle-post structures created a backwater flow profile which acts to slow an approach flow. The value of y_0 for an approach flow (or flow prior to installation of a baffle-post structure) can be calculated, using Manning's equation together with the two values of Fr_0 for the approach flow. Figure 4-18 through Figure 4-22 can then be used to estimate y_1 for the given s/D

spacing and Fr_0 value. Furthermore, if the relative increase in flow depth is known, the figures become useful in choosing an appropriate spacing.

4.4.5. Choked Flow Conditions

To determine if the width constriction of the structure resulted in choked flow, the critical width, B_c , for the given E_0 , was compared to the effective width, B_{eff} . The effective width for the single-row baffle posts for various spacing is presented in Table 3-1. Equation 3-3 was used to calculate B_c , whose values are presented in Table 4-4. As expected, the flow at a lower Fr_0 could pass flow through a much larger contraction (or smaller critical width), as q_0 is much smaller.

Based on the B_c results, the width contraction due to the baffle-post structure was not enough to induce choked flow at $Fr_0 = 0.15$. Graphical results are presented in Figure 4-23. However, with a larger flow rate associated with $Fr_0 = 0.45$, B_c was much larger. Choked flow conditions occurred when the number of bars, n , was greater than or equal to 4, or $B_{eff} \leq 0.147\text{m}$. The choked flow condition results were verified by plotting the experimental results on the specific energy diagram for $Fr_0 = 0.45$, Figure 4-24.

The specific energy diagrams for $Fr_0 = 0.15$, presented in Figure 4-23, compare the free flow conditions to the flow conditions with $n = 8, 4$, and 1. Both the initial (free flow) and final conditions (with structure) are plotted. The shift in specific energy and upstream flow depth is particularly noticeable for $n = 8$, Figure 4-23 (a). The upstream depth increased as a result of flow resistance from the structure. Therefore, the depth term in the specific energy equation increased, which resulted in a total increase in specific energy upstream of the structure. Notice that both the initial and final flow conditions share an E-y curve within the range of the experimental conditions. As there was no need to shift the specific energy curve to compensate for the width contraction, it can be concluded that the width constriction caused by the structure did not sufficiently “choke” the flow.

On the other hand, Figure 4-24 shows specific energy curves for $Fr_0 = 0.45$. These curves show a clear shift in specific energy for free flow conditions versus final conditions. As the width further contracted past B_c , the upstream available energy must increase to push the same discharge through the structure. The data imply that decreasing B_{eff} produced a linear relationship on the E-y plane, with E_1 increasing at a faster rate than y_1 .

4.5. Double-Row of Baffle Posts

4.5.1. Analysis Approach

The hydraulic performance of a double-row of baffle posts depends upon the same parameters as the single-row structures, s/D and y_0/D , as well as an additional parameter expressing streamwise, l/D , spacing. As explained in Section 2.2, C'_L is based on the change in upstream flow depth. The variation in flow depth due to the baffle post was measured along the flume, as described in Section 3.4.2.

4.5.2. Influence of Froude Number, Fr_0

As shown in all the graphical results presented in Figure 4-5, the headloss coefficient consistently increased with increasing Fr_0 values. The discharge coefficient remained relatively constant over a range of Fr_0 values, only slightly decreasing as Fr_0 increased.

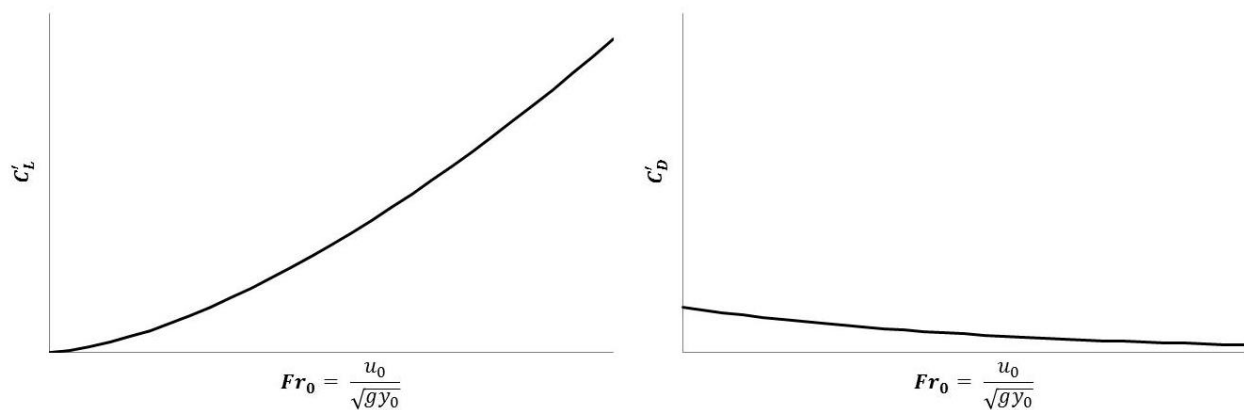


Figure 4-5: General trends for C'_L and C'_D over a range of Fr_0 values

As explained in Section 4.4.1, C'_L increased with Fr_0 due to the increase in relative flow depth and the magnitude and extent of the flow vortices. Discharge coefficient values remained relatively constant over the range of Fr_0 . A constant C'_D implies that the relationship between Q and y_1 is constant over the entire range of Fr_0 , similar to a weir or sluice gate, which simplifies the design and implementation of these structures. The slight decrease in C'_D with an increase in Fr_0 results from a more energetic flow field. An increase in the initial specific energy resulted in higher capacity to push more flow through the structure.

4.5.3. Influence of Lateral Spacing, s/D

The general trends depicting the impact of lateral spacing on the double row structure are presented in Figure 4-6. Experimental results for the double-row baffle-post structure are presented in Table 4-5 and Table 4-6. The graphical results of C'_L are presented in Figure 4-25 through Figure 4-29.

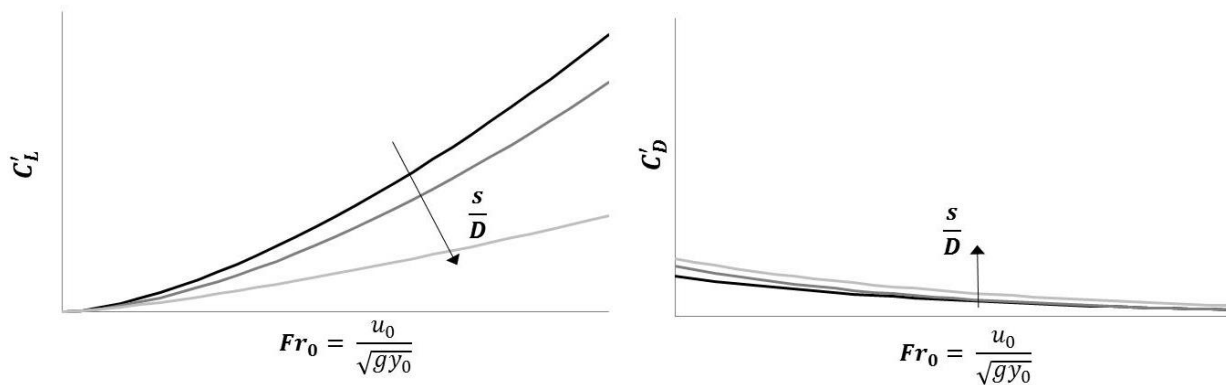


Figure 4-6: General trends for C'_L and C'_D over a range of Fr_0 values, varying s/D spacing

Similar to the single-row structures, there was an inverse relationship between C'_L and s/D spacing. As the baffle posts were positioned closer together, B_{eff} of the channel decreased, approaching B_c . Once $B_{eff} < B_c$, the flow will become choked. Furthermore, the flow vortices were more likely to interact at closer post spacing, resulting in higher ΔE values, as discussed earlier in this study. This phenomenon is clearly presented in Figure 4-27, showing the water surface profiles surrounding the structure at an

initial flow depth of 0.08m. The values of ΔE are visibly higher when s/D spacing is smaller, which can be seen in the higher y_1 value and the position and relative value of the downstream dip in the water surface profile.

The coefficient C'_D remained constant as Fr_0 varied, but decreased as s/D increased. As B_{eff} of the structure increased, the available upstream specific energy can push more flow through the structure, thereby increasing C'_D .

4.5.4. Influence of Streamwise Spacing, l/D

Figure 4-7 shows the general impact of l/D spacing on C'_L and C'_D . As compared to the s/D spacing, l/D spacing has a much smaller impact on both coefficients. Experimental results showing l/D spacing are presented in Figure 4-30 through Figure 4-33 below. Compared to the effects of s/D spacing, the trend is not clear. The experimental data show much more scatter and irregularity than the idealized curves presented in Figure 4-7.

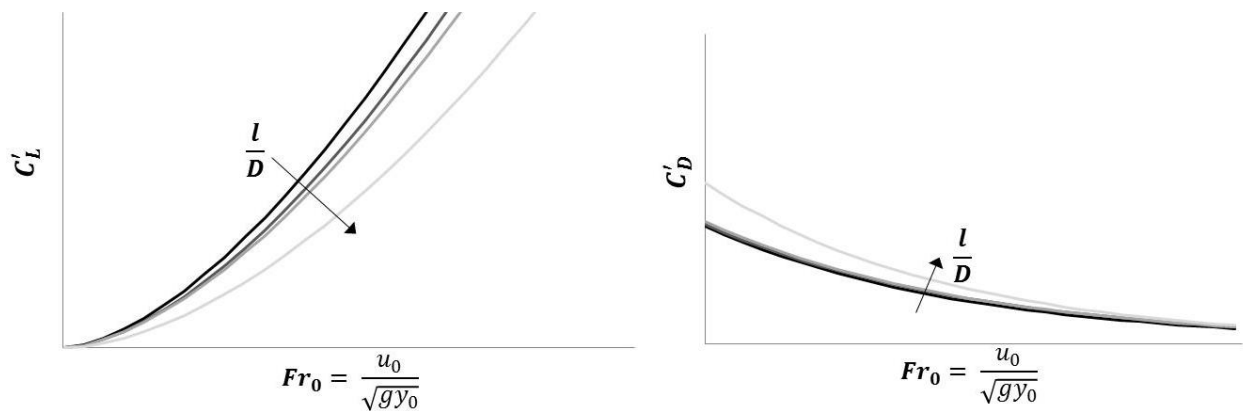


Figure 4-7: General trends for C'_L and C'_D over a range of Fr_0 , varying l/D spacing

In general, it appears that the closest relative spacing, $l/D = 2$, has the highest C'_L values. However, the difference between that and indefinite spacing, $l/D = \infty$, was minimal for all three flow depths. For all four experimental structures, the number of baffle posts, thus the effective width, was constant. The change in y_1 between the four structures was minimal, explaining the similar C'_L values.

Similar ΔE through all four structures is verified in the experimental photos, presented in Figure 4-31. Unlike the photographs presenting the experimental results from s/D spacing, the difference between the tight and loose spacing was not evident. While the position of the dip in water surface profile varies, the minimum flow depth is not significantly different, implying similar values of kinetic energy dissipation.

However, for the same Fr_0 and different l/D spacing, Figure 4-31 shows two different water surface profile shapes. When $l/D = 2$, the two rows appeared to act as one uniform structure, resulting in only one downstream dip. When the streamwise distance increased, there were two dips in water surface behind each row, with the larger dip behind the first row. The first row of baffle posts was the first flow barrier; the flow energy reaching these baffles was larger than the flow passing through the second row of baffles. Therefore, one would expect the dip in the water surface to be larger after the first row. Several other studies have found similar results when analyzing flow past paired cylinders (Li & Shen, 1973 and Bokaian & Geoola, 1984) or the drag coefficient in a forested floodplain (Luo, Gan, & Chew, 1996).

While the middle flow depth (0.15m) depicted the clearest trend in l/D spacing values, that trend was not evident at other flow depths (i.e., 0.08m and 0.20m). Therefore, it must be concluded that there was no clear trend for l/D spacing, implying that the existence and placement of the second row has minimal impacts on ΔE through the structure.

4.5.5. Influence of Baffle Post Diameter, D

Figure 4-8 presents the idealized trends for C'_L and C'_D , when the baffle post diameter, expressed as the dimensionless term y_0/D , is varied. In general, D had very little impact on C'_L , especially at lower Fr_0 values. Beyond the Fr_0 threshold, larger D (smaller y_0/D) values resulted in slightly higher C'_L values. The post diameter expressed as relative depth, y_0/D , appeared to have negligible impacts on C'_D over

the range of experimental Fr_0 values. The experimental results comparing y_0/D , with the same s/D and l/D spacing are presented in Figure 4-34 through Figure 4-37. For all three y_0 values, the larger D value produced a slightly larger C'_L value after $Fr_0 \approx 0.3$, despite the similar B_{eff} and p values.

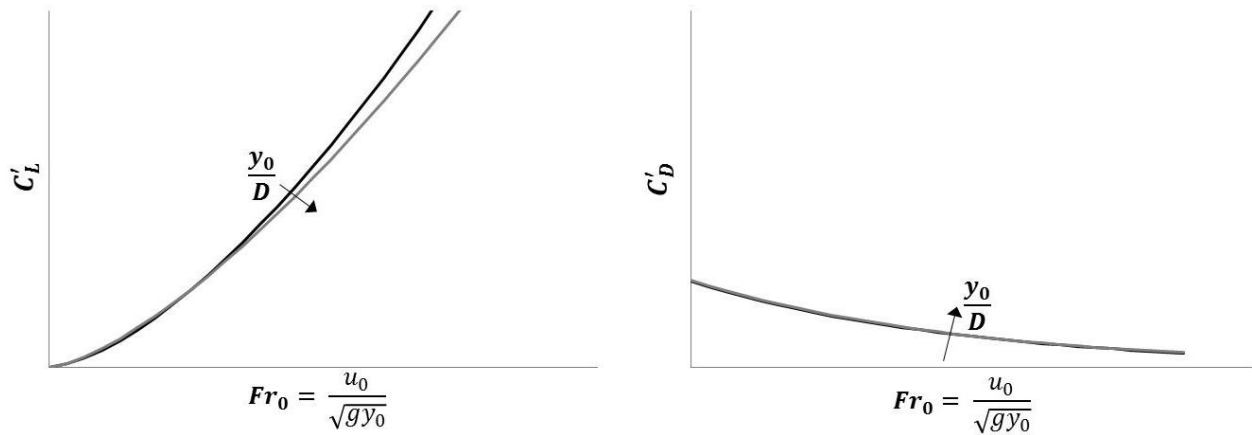


Figure 4-8: General trends for C'_L and C'_D over a range of Fr_0 , varying D , expressed as y_0/D

The larger values of D (smaller values of y_0/D) likely resulted in higher ΔE as a result of the size of the downstream flow vortex, are though this aspect could be a topic for further investigation. To explain this argument, imagine a water droplet flowing directly towards the center of the baffle post. The droplet must flow around the post, resulting in flow vortices and additional turbulence. The larger the baffle post, the longer the flow path around the post, which results in a larger downstream flow vortex.

4.5.6. Influence of Relative Depth, y_0/D

The hydraulic performance of the structure can be customized to a particular situation given the appropriate geometric design; however, the flow depth entering the structure cannot consistently be controlled in a natural river system. To determine the impact on hydraulic performance of y_0/D , the 16-2-2 configuration was plotted for all three y_0 values, shown in Figure 4-38. Figure 4-39 plots the relative depth for the 16-3- ∞ configuration. This plot includes a range of $y_0/D = 2.0$, used in the single-row baffle-post structure, to $y_0/D = 12.4$, which was the highest value tested in the double-row

baffle-post structure experiments. The 16-3-∞ configuration was selected as it was included in both the single-row and double-row baffle-post structure experiments and analysis.

Based on the results, it can be concluded that y_0/D has minimal impacts on C'_L beyond a certain threshold. Figure 4-39 shows that C'_L values were relatively uniform until $y_0/D = 3.0$, where C'_L increased for $Fr_0 = 0.15$. Below the $y_0/D < 3.0$ threshold, the downflow and horseshoe vortices collided with the bottom of the channel, resulting in additional turbulence that increased ΔE through the structure. When $y_0/D > 3.0$, the horseshoe vortex did not interact with the channel bottom, resulting in similar ΔE values, given the same upstream specific energy head. For higher Fr_0 values, that threshold appeared to increase to $y_0/D > 5.0$. Although only two configurations are presented, the overall trends were consistent for all configurations.

4.5.7. Depth Increase Parameter, y_1/y_0

The trends shown in Figure 4-40 illustrate how s/D spacing and Fr_0 influence the values of the depth increase parameter, y_1/y_0 . The structures used to obtain the data for this figure entailed posts set at $l/D = 2$. The value of y_0 for an approach free-flow can be calculated, using a resistance to flow equation together with the value of Fr_0 for the approach flow. The flow depth, y_1 , at the baffle-post structure can be estimated using Figure 4-40. From y_1 , the upstream dimensions of the backwater flow profile (M_1 flow profile) can be calculated. In due course this backwater profile can be interpreted for its effect on the capacity of the approach flow to convey bed sediment. As both coefficients for non-uniform flow are cumbersome and impractical, the y_1/y_0 term becomes increasingly useful, creating a practical approach to analyzing the water effects of this structure.

4.5.8. Choked Flow Conditions

The double-row structure configurations were also analyzed to determine if the structure restricted the channel width enough to induce choked flow conditions. Using the methods described in previous

sections, B_c was calculated for four flow conditions and compared to B_{eff} . As discussed previously in this study, y_0/D values appeared to have little impact on the hydraulic performance of the structure beyond $y_0/D = 3.0$; therefore, only choked flow conditions for the smallest relative depth ($y_0/D = 5.0$) are discussed in this section. Calculations begin at $Fr_0 = 0.33$, as choking did not occur at lower Fr_0 values. The results are presented in Table 4-9.

As Fr_0 increased, the magnitude of B_c increased. Therefore, the upstream specific energy became sufficient to push the higher discharges through a smaller channel width. Figure 4-41 presents the experimental results for all four Fr_0 values.

As the width contracted and the flow approached choked conditions, the available specific energy upstream of the structure must increase to push the same discharge through the structure, shown in Figure 4-41. At the lowest Froude number, $Fr_0 = 0.33$, only the tightest s/D spacing induced choked flow conditions. As Fr_0 increased, two and then all three configurations contracted the width enough to induce choked flow conditions. Furthermore, as the initial discharge and Fr_0 value increased, the amount of energy needed to propel the flow through the structure also increased linearly. For example, in Figure 4-41 (d), both E_1 and y_1 increased when conditions changed from free flow to gradually varied flow as a result of the installation of a structure with $s/D = 5$ spacing. With the next structure, $s/D = 3$, both terms increased again, with E increasing at a faster rate than y . Finally, the last increase occurred with the tightest spacing structure, $s/D = 2$. The gain in E and y between free flow and gradually varied flow conditions with the largest width contraction, $s/D = 2$ at $Fr_0 = 0.53$ is approximately twice as large as the increase when $Fr_0 = 0.33$, because twice as much energy is needed to push the higher discharge through the structure. Notice that the data points form a linear relationship on the E-y (specific energy diagram) plane.

4.6. Bed Sediment Transport to and at a Baffle-Post Structure

The analysis pertaining to bed sediment transport and local scour was a qualitative analysis, largely focusing on experimental photos. A structure with two rows, $D = 16\text{mm}$ and $s/D = l/D = 2$ spacing was selected for this experiment, as it has the tightest lateral spacing, with the highest flow resistance.

4.6.1. Free Flow Conditions

Figure 4-42 shows experimental photographs taken throughout the 300-minute long test. Ripples quickly began forming at the upstream end of the flume, migrating downstream with time. By $t = 90$ minutes, ripples were observed along the entire length of the sandbed. As time progressed, the ripples transitioned from being two-dimensional, varying with depth and streamwise length, to three-dimensional, as seen at $t = 180$ minutes. By the end of the testing period, the amplitude and wavelength of the ripples was relatively consistent throughout the flume length with average values of 2.6 cm and 19.3 cm, respectively. The measured values are presented in Appendix A.

4.6.2. Retarded Flow Conditions with no Armoring

The second experiment included the structure installed in the sand bed 6.4 m from the flume inlet. No armoring was placed at the base of the structure to assess its susceptibility to local scour. Photographs from this experiment are presented in Figure 4-43. Due to the mix of downflows and secondary flows at the structure, a horseshoe vortex formed at the base of each post, displacing bed material. These flow vortices are very similar to those seen at a bridge pier. Several studies have documented scour at bridge piers including Julien, 2002, Melville & Coleman, 2000, and Novaket al., 1996. Halfway through the test, at $t = 180$ minutes, the flow had eroded through the entire depth of the sand bed.

Again, ripples formed at the upstream edge of the flume, slowly working their way down the flume. Due to the bed material displaced at the foot of the structure, large 3D ripples immediately began to form

downstream of the scour hole, quickly moving downstream. As compared to the free flow conditions, ripples did not form along the entire length of the flume until $t = 180$ minutes.

4.6.3. Retarded Flow Conditions with Armoring

During the final experiment, gravel armoring was installed at the base of the structure to determine the effect armoring would have on the hydraulic performance, local scour, and sediment transport. As shown in Figure 4-44, the armoring proved to be effective at mitigating local scour. The gravel also appeared to have increased ΔE through the structure, as the change in flow depth upstream and just downstream of the structure is much more pronounced than the change in flow depths seen in Figure 4-43.

Large ripples quickly formed immediately downstream of the structure, which indicated high sediment transport rates. Ripples formed throughout the length of the sand bed much sooner at $t = 37$ minutes. The ripples downstream of the structure appeared to have higher amplitudes and lower frequencies than those seen immediately upstream of the structure. Overall, the sand depth upstream of the structure maintained a higher depth than downstream of the structure, indicating aggradation.

4.7. Environmental Impacts

Before an in-stream structure can be installed, its impact on the local environment must be assessed. The structure must be designed to best maintain and mimic natural and stable hydraulic, geomorphic, hydrologic, and ecological functions of the stream. This functionality can be accomplished by accommodating natural watercourse functions such as:

- 1) Modifying the mobility of sediment and woody debris;
- 2) Preventing increased scour and erosion on the stream bed or banks;
- 3) Maintaining low flow depth;

- 4) Limiting the alteration of the bed gradient; and,
- 5) Adjusting the channel and corresponding floodplain so as to be based on 'natural' roughness coefficients, etc.

Factors briefly discussed in this report include fish passage and the structures' impact on local aquatic habitat.

4.7.1. Fish Passage

A structure can become a fish passage barrier with excessive drops, flow velocity, and insufficient depth (Hotchkiss & Frei, 2007). None of the baffle-post structure configurations discussed in this report block the entire stream width; therefore, it is not considered to be a drop barrier. However, the concentration of flow could result in velocities exceeding fishes' biological swimming ability. When considering in-stream structures, there are three classifications of fish swimming capabilities:

- 1) Cruising speeds which can be maintained for hours.
- 2) Sustained speeds which can be maintained for minutes.
- 3) Darting speeds, which are a single effort, and can only be maintained for seconds.

It has been observed after implementing sustained or darting speeds, it can take up to two hours for fish to recover and resume normal movement (Bell, 1986). Therefore, the velocity increase parameter, u_2/u_0 , through the structure is instrumental in determining if the structure will become a velocity barrier. The u_2/u_0 term was calculated for all double-row structures. The velocity through the structure was calculated as

$$u_2 = \frac{Q}{(y_2)(b_{eff})} \quad (4-4)$$

Only the results for the 0.08 m depth are presented below in Figure 4-45 and Figure 4-46, as Section 4.5.6 proved that y_0/D had negligible impacts on the flow hydraulics after $y_0/D = 3.0$. Further increasing the flow depth would only additionally decrease the velocity at the same flow rate.

As shown in the relevant figures, Fr_0 has the largest impact on u_1/u_0 . The velocity is expected to increase up to a factor of about 2.2 for $Fr_0 = 0.11$ and the tightest s/D spacing. As an estimate, most streams flow at approximately $Fr_0 \approx 0.2$. Therefore, one can expect the velocity to increase by approximately 2-fold given tight s/D spacing. As Fr_0 increased, u_0 increased, making the relative difference smaller.

The s/D spacing appears to also have second significant impact on u_2/u_0 . As expected, tighter s/D spacing leads to smaller B_{eff} values, which leads to higher increases in u_1 as the flow navigates around the baffles. Streamwise spacing, l/D , appears to have the minimal impact on u_1/u_0 , which is expected as all four structures have the same effective width. Finally, D also appeared to have little to no effect on u_2/u_0 .

4.7.2. Aquatic Habitat

While no definitive information is available on the impacts of this structure on aquatic habitat, some generalizations can be made. Hydraulic complexity or habitat diversity is essential for a healthy aquatic ecosystem (Maddock, 1999). These structures can add hydraulic complexity to the system by increasing the flow depth and decreasing the average velocity upstream of the structures, creating a pool-like environments. Pools are a crucial physical component for the life stages of many aquatic organisms, providing lower velocities and rearing habitat (Abbe & Montgomery, 1996). Downstream of the structure, the experimental results show that the flow is likely to accelerate, decreasing the flow depth and increasing the average velocity, thus creating a riffle-like environment.

4.8. Tables and Figures

Table 4-1: Hydraulic experiment results for single-row baffle-post structures for $Fr_0 = 0.15$ at three different y_0/D values, varying l/D spacing.

y_0/D	s/D	n	p	y_0 [m]	Re_0	Fr_0	C'_L	C'_D	y_1/y_0
2.0	1.5	8	63%	0.033	2,787	0.15	20.76	0.22	1.47
	2	7	55%	0.033	2,787	0.15	17.94	0.24	1.34
	3	5	39%	0.033	2,787	0.15	11.52	0.29	1.17
	4	4	31%	0.032	2,787	0.16	10.48	0.31	1.14
	5	3	23%	0.032	2,787	0.16	8.60	0.34	1.11
	6	2	16%	0.033	2,787	0.15	3.90	0.51	1.05
2.8	1.5	8	63%	0.045	4,599	0.15	9.36	0.33	1.20
	2	7	55%	0.046	4,599	0.15	7.25	0.37	1.14
	3	5	39%	0.046	4,599	0.15	3.26	0.55	1.05
	4	4	31%	0.044	4,599	0.16	3.55	0.53	1.06
	5	3	23%	0.045	4,599	0.15	1.42	0.84	1.02
	6	2	16%	0.044	4,599	0.16	0.77	1.14	1.01
	6.4	1	8%	0.043	4,599	0.16	0.79	1.12	1.01
4.9	1.5	8	63%	0.078	9,755	0.14	1.58	0.80	1.04
	2	7	55%	0.078	10,452	0.15	1.37	0.85	1.04
	3	5	39%	0.078	9,755	0.14	0.48	1.44	1.01
	4	4	31%	0.076	10,452	0.16	0.26	1.98	1.01
	5	3	23%	0.078	9,755	0.14	0.25	2.01	1.01
	6.4	1	8%	0.079	10,452	0.15	0.24	2.04	1.01

Table 4-2: Hydraulic experiment results for single-row baffle-post structures at $Fr_0 = 0.45$. Four different y_0/D were tested, varying the s/D spacing at each depth.

y_0/D	s/D	n	p	y_0 [m]	Re_0	Fr_0	C'_L	C'_D	y_1/y_0
6.4	1.5	8	63%	0.101	45,987	0.46	6.64	0.39	1.44
	2	7	55%	0.101	45,987	0.46	5.30	0.43	1.29
	3	5	39%	0.101	45,987	0.46	3.64	0.52	1.16
	4	4	31%	0.102	45,987	0.45	2.50	0.63	1.10
	5	3	23%	0.101	45,987	0.46	1.47	0.82	1.05
	6	2	16%	0.102	45,987	0.45	1.19	0.92	1.04
	6.4	1	8%	0.102	45,987	0.45	0.94	1.03	1.03
4.9	1.5	8	63%	0.077	31,355	0.47	8.65	0.34	1.44
	2	7	55%	0.078	31,355	0.46	6.99	0.38	1.30
	3	5	39%	0.078	31,355	0.46	4.93	0.45	1.17
	4	4	31%	0.078	31,355	0.46	3.46	0.54	1.11
	5	3	23%	0.078	31,355	0.46	2.59	0.62	1.08
	6	2	16%	0.078	31,355	0.46	1.39	0.85	1.04
	6.4	1	8%	0.077	31,355	0.47	0.49	1.42	1.01
3.1	1.5	8	63%	0.050	15,329	0.44	11.68	0.29	1.33
	2	7	55%	0.049	15,329	0.46	9.17	0.33	1.22
	3	5	39%	0.049	15,329	0.46	6.48	0.39	1.13
	4	4	31%	0.049	15,329	0.46	3.40	0.54	1.06
	5	3	23%	0.049	15,329	0.46	1.80	0.75	1.03
	6	2	16%	0.049	15,329	0.46	3.89	0.51	1.07
	6.4	1	8%	0.048	15,329	0.47	1.28	0.89	1.02
2.1	1.5	8	63%	0.033	8,361	0.46	22.81	0.21	1.57
	2	7	55%	0.034	8,361	0.45	19.47	0.23	1.41
	3	5	39%	0.034	8,361	0.46	15.99	0.25	1.28
	4	4	31%	0.033	8,361	0.45	10.46	0.31	1.15
	5	3	23%	0.033	8,361	0.45	6.96	0.38	1.09
	6	2	16%	0.033	8,361	0.45	4.90	0.45	1.06
	6.4	1	8%	0.033	8,361	0.45	1.34	0.86	1.02

Table 4-3: Hydraulic experimental results for single-row baffle-post structures, varying Fr_0 , y_0 , and s/D spacing.

Structure Geometry			$y_0 = 0.08 \text{ m}$					$y_0/D = 5.0$					$y_0 = 0.15 \text{ m}$					$y_0/D = 9.5$					$y_0 = 0.20 \text{ m}$					$y_0/D = 12.4$				
s/D	n	p	Re_0	Fr_0	C'_L	C'_D	y_1/y_0	Re_0	Fr_0	C'_L	C'_D	y_1/y_0	Re_0	Fr_0	C'_L	C'_D	y_1/y_0	Re_0	Fr_0	C'_L	C'_D	y_1/y_0	Re_0	Fr_0	C'_L	C'_D	y_1/y_0					
2	7	55%	12,124	0.17	2.44	0.64	1.08	27,174	0.15	0.57	1.33	1.03	24,387	0.09	0.15	2.59	1.01															
2	7	55%	12,124	0.17	2.13	0.69	1.06	49,750	0.27	0.82	1.10	1.05	57,135	0.20	0.32	1.78	1.02															
2	7	55%	16,026	0.23	2.85	0.59	1.09	65,497	0.36	0.91	1.05	1.05	87,793	0.32	0.41	1.57	1.03															
2	7	55%	17,837	0.25	3.23	0.56	1.11	85,006	0.47	1.17	0.92	1.07	124,026	0.44	0.53	1.38	1.04															
2	7	55%	21,879	0.31	3.72	0.52	1.13	105,909	0.58	1.27	0.89	1.07	160,258	0.56	0.66	1.23	1.05															
2	7	55%	26,895	0.37	3.92	0.51	1.14																									
2	7	55%	32,052	0.45	4.28	0.48	1.15																									
2	7	55%	37,626	0.53	4.79	0.46	1.18																									
2	7	55%	44,593	0.62	5.32	0.43	1.20																									
3	5	39%	12,124	0.18	1.37	0.85	1.04	27,174	0.15	0.32	1.76	1.02	23,969	0.09	0.15	2.57	1.01															
3	5	39%	16,026	0.23	1.54	0.80	1.04	49,750	0.27	0.66	1.23	1.04	57,135	0.20	0.18	2.37	1.01															
3	5	39%	21,879	0.31	2.44	0.64	1.08	65,497	0.36	0.51	1.41	1.03	87,793	0.32	0.26	1.95	1.02															
3	5	39%	27,174	0.38	2.61	0.62	1.08	85,006	0.47	0.74	1.16	1.04	124,026	0.45	0.33	1.75	1.02															
3	5	39%	32,052	0.45	2.78	0.60	1.09	105,909	0.58	0.85	1.09	1.05	160,258	0.56	0.35	1.70	1.02															
3	5	39%	37,626	0.52	3.04	0.57	1.10																									
3	5	39%	44,593	0.62	2.91	0.59	1.09																									
3	5	39%	45,290	0.64	3.50	0.53	1.11																									
5	3	23%	12,124	0.17	0.87	1.07	1.02	27,174	0.15	0.26	1.96	1.01	23,969	0.09	0.11	2.96	1.01															
5	3	23%	12,124	0.18	0.48	1.44	1.01	49,471	0.26	0.25	2.01	1.01	57,135	0.20	0.14	2.64	1.01															
5	3	23%	16,026	0.24	1.39	0.85	1.04	65,497	0.36	0.32	1.76	1.02	87,793	0.32	0.19	2.29	1.01															
5	3	23%	17,837	0.25	1.29	0.88	1.04	85,006	0.47	0.45	1.49	1.02	124,026	0.45	0.22	2.13	1.02															
5	3	23%	21,879	0.31	1.51	0.81	1.04	105,909	0.58	0.50	1.41	1.03	160,258	0.56	0.25	2.02	1.02															
5	3	23%	27,871	0.38	1.44	0.83	1.04																									
5	3	23%	32,052	0.45	1.31	0.87	1.04																									
5	3	23%	37,626	0.52	1.64	0.78	1.05																									

Table 4-4: B_c values for single-row baffle-post structure experiments

Parameter	$Fr_0 = 0.15$	$Fr_0 = 0.45$
Q_0 [m^3/s]	0.0009	0.0093
E_0 [m]	0.045	0.111
y_c [m]	0.030	0.074
q_c [m^2/s]	0.016	0.064
B_c [m]	0.057	0.147

Table 4-5: Hydraulic experiment results for double-row baffle-post structures at three different y_0/D values, varying post s/D spacing with $D = 16$ mm over a range of subcritical Fr_0 values. Graphical results are presented in the upper graph of Figure 4-25, Figure 4-28, and Figure 4-29. Experiment photographs for $y_0/D = 5.0$ are presented in Figure 4-26.

	Structure Geometry			$y_0 = 0.08$ m		$y_0/D = 5.0$			$y_0 = 0.15$ m		$y_0/D = 9.5$			$y_0 = 0.20$ m		$y_0/D = 12.4$		
	s/D	n	p	Re_0	Fr_0	C'_L	C'_D	y_1/y_0	Re_0	Fr_0	C'_L	C'_D	y_1/y_0	Re_0	Fr_0	C'_L	C'_D	y_1/y_0
16-2-2	2	13	102%	7,943	0.11	0.90	1.05	1.03	17,419	0.10	0.34	1.70	1.02	27,453	0.10	0.29	1.87	1.02
	2	13	102%	14,354	0.21	2.01	0.71	1.06	32,052	0.18	1.04	0.98	1.06	49,471	0.18	0.96	1.02	1.07
	2	13	102%	22,297	0.33	5.67	0.42	1.21	48,774	0.27	2.35	0.65	1.15	70,374	0.26	1.72	0.76	1.15
	2	13	102%	27,871	0.39	6.81	0.38	1.30	69,677	0.38	3.49	0.54	1.28	88,490	0.32	2.21	0.67	1.21
	2	13	102%	32,330	0.45	7.48	0.37	1.37	89,187	0.50	4.58	0.47	1.46	113,574	0.42	2.97	0.58	1.34
	2	13	102%	36,929	0.53	9.30	0.33	1.54	111,484	0.56	4.61	0.47	1.56					
	2	13	102%	41,110	0.56	9.25	0.33	1.60										
16-3-2	3	9	70%	7,943	0.11	0.69	1.21	1.02	17,419	0.10	0.28	1.88	1.01	27,453	0.10	0.07	3.68	1.00
	3	9	70%	14,354	0.21	1.54	0.80	1.04	32,052	0.18	0.90	1.05	1.05	49,471	0.18	0.61	1.28	1.04
	3	9	70%	22,297	0.33	3.62	0.53	1.12	48,774	0.27	1.65	0.78	1.10	70,374	0.26	0.96	1.02	1.07
	3	9	70%	27,871	0.39	5.27	0.44	1.20	69,677	0.38	2.54	0.63	1.17	88,490	0.32	1.56	0.80	1.13
	3	9	70%	32,330	0.42	5.16	0.44	1.21	89,187	0.53	4.01	0.50	1.32	113,574	0.42	2.22	0.67	1.21
	3	9	70%	32,330	0.45	6.40	0.40	1.27	111,484	0.70	5.49	0.43	1.59					
	3	9	70%	36,929	0.54	7.85	0.36	1.37										
16-5-2	5	5	39%	7,943	0.12	0.49	1.42	1.01	17,001	0.10	0.27	1.91	1.01	27,453	0.10	0.08	3.63	1.01
	5	5	39%	14,354	0.21	1.14	0.94	1.03	32,052	0.19	0.41	1.56	1.02	49,471	0.18	0.27	1.94	1.02
	5	5	39%	22,297	0.33	1.60	0.79	1.05	48,774	0.28	0.71	1.18	1.04	70,374	0.26	0.33	1.74	1.02
	5	5	39%	27,871	0.39	2.44	0.64	1.08	69,677	0.39	1.31	0.87	1.07	89,187	0.33	0.77	1.14	1.06
	5	5	39%	32,052	0.44	2.52	0.63	1.08	88,490	0.51	2.62	0.62	1.17	112,877	0.42	1.26	0.89	1.10
	5	5	39%	36,929	0.53	4.14	0.49	1.14										

Table 4-6: Hydraulic experiment results for the double-row baffle-post structures at three different y_0/D values, varying s/D post spacing, maintaining $D = 8$ mm, over a range of subcritical Fr_0 values. Graphical results are presented in the lower graph of Figure 4-25, Figure 4-28, and Figure 4-29. Experiment photographs for $y_0/D = 9.9$ are presented in Figure 4-27.

		Structure Geometry			$y_0 = 0.08$ m		$y_0/D = 9.9$			$y_0 = 0.15$ m		$y_0/D = 18.4$		$y_0 = 0.20$ m		$y_0/D = 24.6$			
		s/D	n	p	Re_0	Fr_0	C'_L	C'_D	y_1/y_0	Re_0	Fr_0	C'_L	C'_D	y_1/y_0	Re_0	Fr_0	C'_L	C'_D	y_1/y_0
8-4-4	4	13	51%	7,943	0.12	0.49	1.42	1.01	17,001	0.10	0.14	2.68	1.01	27,174	0.10	0.15	2.59	1.01	
	4	13	51%	14,354	0.21	0.94	1.03	1.03	32,052	0.18	0.40	1.58	1.02	49,471	0.18	0.34	1.72	1.02	
	4	13	51%	22,297	0.34	2.46	0.64	1.07	48,774	0.28	1.00	1.00	1.05	70,374	0.26	0.54	1.37	1.04	
	4	13	51%	32,052	0.44	3.11	0.57	1.10	69,677	0.39	1.79	0.75	1.11	89,187	0.33	1.07	0.97	1.08	
	4	13	51%	36,929	0.53	3.60	0.53	1.12	88,490	0.53	2.50	0.63	1.16	112,180	0.42	1.59	0.79	1.13	
	4	13	51%	37,626	0.53	4.51	0.47	1.16											
8-6-4	6	9	35%	6,968	0.11	0.51	1.40	1.01	17,001	0.10	0.07	3.77	1.00	27,174	0.10	0.43	1.53	1.03	
	6	9	35%	14,354	0.21	1.17	0.92	1.03	32,052	0.18	0.34	1.71	1.02	49,471	0.18	0.19	2.28	1.01	
	6	9	35%	22,297	0.34	1.20	0.91	1.03	48,774	0.28	0.46	1.47	1.02	70,374	0.26	0.30	1.84	1.02	
	6	9	35%	27,871	0.39	1.31	0.87	1.04	69,677	0.39	1.20	0.91	1.07	89,187	0.33	0.64	1.25	1.05	
	6	9	35%	27,871	0.40	2.13	0.69	1.06	88,490	0.50	1.81	0.74	1.11	112,180	0.42	1.10	0.95	1.08	
	6	9	35%	32,052	0.44	2.18	0.68	1.07											
	6	9	35%	36,929	0.53	2.70	0.61	1.08											
8-10-4	10	5	20%	6,968	0.11	0.51	1.40	1.01	17,001	0.10	0.07	3.77	1.00	27,174	0.10	0.08	3.64	1.01	
	10	5	20%	14,354	0.21	0.72	1.18	1.02	32,052	0.18	0.14	2.68	1.01	48,774	0.18	0.08	3.62	1.01	
	10	5	20%	22,297	0.35	1.01	0.99	1.03	48,774	0.28	0.27	1.91	1.01	70,374	0.26	0.19	2.31	1.01	
	10	5	20%	27,871	0.39	0.46	1.48	1.01	69,677	0.39	0.87	1.07	1.05	89,187	0.33	0.44	1.51	1.03	
	10	5	20%	32,052	0.44	1.26	0.89	1.04	89,187	0.51	2.02	0.70	1.12	112,180	0.44	1.26	0.89	1.10	
	10	5	20%	36,929	0.53	2.85	0.59	1.09											

Table 4-7: Hydraulic experiment results for double-row baffle-post structures at three different y_0/D , varying l/D post spacing over a range of subcritical Fr_0 values. Graphical results are presented in Figure 4-30, Figure 4-32, and Figure 4-33. Experiment photographs for $y_0/D = 5.0$ are presented in Figure 4-31.

		Structure Geometry			$y_0 = 0.08$ m		$y_0/D = 5.0$			$y_0 = 0.15$ m		$y_0/D = 9.5$			$y_0 = 0.20$ m		$y_0/D = 12.4$		
		l/D	n	p	Re_0	Fr_0	C'_L	C'_D	y_1/y_0	Re_0	Fr_0	C'_L	C'_D	y_1/y_0	Re_0	Fr_0	C'_L	C'_D	y_1/y_0
16-3-2	2	9	70%	7,943	0.11	0.69	1.21	1.02	17,419	0.10	0.28	1.88	1.01	27,453	0.10	0.07	3.68	1.00	
	2	9	70%	22,297	0.33	1.54	0.80	1.04	32,052	0.18	0.90	1.05	1.05	49,471	0.18	0.61	1.28	1.04	
	2	9	70%	27,871	0.39	3.62	0.53	1.12	48,774	0.27	1.65	0.78	1.10	70,374	0.26	0.96	1.02	1.07	
	2	9	70%	32,330	0.42	5.27	0.44	1.20	69,677	0.38	2.54	0.63	1.17	88,490	0.32	1.56	0.80	1.13	
	2	9	70%	32,330	0.45	5.16	0.44	1.21	89,187	0.53	4.01	0.50	1.32	113,574	0.42	2.22	0.67	1.21	
	2	9	70%	36,929	0.54	6.40	0.40	1.27											
16-3-3	3	9	70%	7,943	0.12	0.71	1.19	1.02	17,419	0.10	0.28	1.88	1.01	27,453	0.10	0.15	2.60	1.01	
	3	9	70%	14,354	0.21	1.16	0.93	1.03	32,052	0.18	0.72	1.18	1.04	49,471	0.18	0.51	1.40	1.04	
	3	9	70%	22,297	0.33	3.62	0.53	1.12	48,774	0.27	1.41	0.84	1.08	70,374	0.26	0.96	1.02	1.07	
	3	9	70%	27,871	0.39	4.79	0.46	1.18	69,677	0.38	2.47	0.64	1.17	88,490	0.32	1.42	0.84	1.12	
	3	9	70%	32,052	0.44	5.63	0.42	1.23	89,187	0.51	3.48	0.54	1.27	113,574	0.42	2.07	0.70	1.19	
	3	9	70%	41,110	0.52	7.12	0.37	1.32											
	3	9	70%	36,929	0.56	7.41	0.37	1.36											
16-3-4	4	9	70%	8,361	0.13	0.72	1.18	1.02	17,419	0.10	0.21	2.17	1.01	27,174	0.10	0.11	2.98	1.01	
	4	9	70%	14,911	0.21	1.32	0.87	1.04	32,052	0.18	0.66	1.23	1.03	49,471	0.18	0.48	1.45	1.03	
	4	9	70%	22,297	0.32	3.11	0.57	1.10	48,774	0.28	1.43	0.84	1.08	70,374	0.26	0.88	1.07	1.07	
	4	9	70%	32,052	0.45	5.32	0.43	1.20	69,677	0.38	2.24	0.67	1.15	89,187	0.33	1.44	0.83	1.12	
	4	9	70%	36,929	0.52	6.47	0.39	1.28	89,187	0.52	3.50	0.53	1.26	113,574	0.42	2.07	0.70	1.19	
16-3-∞	∞	5	39%	7,665	0.12	0.50	1.41	1.01	17,419	0.10	0.14	2.65	1.01	27,453	0.10	0.11	2.98	1.01	
	∞	5	39%	14,911	0.21	0.69	1.21	1.02	32,052	0.18	0.47	1.45	1.02	49,471	0.18	0.30	1.82	1.02	
	∞	5	39%	22,297	0.32	2.08	0.69	1.06	48,774	0.28	0.89	1.06	1.05	70,374	0.26	0.47	1.46	1.03	
	∞	5	39%	32,052	0.45	4.10	0.49	1.14	69,677	0.39	1.79	0.75	1.11	89,187	0.33	0.89	1.06	1.07	
	∞	5	39%	36,929	0.54	5.90	0.41	1.23	89,187	0.54	3.51	0.53	1.26	113,574	0.42	1.62	0.79	1.13	

Table 4-8: Hydraulic experiment results for the double-row baffle-post structures at three different y_0/D values, varying D over a range of subcritical Fr_0 values, maintaining the same relative s/D and l/D spacing. Graphical results are presented in Figure 4-34, Figure 4-36, and Figure 4-37. Experiment photographs for $y_0/D = 9.9$ are presented in Figure 4-27.

Structure Geometry		$y_0 = 0.08 \text{ m}$						$y_0 = 0.15 \text{ m}$					$y_0 = 0.20 \text{ m}$				
		N	p	Re_0	Fr_0	C'_L	C'_D	y_1/y_0	Re_0	Fr_0	C'_L	C'_D	y_1/y_0	Re_0	Fr_0	C'_L	C'_D
$D = 16 \text{ mm}$	13	102%	7,943	0.11	0.90	1.05	1.03	17,419	0.10	0.34	1.70	1.02	27,453	0.10	0.29	1.87	1.02
	13	102%	14,354	0.21	2.01	0.71	1.06	32,052	0.18	1.04	0.98	1.06	49,471	0.18	0.96	1.02	1.07
	13	102%	22,297	0.33	5.67	0.42	1.21	48,774	0.27	2.35	0.65	1.15	70,374	0.26	1.72	0.76	1.15
	13	102%	27,871	0.39	6.81	0.38	1.30	69,677	0.38	3.49	0.54	1.28	88,490	0.32	2.21	0.67	1.21
	13	102%	32,330	0.45	7.48	0.37	1.37	89,187	0.50	4.58	0.47	1.46	113,574	0.42	2.97	0.58	1.34
	13	102%	36,929	0.53	9.30	0.33	1.54	111,484	0.56	4.61	0.47	1.56					
	13	102%	41,110	0.56	9.25	0.33	1.60										
$D = 8 \text{ mm}$	25	98%	7,246	0.11	0.96	1.02	1.03	17,001	0.10	0.34	1.71	1.02	27,174	0.10	0.11	3.01	1.01
	25	98%	14,354	0.21	1.99	0.71	1.06	32,052	0.18	1.00	1.00	1.05	49,471	0.18	0.87	1.07	1.06
	25	98%	22,297	0.34	5.18	0.44	1.18	48,774	0.28	2.25	0.67	1.14	70,374	0.26	1.52	0.81	1.13
	25	98%	27,871	0.39	4.79	0.46	1.18	69,677	0.39	3.44	0.54	1.27	89,187	0.33	2.07	0.70	1.19
	25	98%	27,871	0.41	6.92	0.38	1.29	88,490	0.51	4.46	0.47	1.41	112,180	0.42	2.85	0.59	1.31
	25	98%	32,052	0.46	6.96	0.38	1.31										
	25	98%	32,052	0.46	7.42	0.37	1.34										
	25	98%	36,929	0.52	8.45	0.34	1.46										
	25	98%	36,929	0.54	8.85	0.34	1.47										

Table 4-9: B_c results for flow conditions for the double-row post structure experiments when $y_0/D = 5.0$

Parameter	$Fr_0 = 0.33$	$Fr_0 = 0.39$	$Fr_0 = 0.44$	$Fr_0 = 0.54$
Q_0 [m^3/s]	0.0045	0.0057	0.0066	0.0075
E_0 [m]	0.0817	0.0862	0.0902	0.0895
y_c [m]	0.0545	0.0575	0.0601	0.0597
q_c [m^2/s]	0.0398	0.0431	0.0461	0.0457
B_c [m]	0.1138	0.1313	0.1419	0.1643

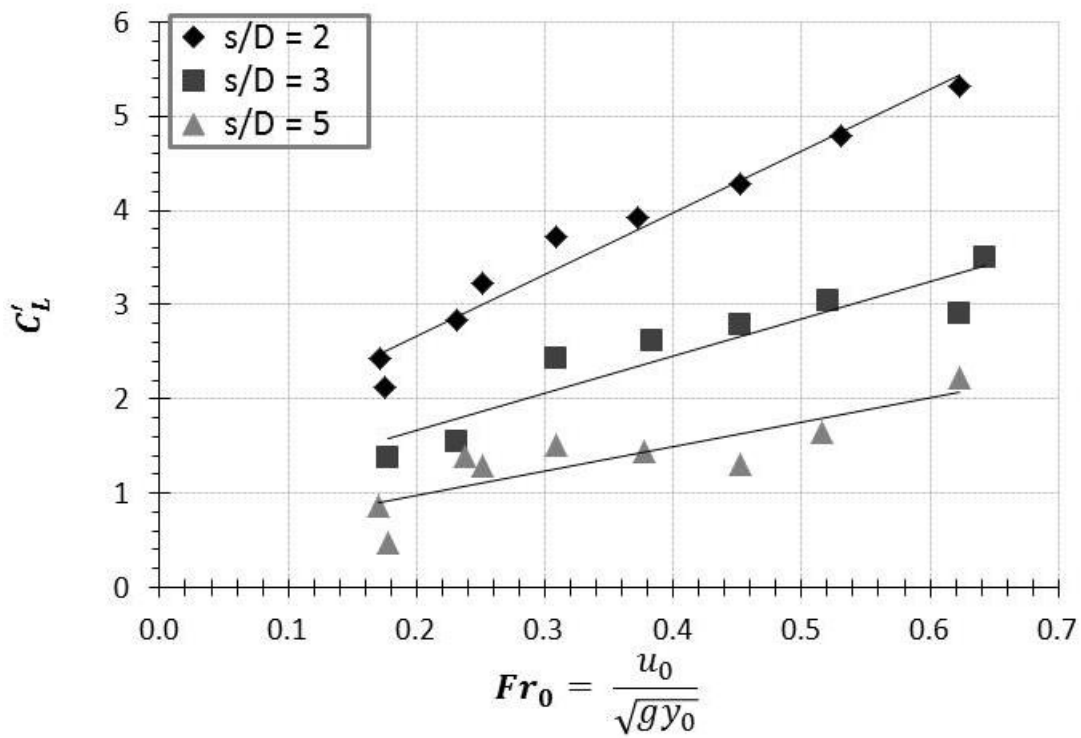


Figure 4-9: C_L' results for single-row baffle-post structures for $y_0 = 0.08$ m, over a range of Fr_0 values.

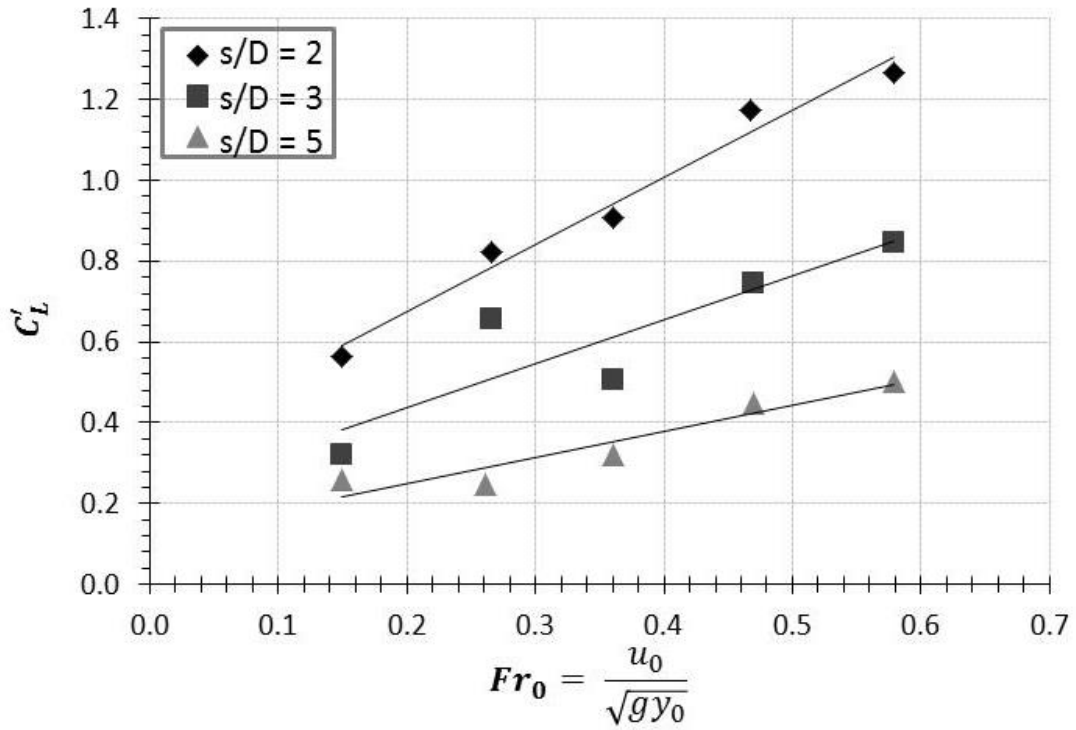


Figure 4-10: C'_L results for single-row baffle-post structures for $y_0 = 0.15$ m, over a range of Fr_0 values.

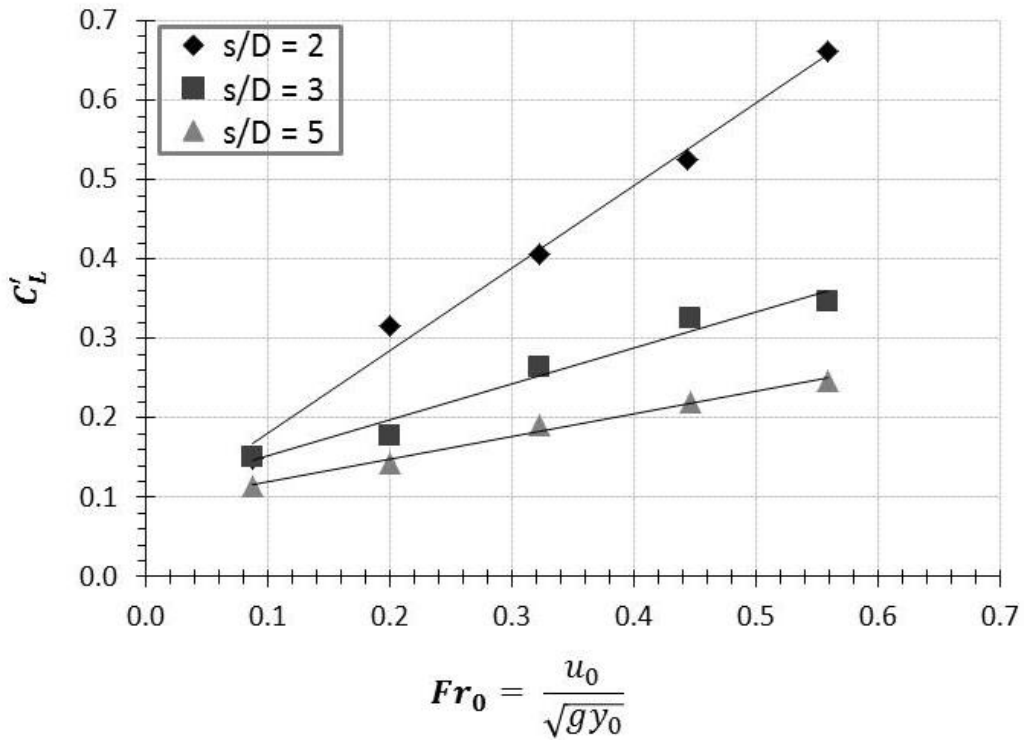


Figure 4-11: C'_L results for single-row baffle-post structures for $y_0 = 0.20$ m, over a range of Fr_0 values.

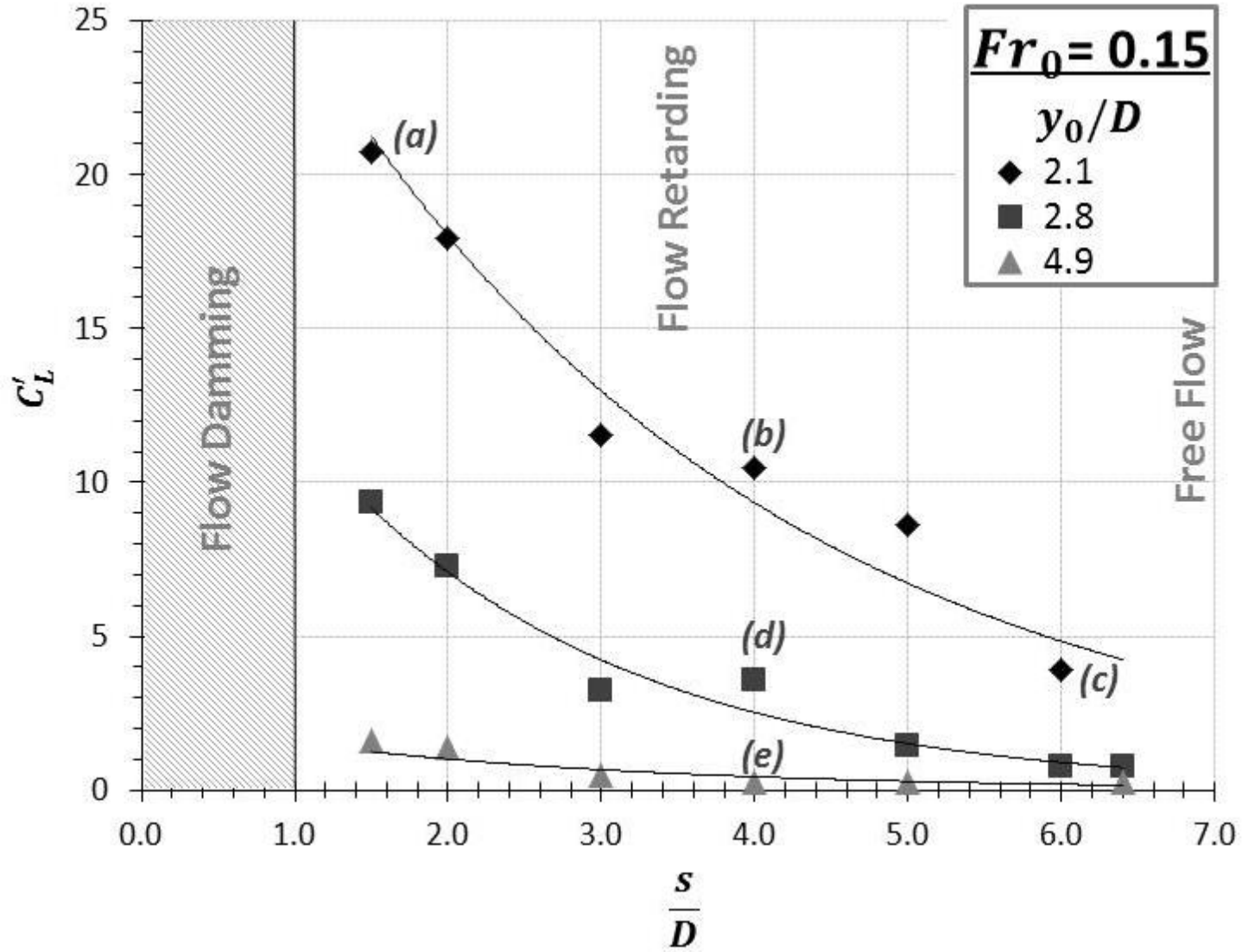


Figure 4-12: C_L results over a range of s/D spacing values for $Fr_0 = 0.15$ and three y_0/D values. Results show that the lowest flow depth ($y_0/D = 2.1$) resulted in the highest C_L values over the range of s/D spacing.

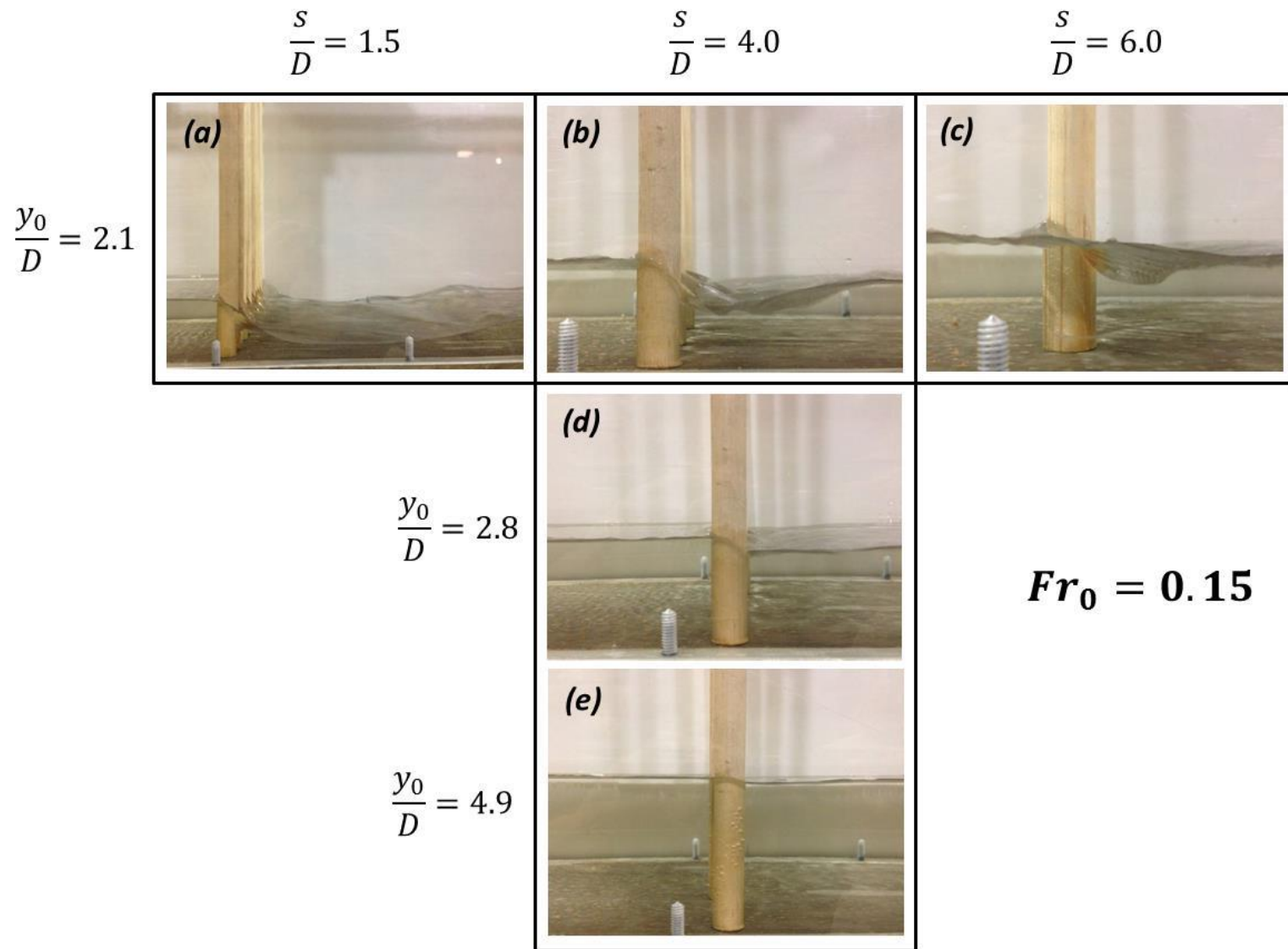


Figure 4-13: Result photographs single-row baffle-post structure performance tests at $Fr_0 = 0.15$, corresponding to the letters in Figure 4-12. As anticipated, the magnitude and extent of the downstream wake decreases with an increasing s/D ratio and y_0/D ratio.

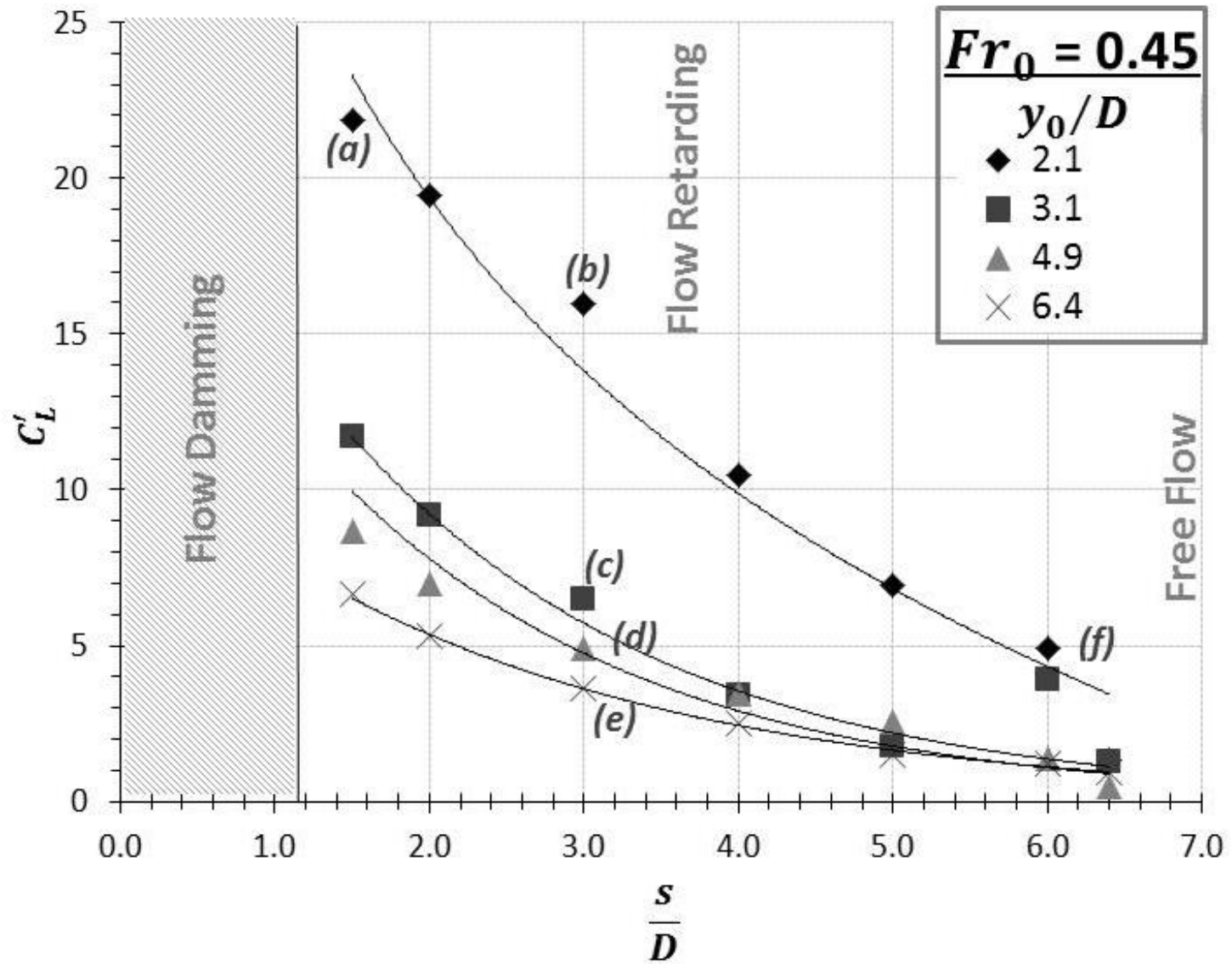


Figure 4-14: C'_L results over a range of s/D spacing values at $Fr_0 = 0.45$ and four y_0/D values.

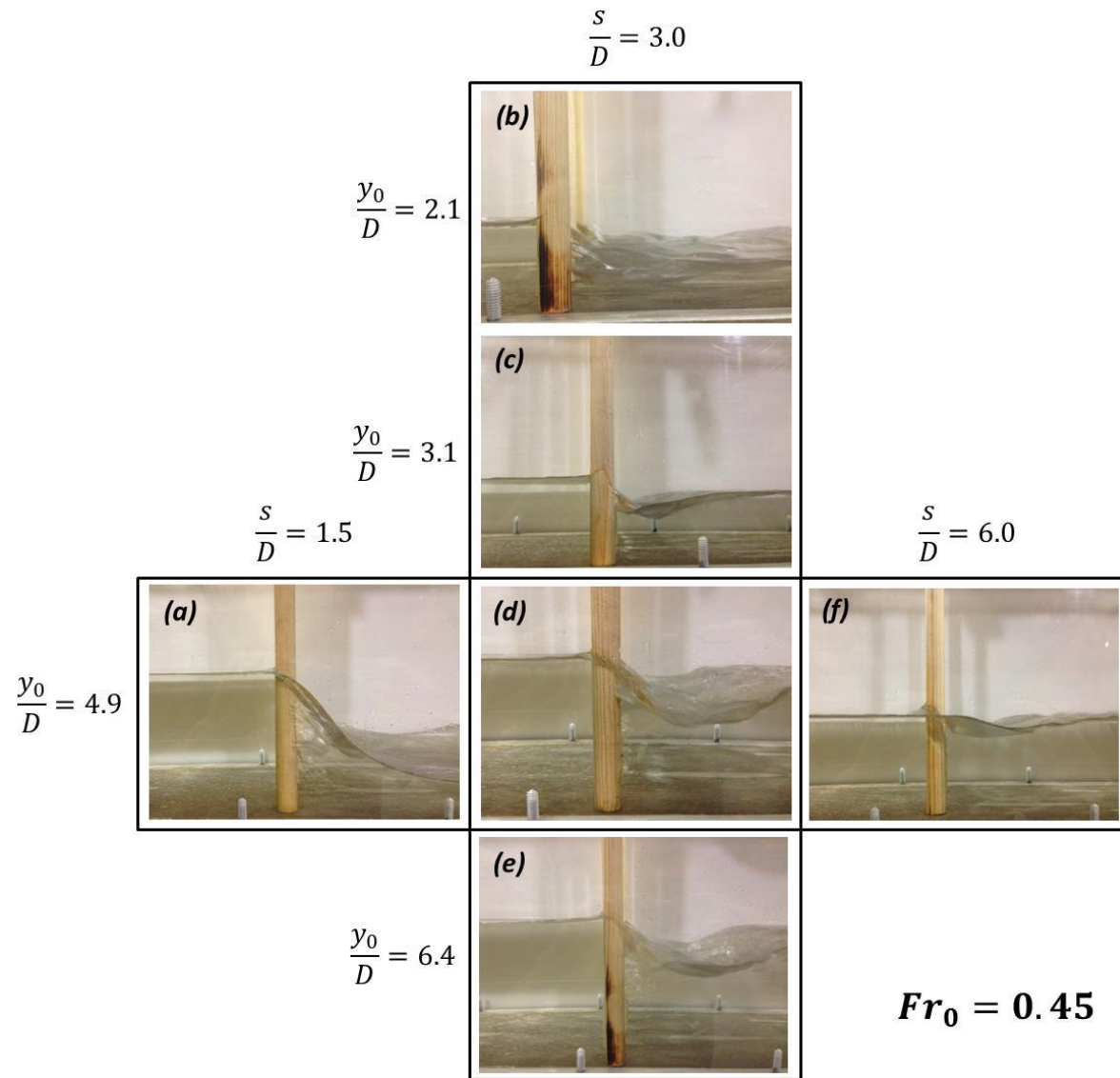


Figure 4-15: Result photographs for single-row baffle-post structure performance experiments at $Fr_0 = 0.45$, corresponding to the letters in Figure 4-13. As anticipated, the magnitude and extent of the downstream wake decreases with an increasing s/D ; however, y_0/D values appear to have little impact on C'_L , particularly in comparison to the $Fr_0 = 0.15$ results.

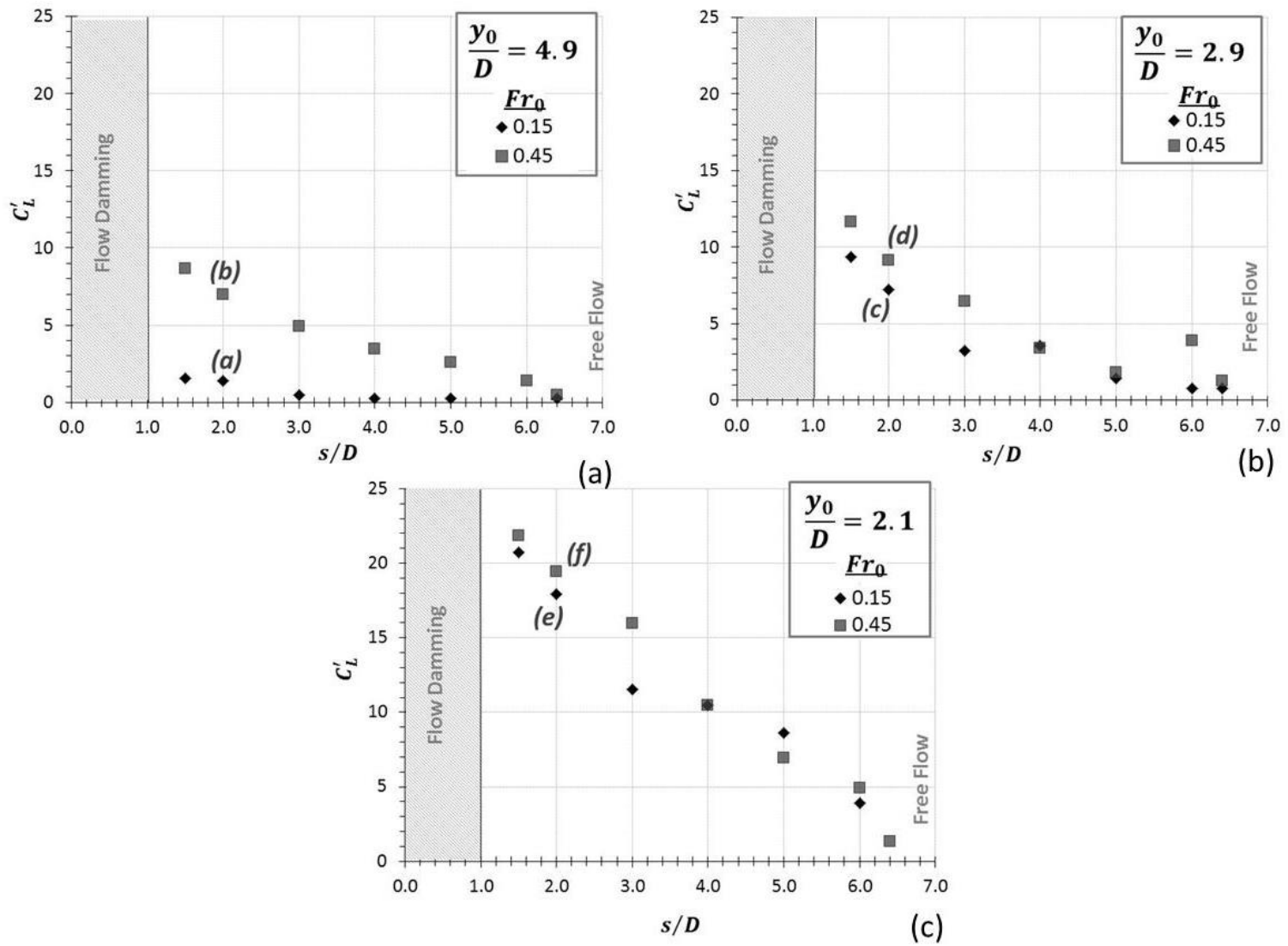


Figure 4-16: C'_L results, comparing Fr_0 for the same y_0/D . Notice that as y_0/D increases, the discrepancy between the two C'_L becomes larger, especially at lower s/D ratios.

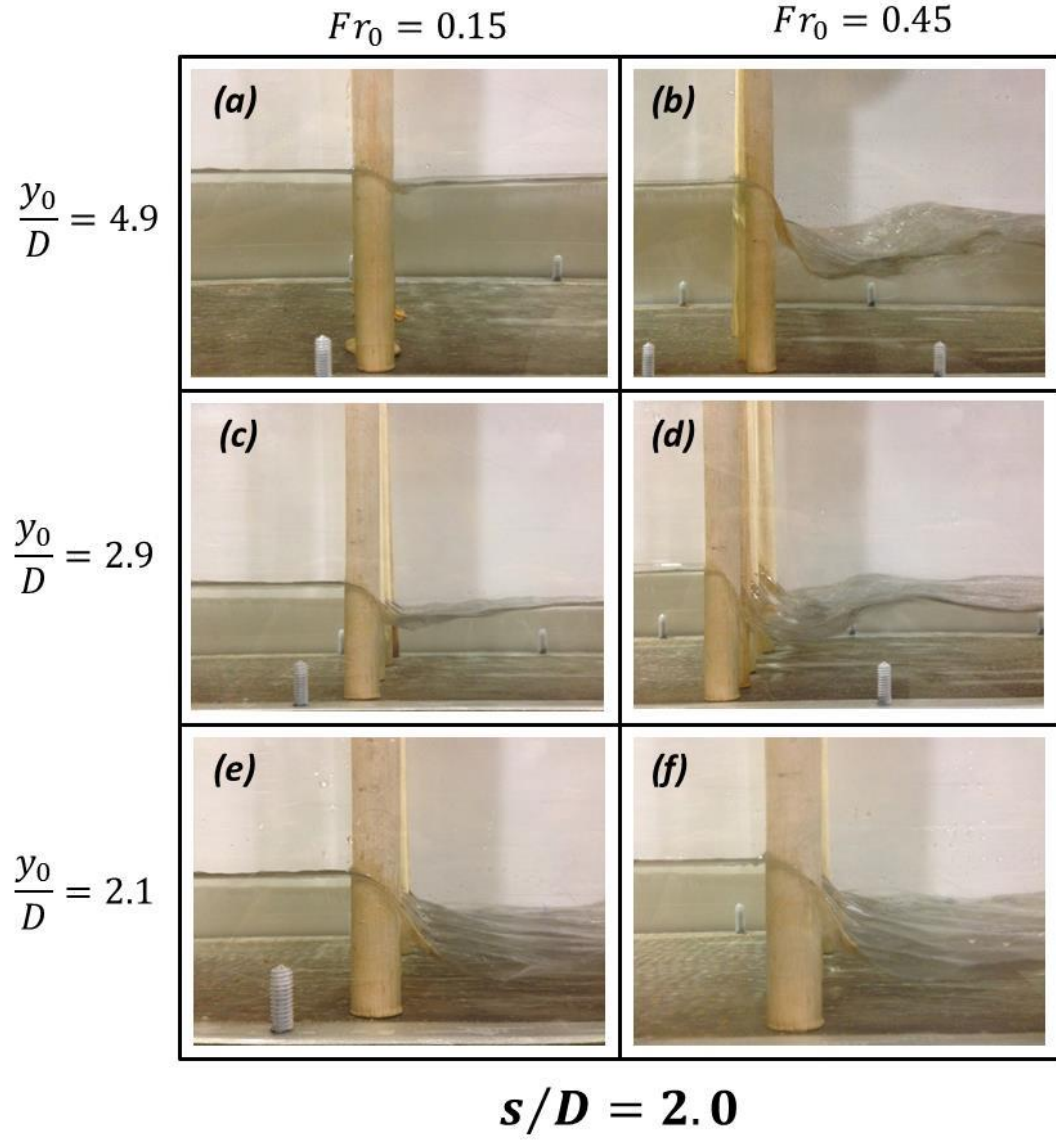


Figure 4-17: Result photographs for single-row baffle-post structures experiments corresponding to the letters in Figure 4-16.

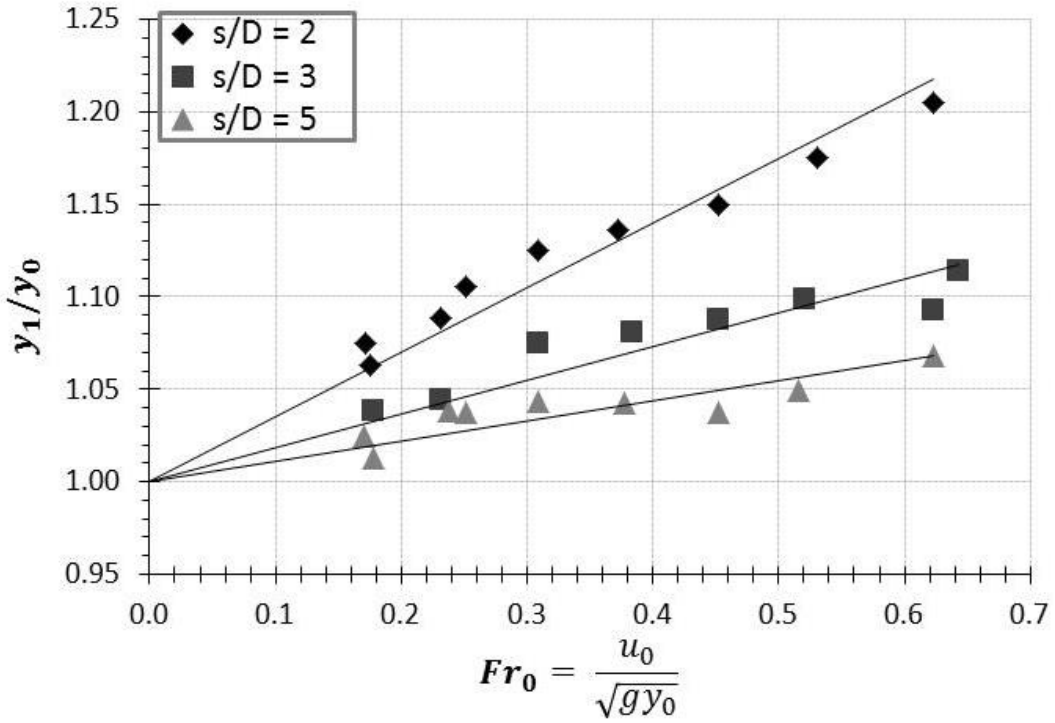


Figure 4-18: Depth increase parameter for a single-row of baffle posts at $y_0 = 0.08$ m, varying Fr_0 and s/D spacing.

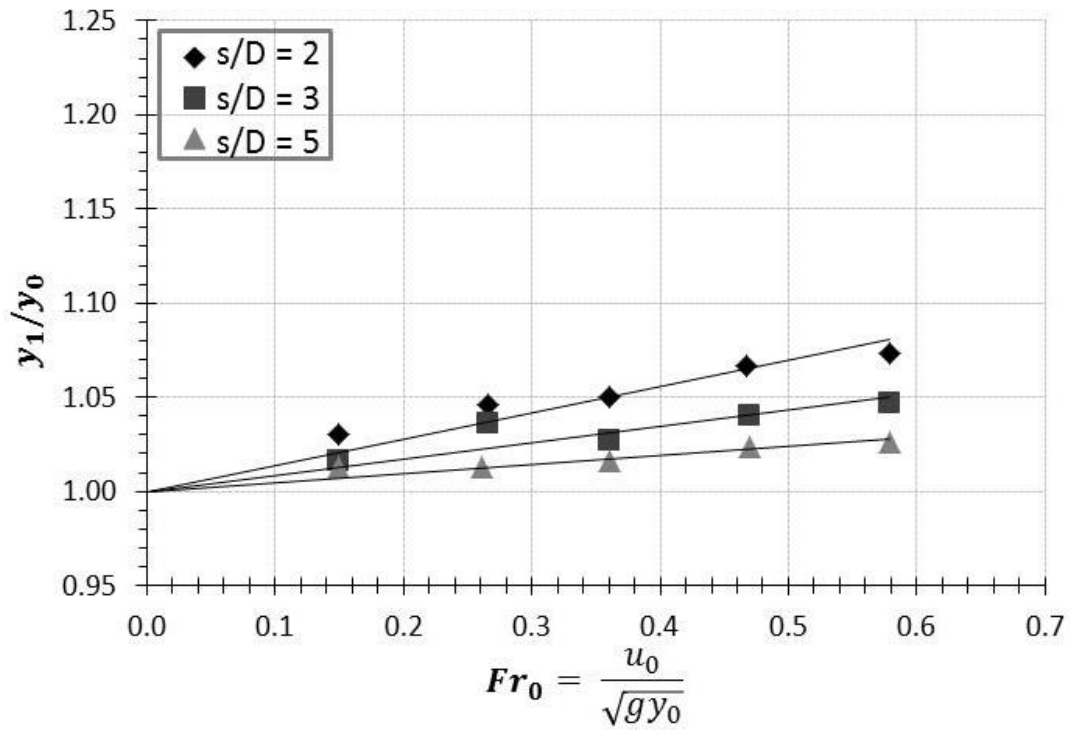


Figure 4-19: Depth increase parameter for a single-row of baffle posts at $y_0 = 0.15$ m, varying Fr_0 and s/D spacing.

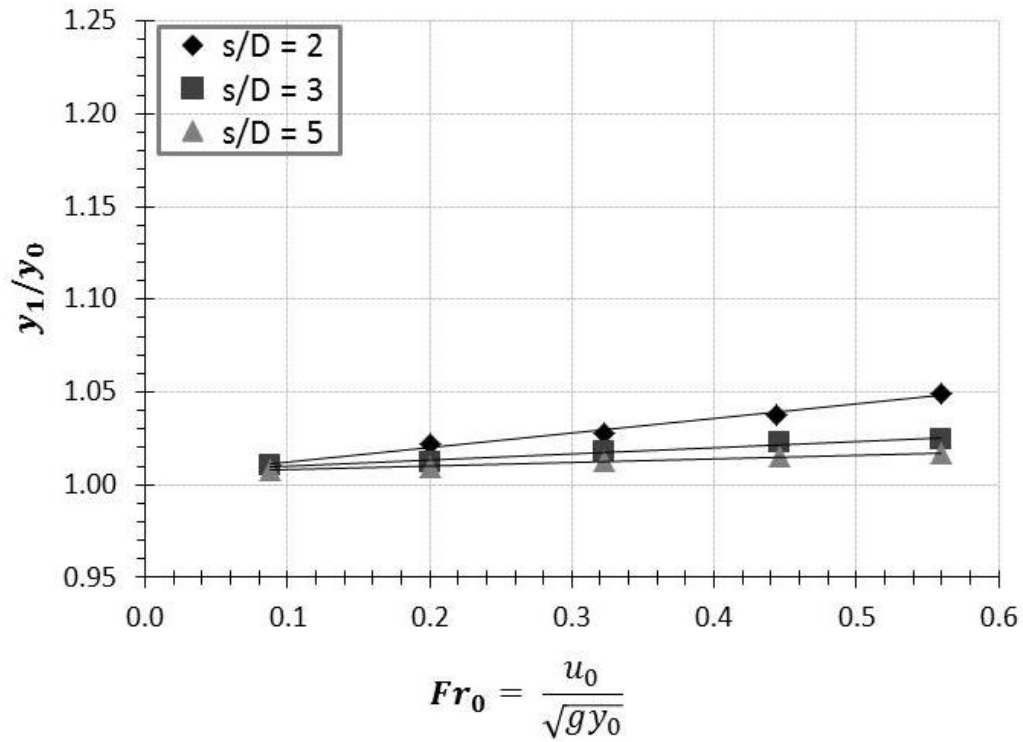


Figure 4-20: Depth increase parameter for a single-row of baffle posts at $y_0 = 0.20$ m, varying Fr_0 and s/D spacing.

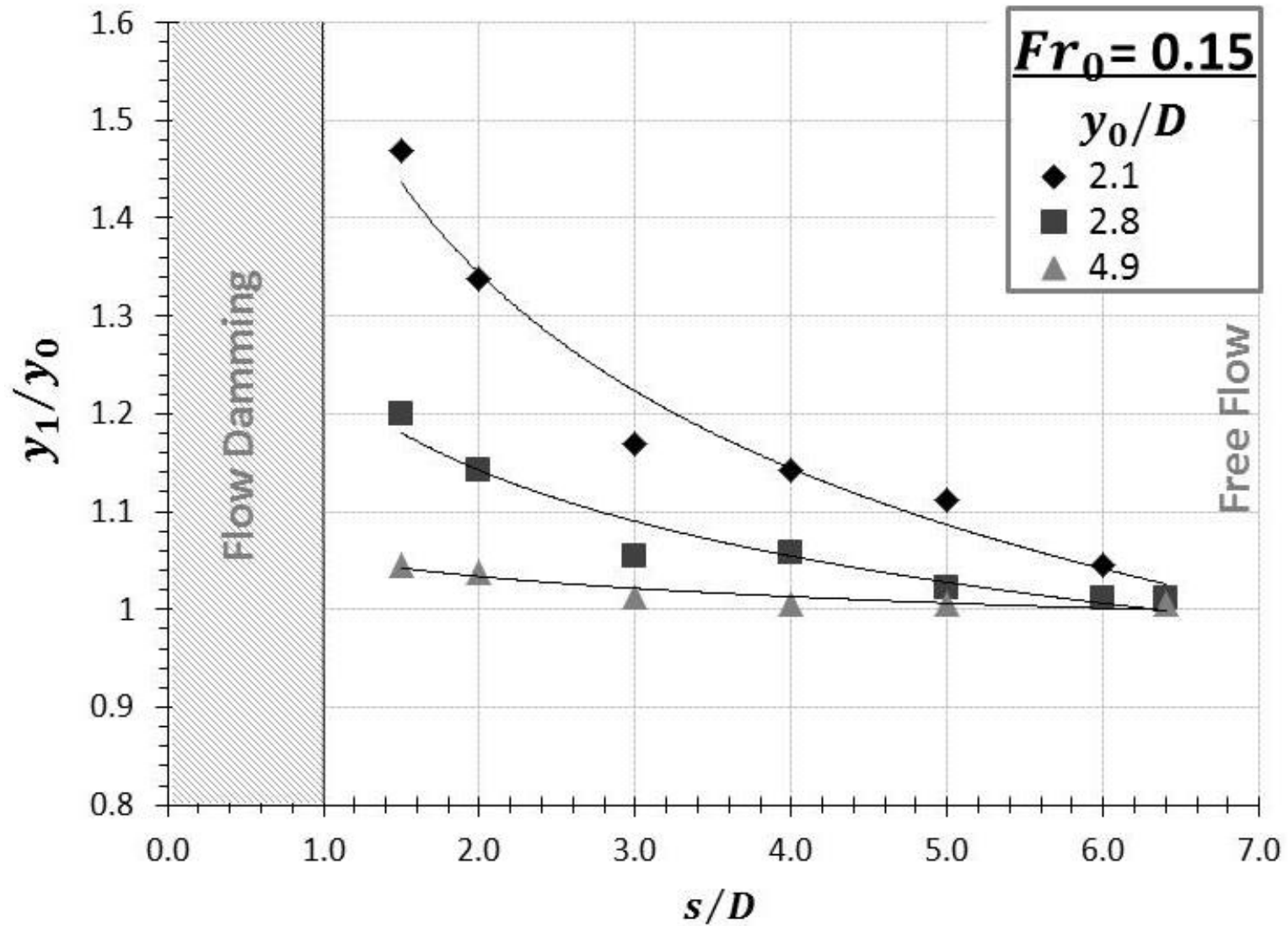


Figure 4-21: Depth increase parameter, y_1/y_0 , for a single-row of baffle posts at $Fr_0 = 0.15$.

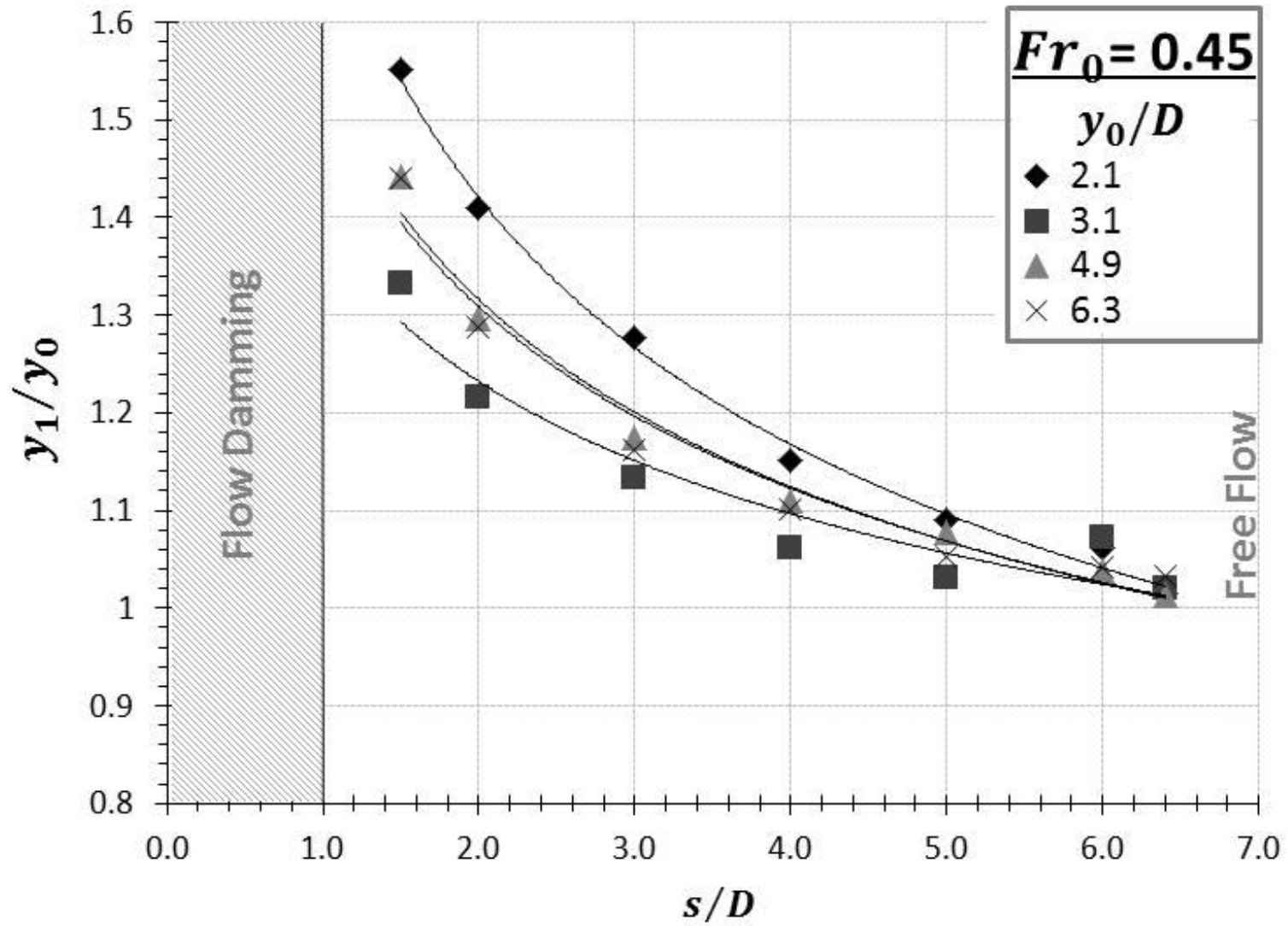


Figure 4-22: Depth increase parameter, y_1/y_0 , for a single-row of baffle posts at $Fr_0 = 0.45$.

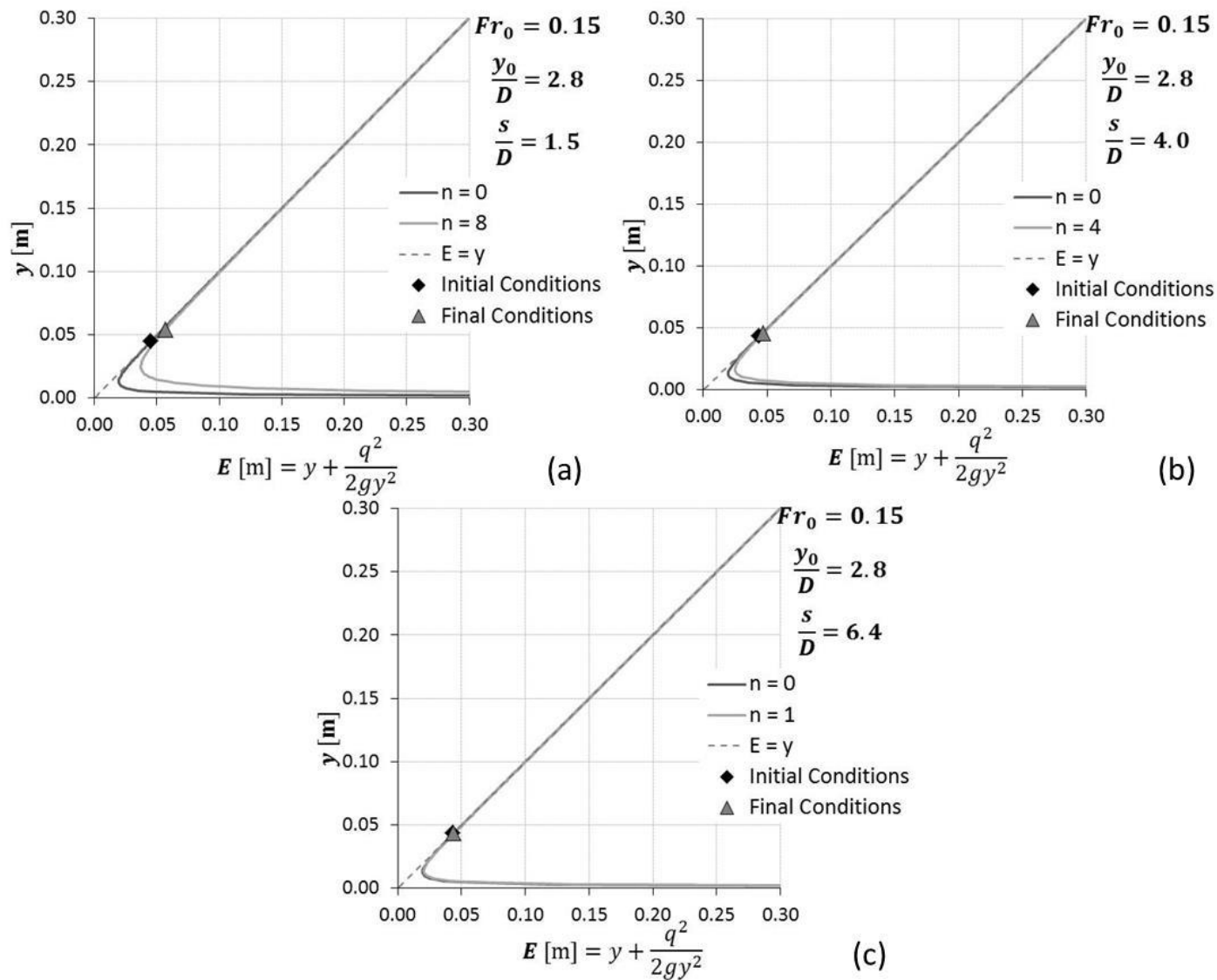


Figure 4-23: Specific energy diagram for baffle-post structure at various spacings.

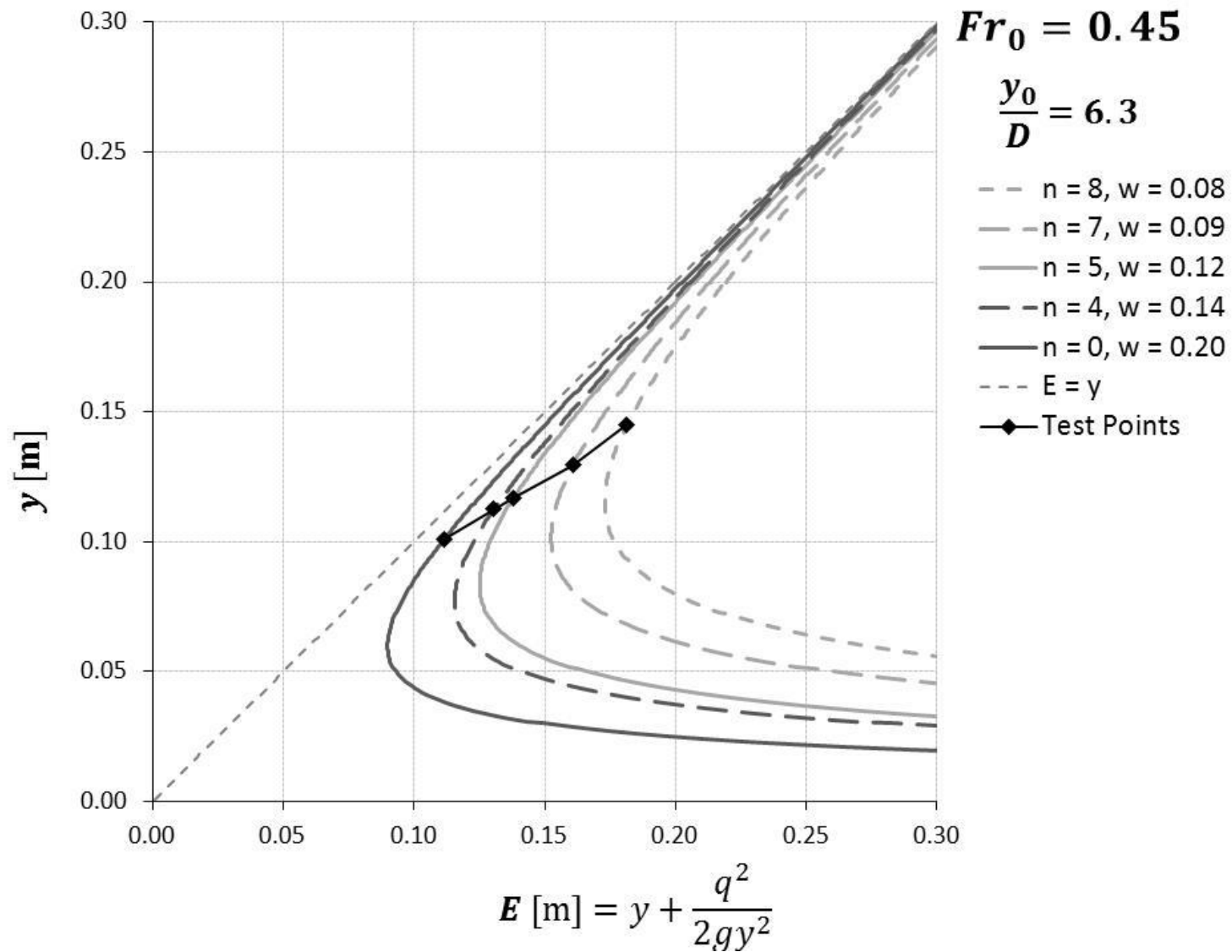


Figure 4-24: Experimental results on the specific energy diagram for free-flow and choked flow conditions at $Fr_0 = 0.45$

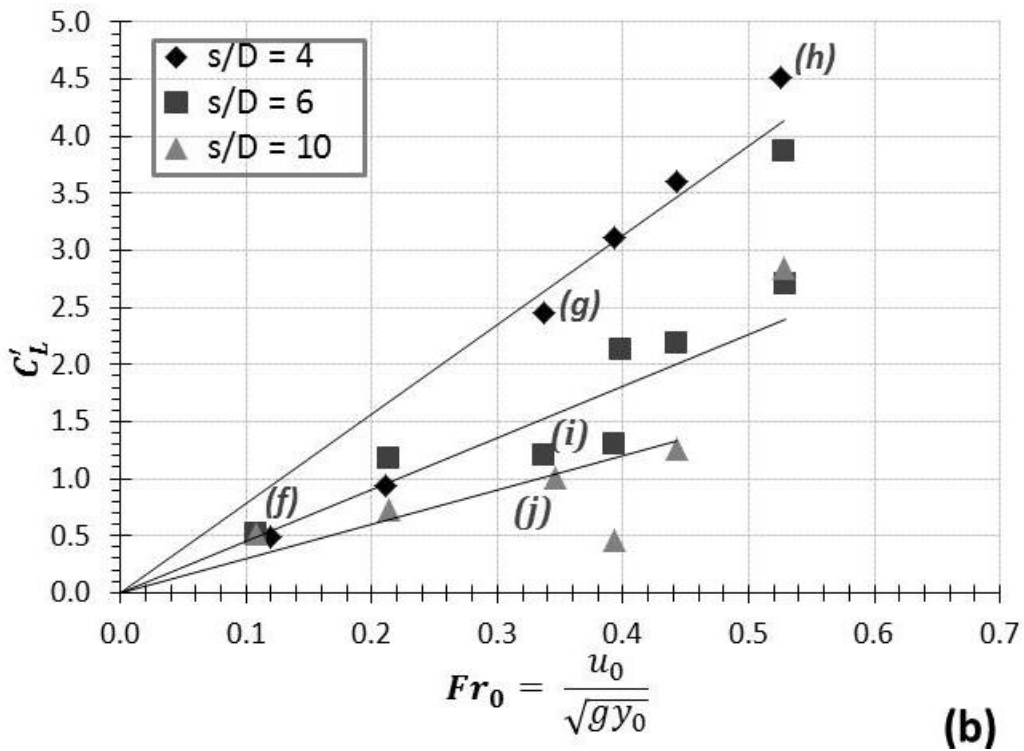
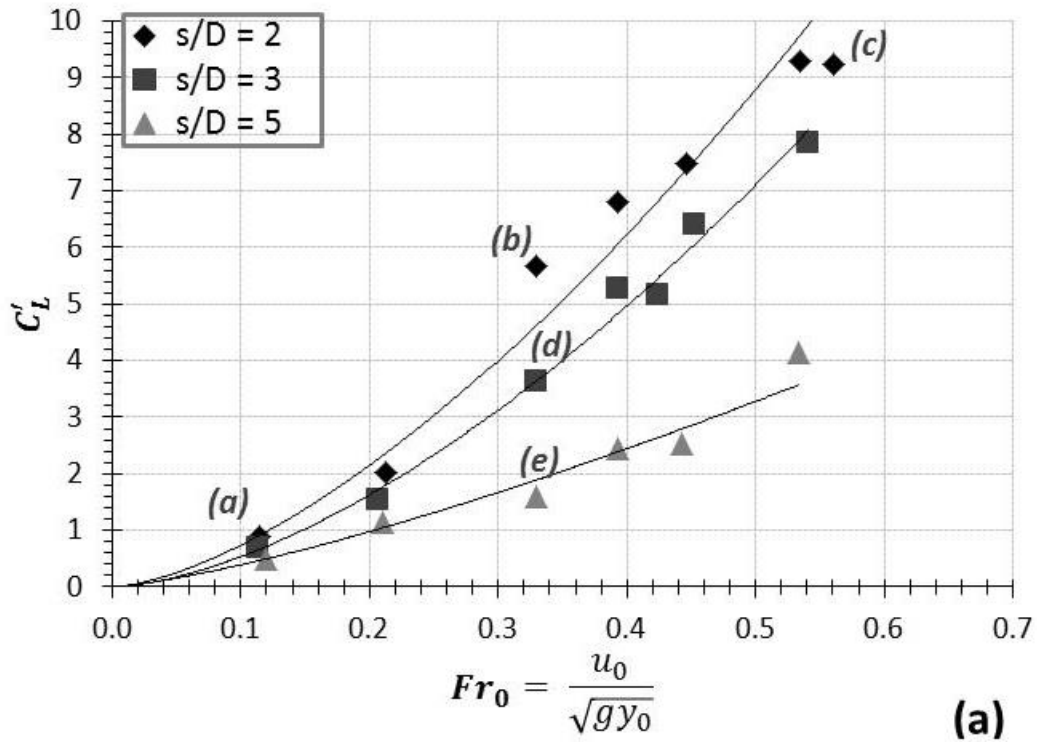


Figure 4-25: C_L' results for a depth of 0.08 m, over a range of Fr_0 values, varying s/D spacing for two D values. The letters in the graphs correspond to experiment photographs presented in Figure 4-26 and Figure 4-27 below.

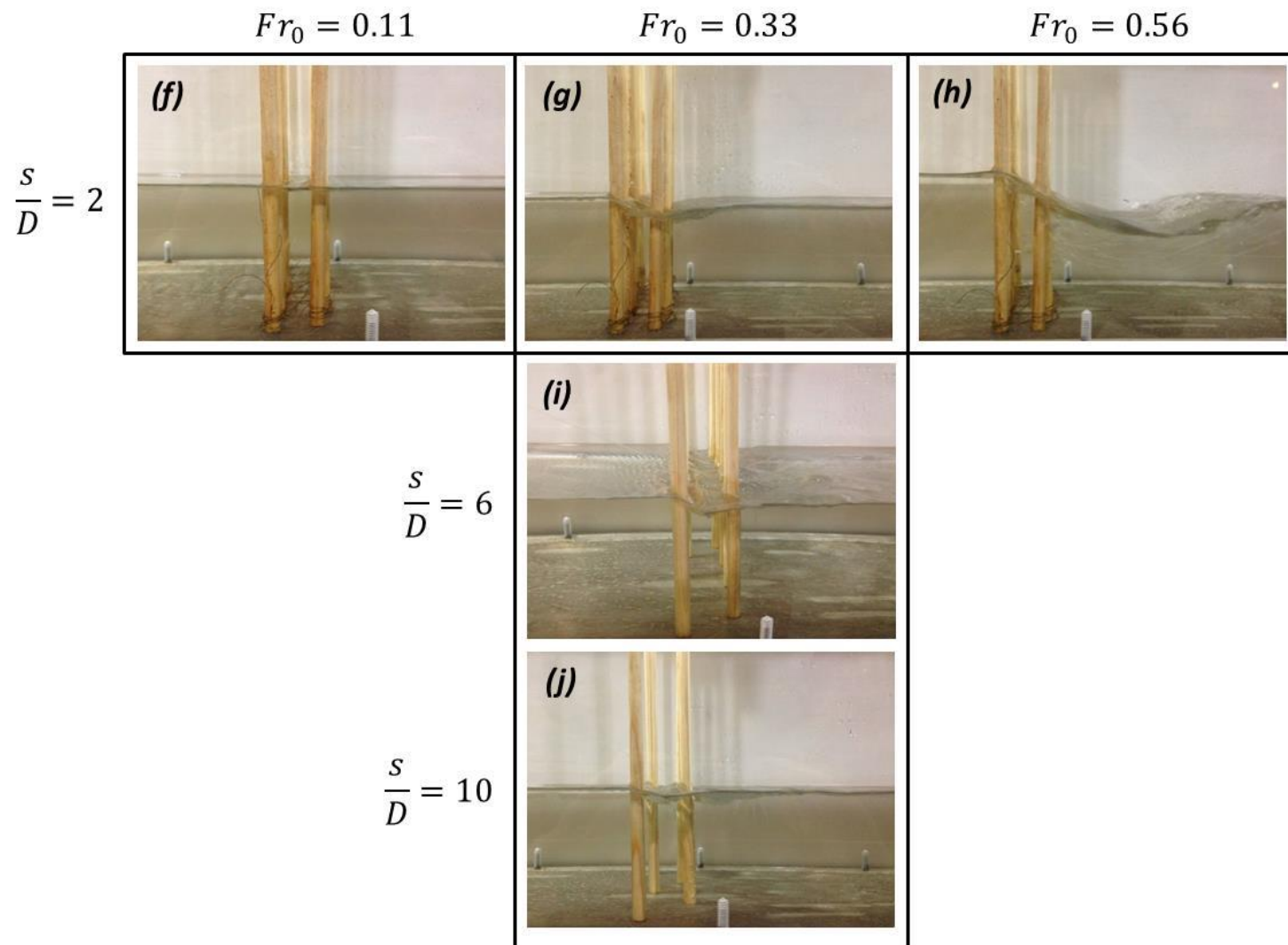


Figure 4-26: Photographs of s/D spacing results for $y_0/D = 5.0$. The letters correspond to the data points given in Figure 4-25. Notice that ΔE through the structure increases with an increasing Fr_0 , even though C'_L decreases with the Fr_0 . On the other hand, ΔE through the structure, and corresponding C'_L , decreases as s/D spacing of the structure increases.

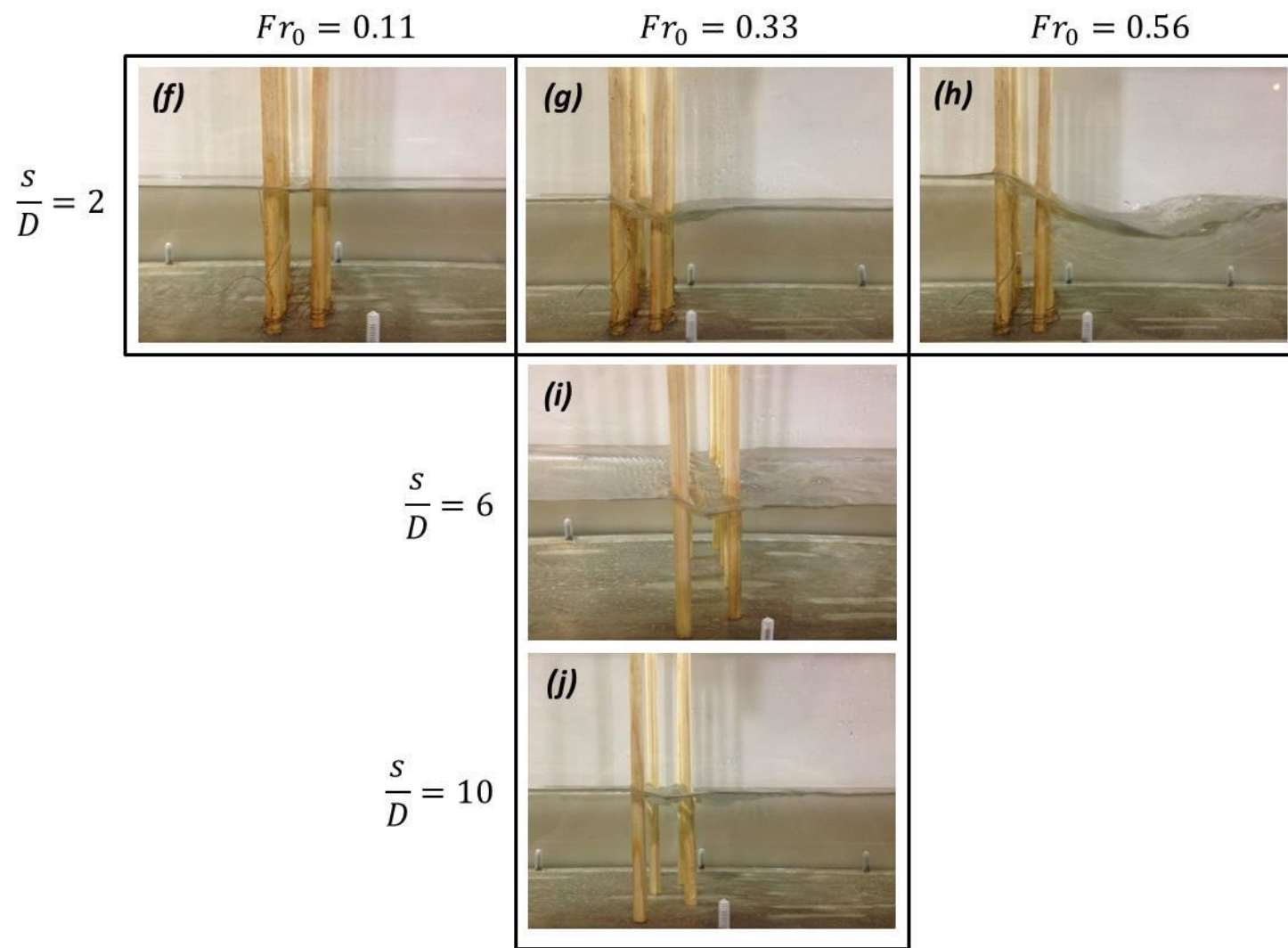


Figure 4-27: Photographs of lateral spacing results for $y_0/D = 9.9$. The letters correspond to the data points given in Figure 4-25. Notice that ΔE through the structure increases with an increasing Fr_0 , even though the C'_L decreases with the Fr_0 . On the other hand, the ΔE through the structure, and corresponding C'_L , decreases as s/D spacing of the structure increases.

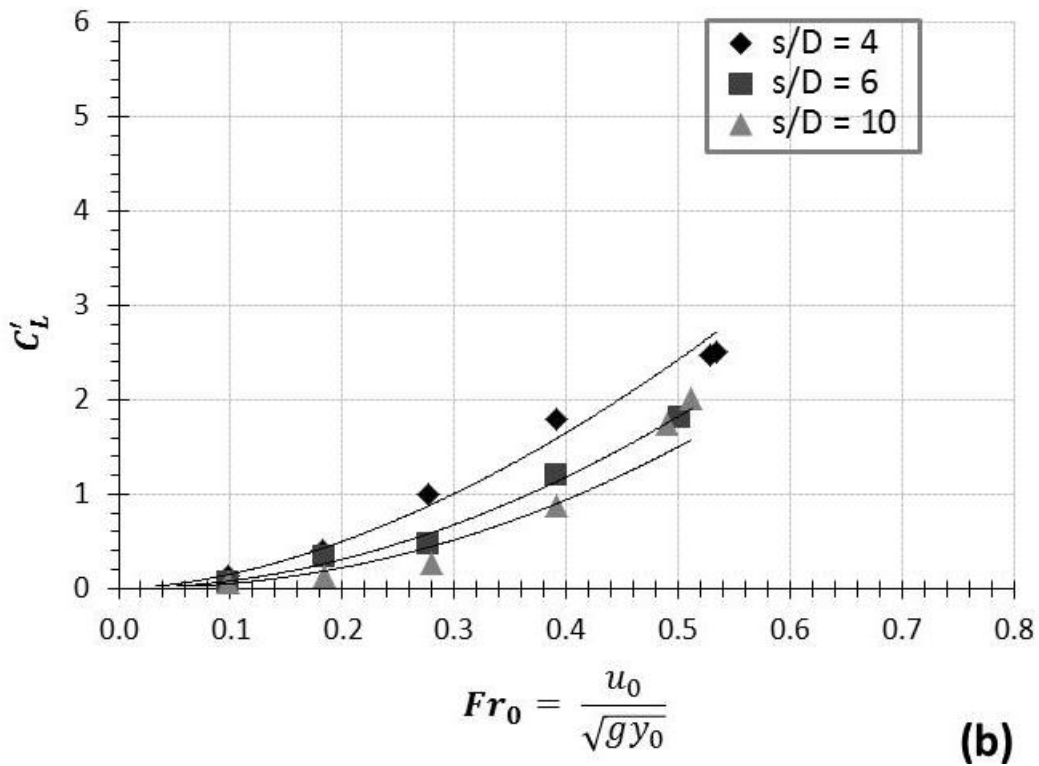
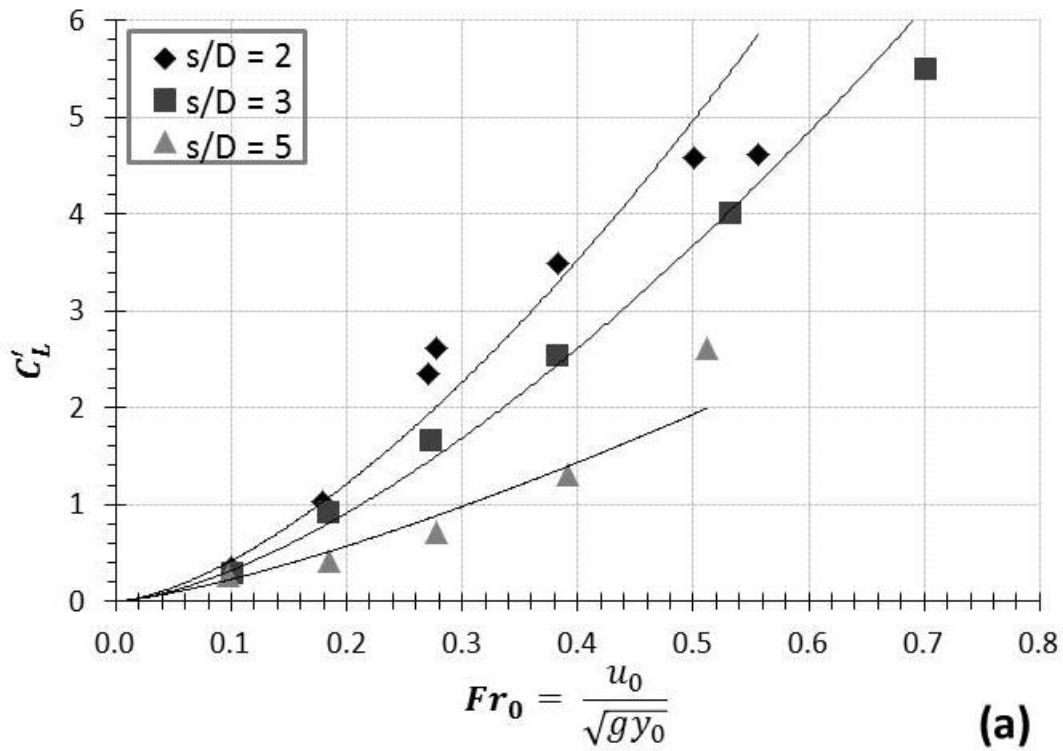


Figure 4-28: C'_L results for $y_0 = 0.15$ m, over a range of Fr_0 , varying s/D spacing for two different D values. (a) $y_0/D = 9.5$; $l/D = 2$ and (b) $y_0/D = 18.4$; $l/D = 4$.

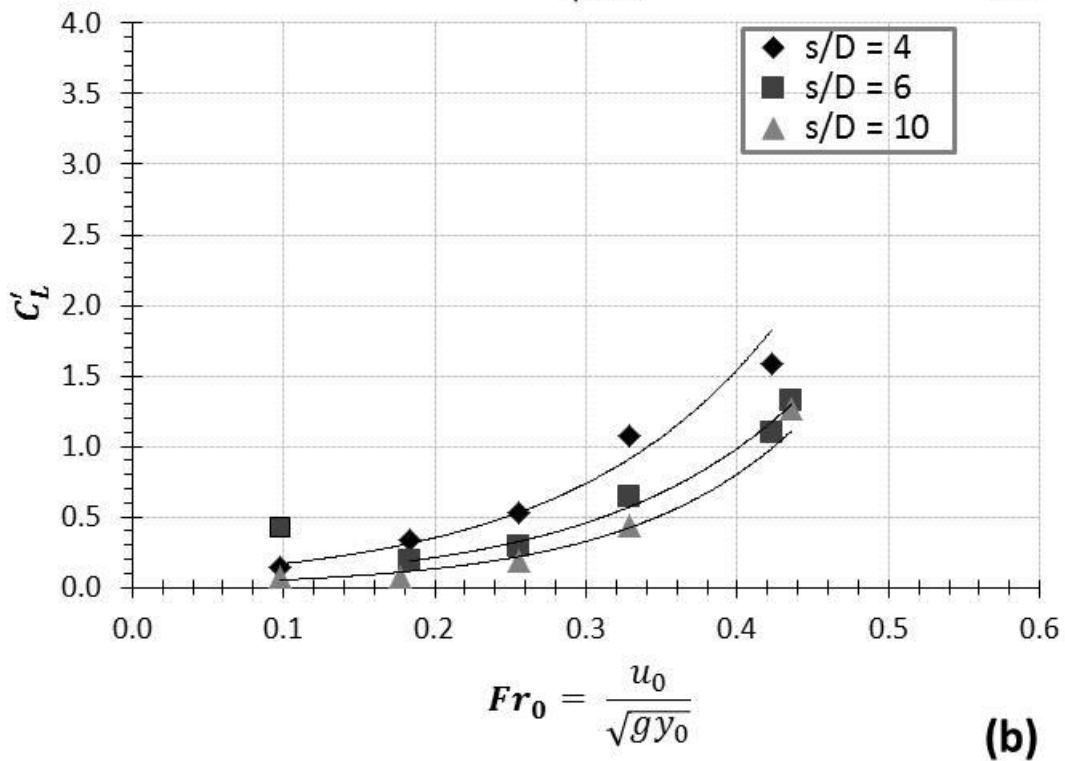
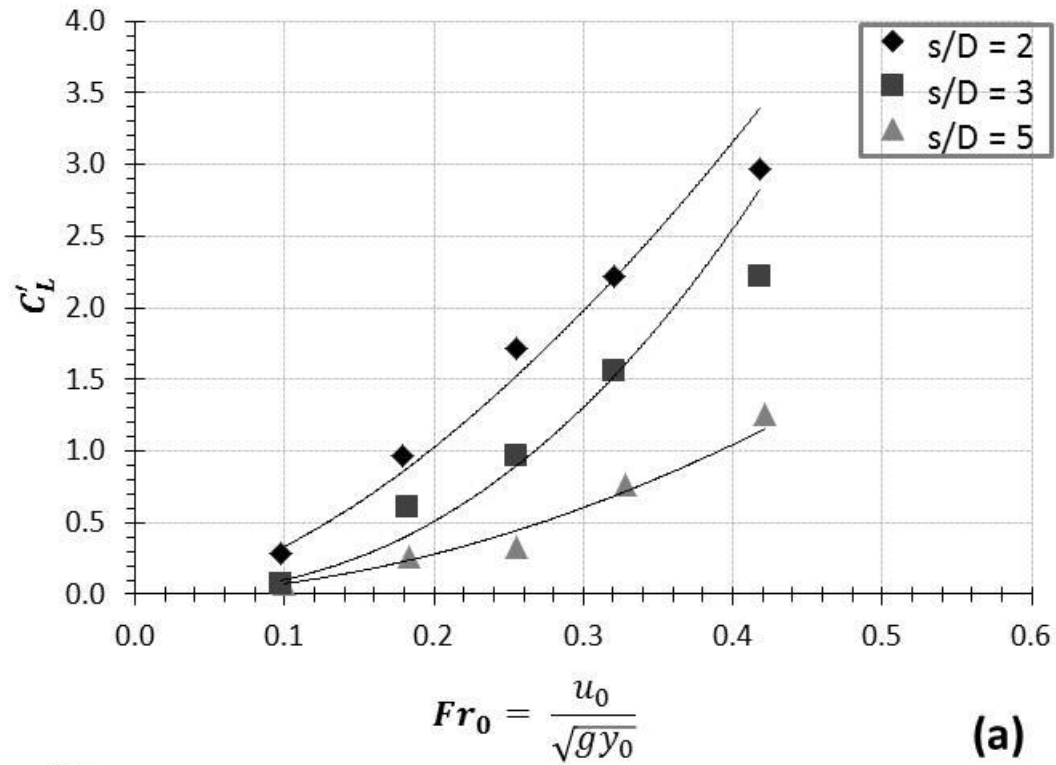


Figure 4-29: C'_L results for $y_0 = 0.20$ m, over a range of Fr_0 values, varying s/D spacing for two different D values. Note: the datum point in Figure 4-29 (b) at $s/D = 6$ and at $Fr_0 = 0.1$, in which $C'_L \approx 6.8$ is an outlier.

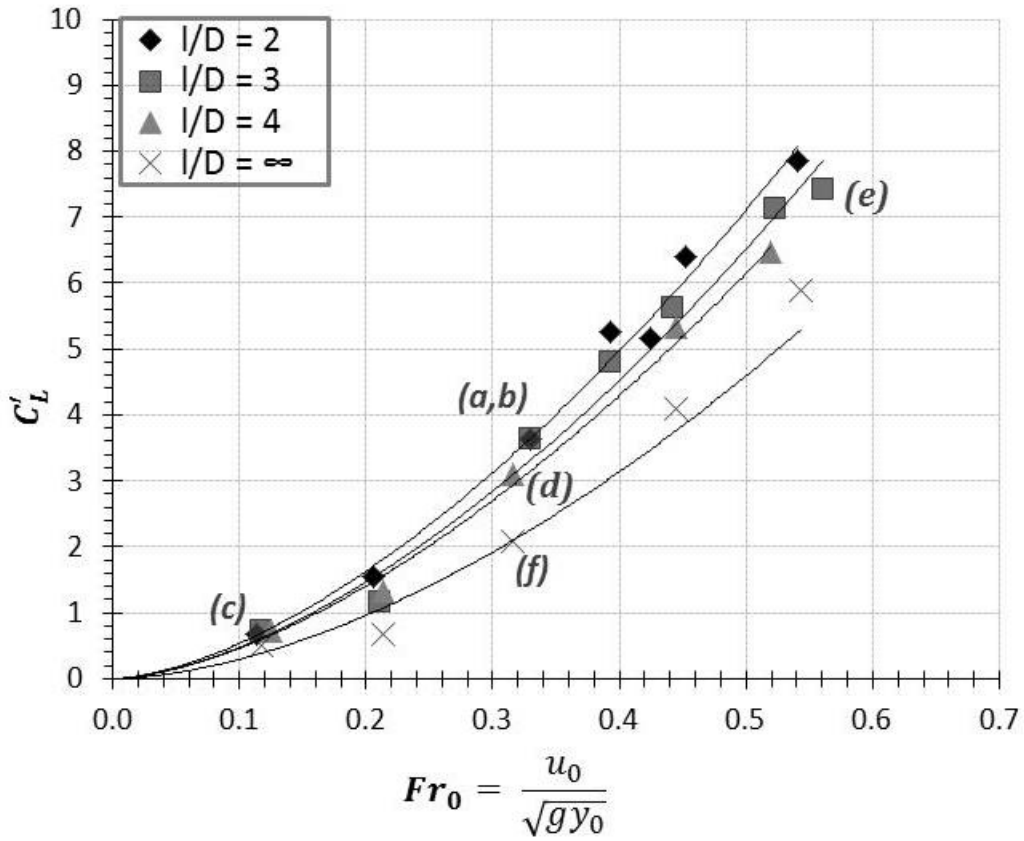


Figure 4-30: C_L' results for $y_0 = 0.08$ m, over a range of Fr_0 , varying l/D spacing for $D = 16$ mm. The letters correspond to experiment photographs presented in Figure 4-31.

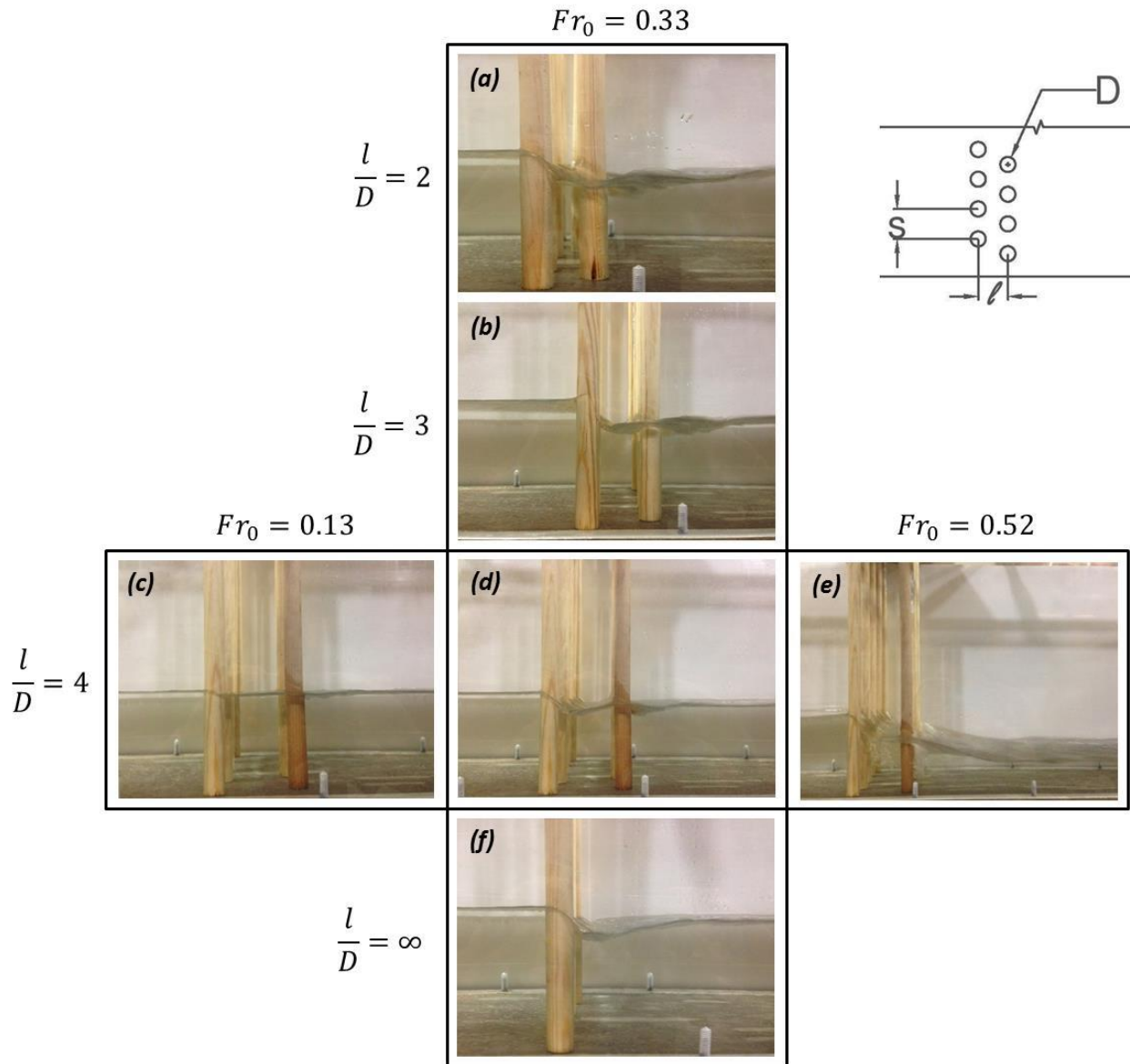


Figure 4-31: Photographs of l/D spacing results for $y_0/D = 5.0$. The letters correspond to the data points given in Figure 4-30. The ΔE value through the structure, and corresponding C'_L , is not significantly different for the varying l/D spacing configurations.

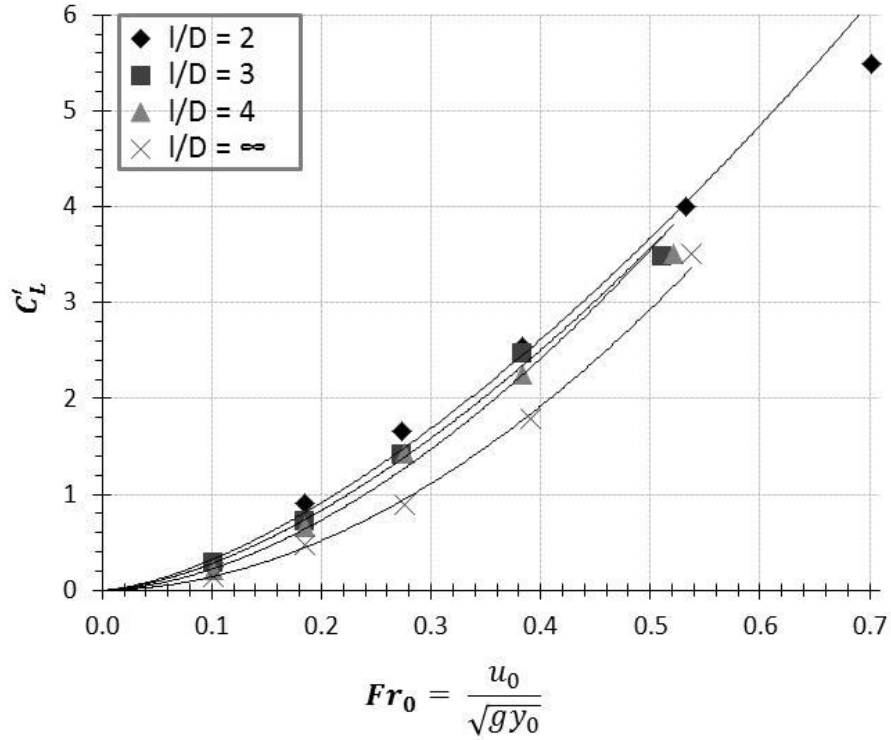


Figure 4-32: C'_L results for $y_0 = 0.15$ m, over a range of Fr_0 , varying l/D spacing for $D = 16$ mm

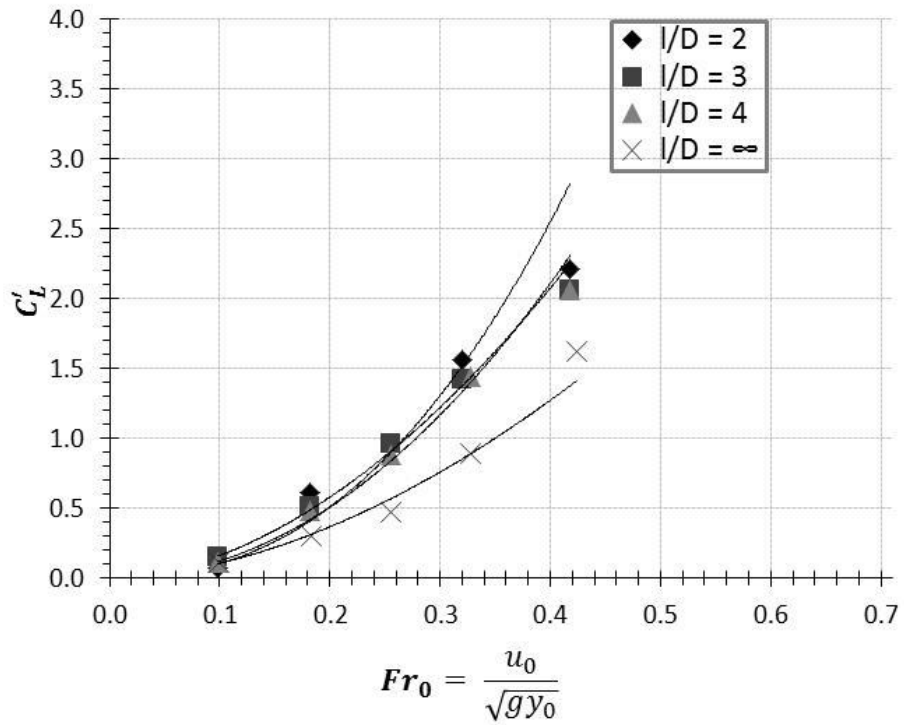


Figure 4-33: C'_L results for $y_0 = 0.20$ m, over a range of Fr_0 , varying l/D spacing for $D = 16$ mm

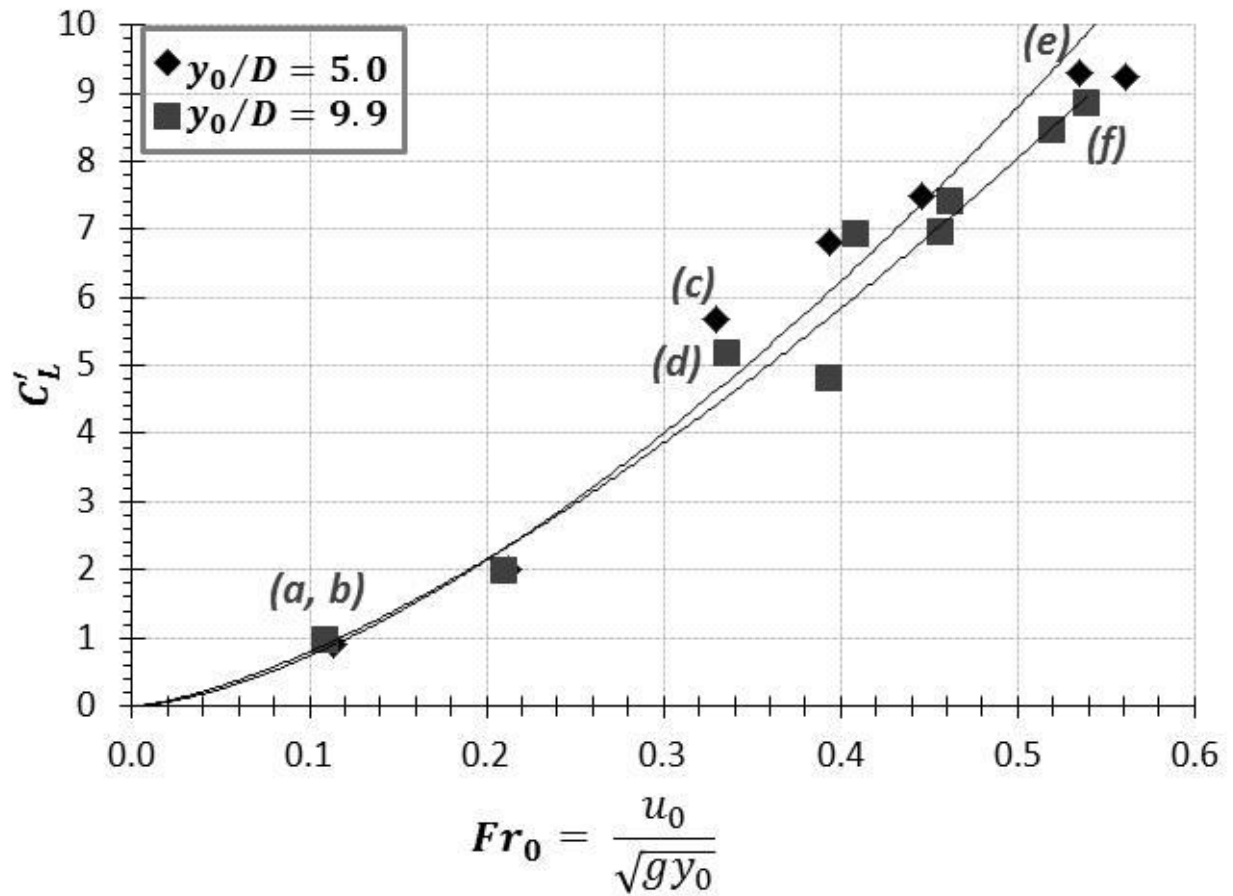


Figure 4-34: C'_L results for $y_0 = 0.08$ m, over a range of Fr_0 , varying D for the same s/D and l/D spacing. The letters correspond to experiment photographs presented in Figure 4-35.

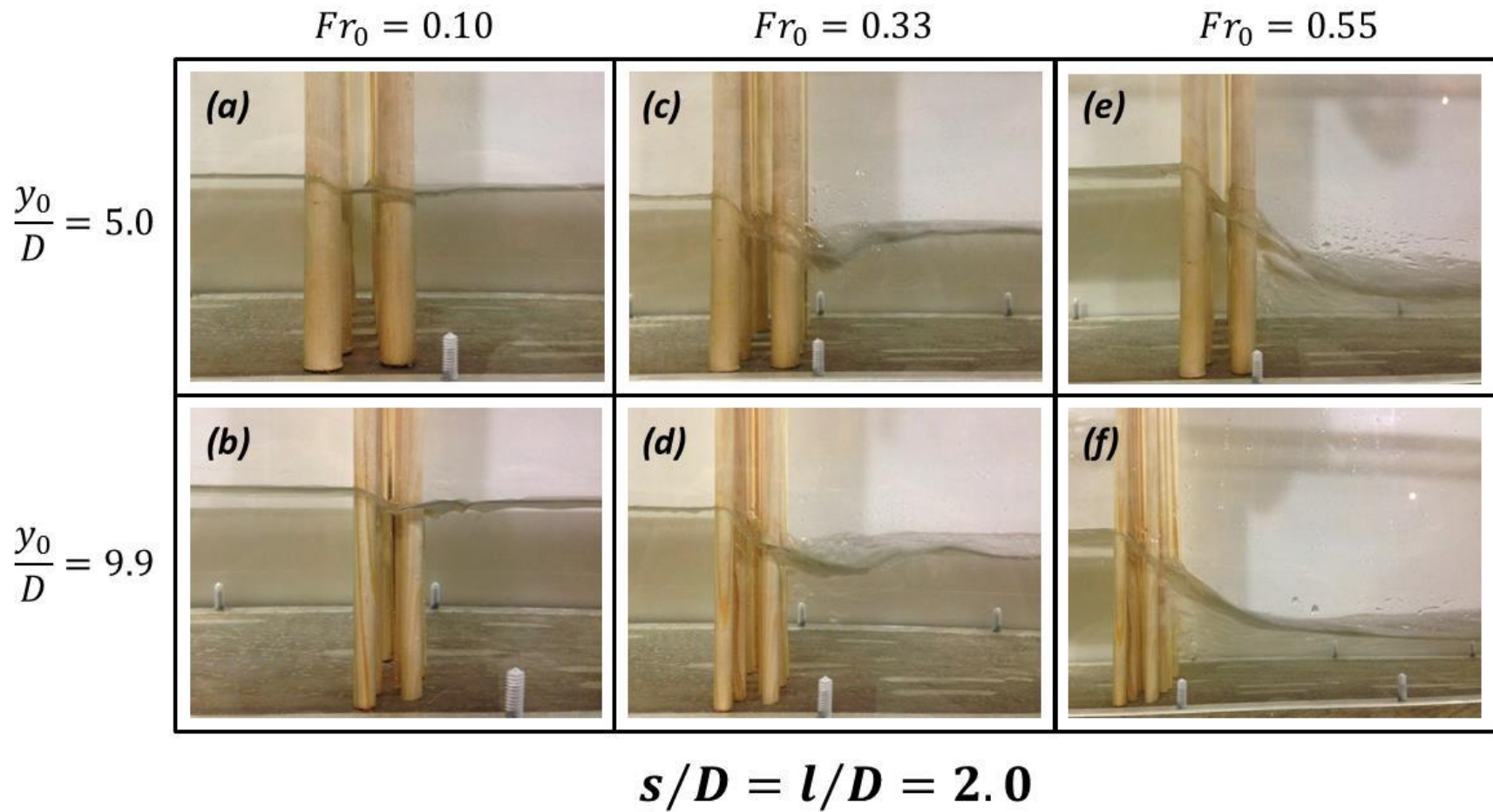


Figure 4-35: Experiment photographs results showing varying D over a range of Fr_0 values for consistent s/D and l/D spacing. The letters correspond to the C_L' values presented in Figure 4-34.

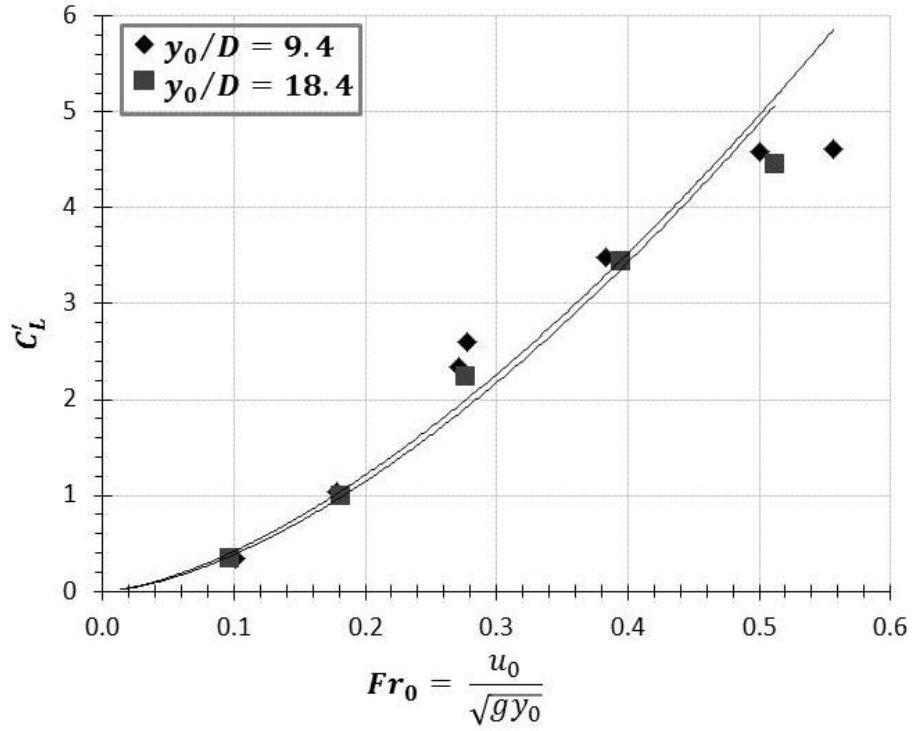


Figure 4-36: C'_L results for $y_0 = 0.15$ m, over a range of Fr_0 values, varying D , expressed as y_0/D for the same relative s/D and l/D spacing.

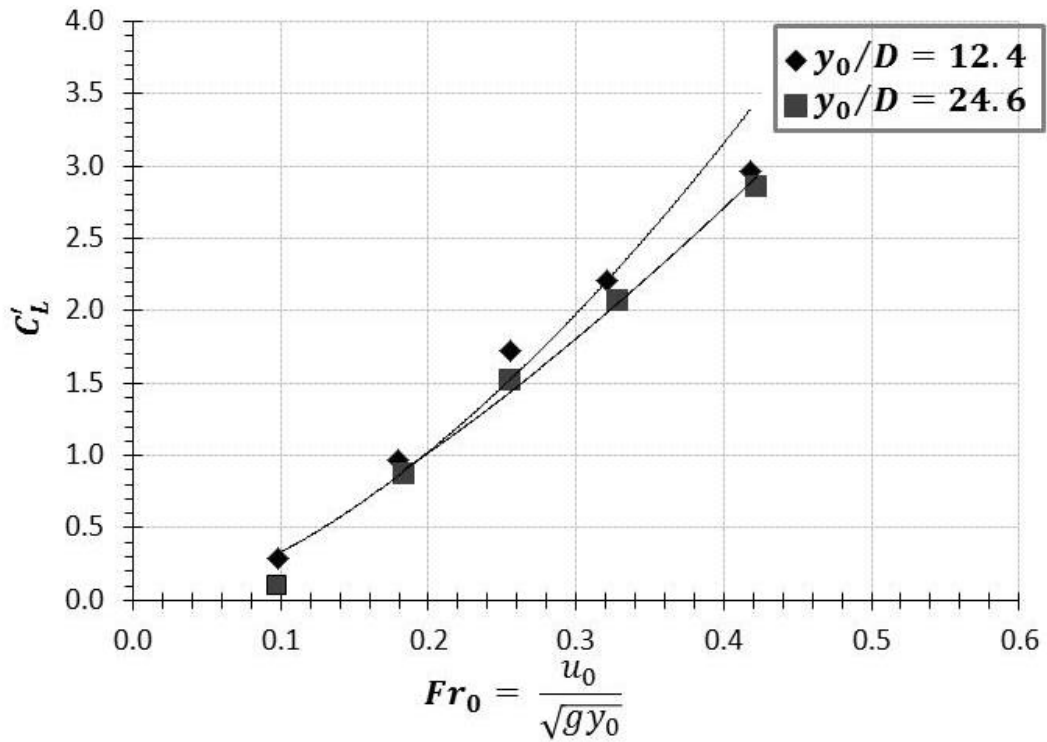


Figure 4-37: C'_L results for $y_0 = 0.20$ m, over a range of Fr_0 values, varying D for the same s/D and l/D spacing.

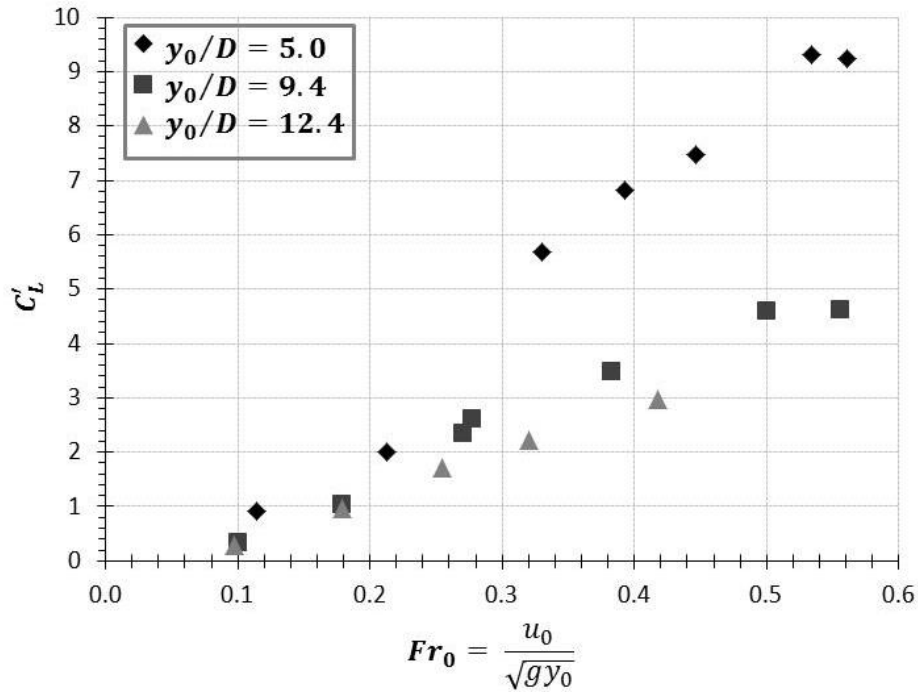


Figure 4-38: Experiment results comparing the 16-2-2 configuration at three different y_0 values, expressed by the dimensionless term, y_0/D .

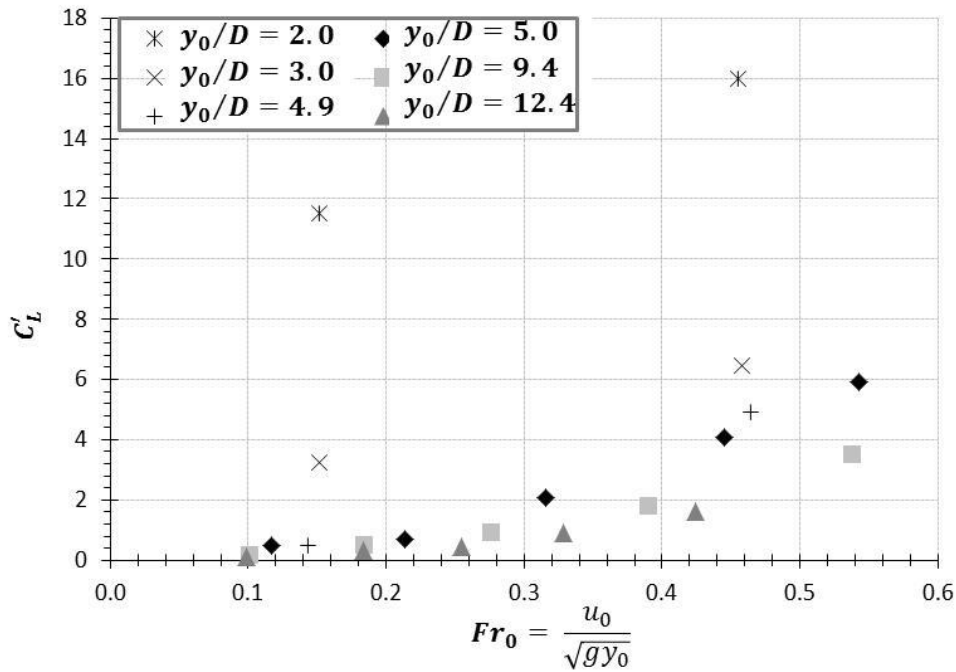


Figure 4-39: C'_L results comparing six y_0/D values for the same single-row structure. Please note that the series presented on the left side of the legend indicate results from the single-row structure experiments, where y_0/D was varied for $Fr_0 = 0.15$ and $Fr_0 = 0.45$. The right side of the legend shows results from the double-row hydraulic performance tests where Fr_0 was varied for three different y_0/D values.

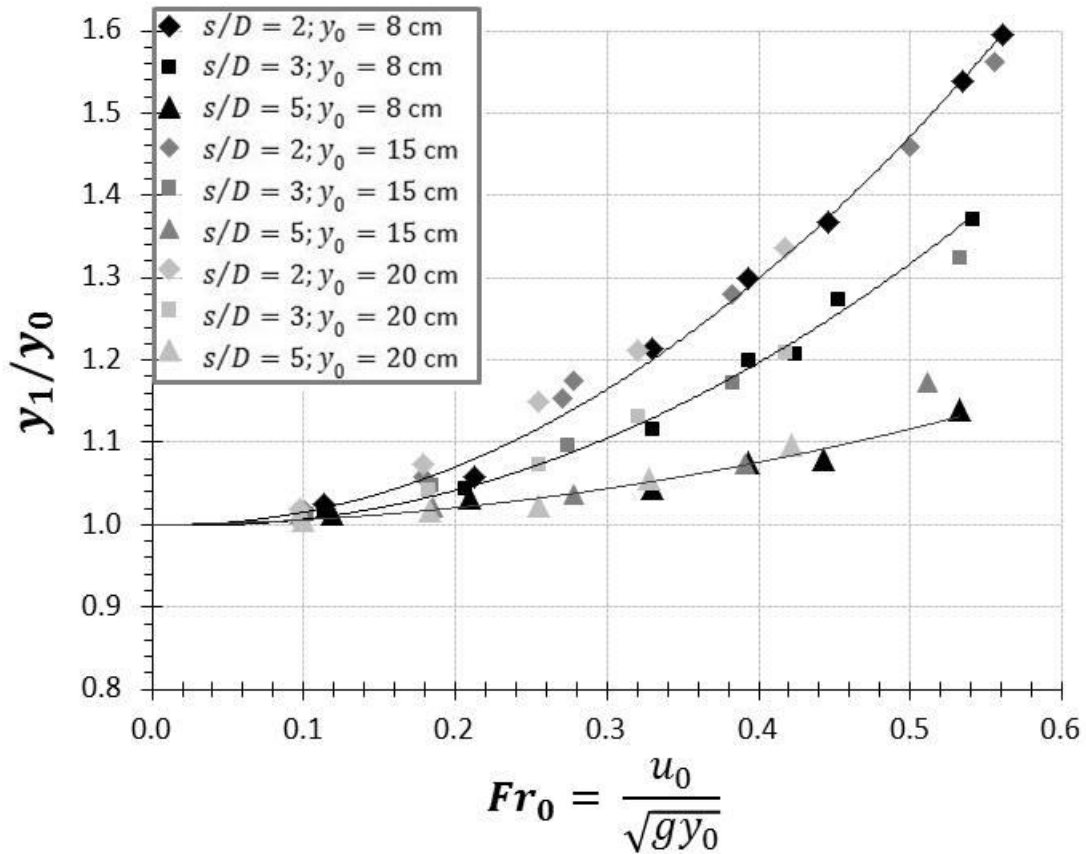


Figure 4-40: The variation of flow depth parameter y_1/y_0 for a double-row baffle-post structure with rows spaced at $l/D = 2$. The additional parameter in this figure is y_0/D , which exerts only a very small effect for the range of values investigated.

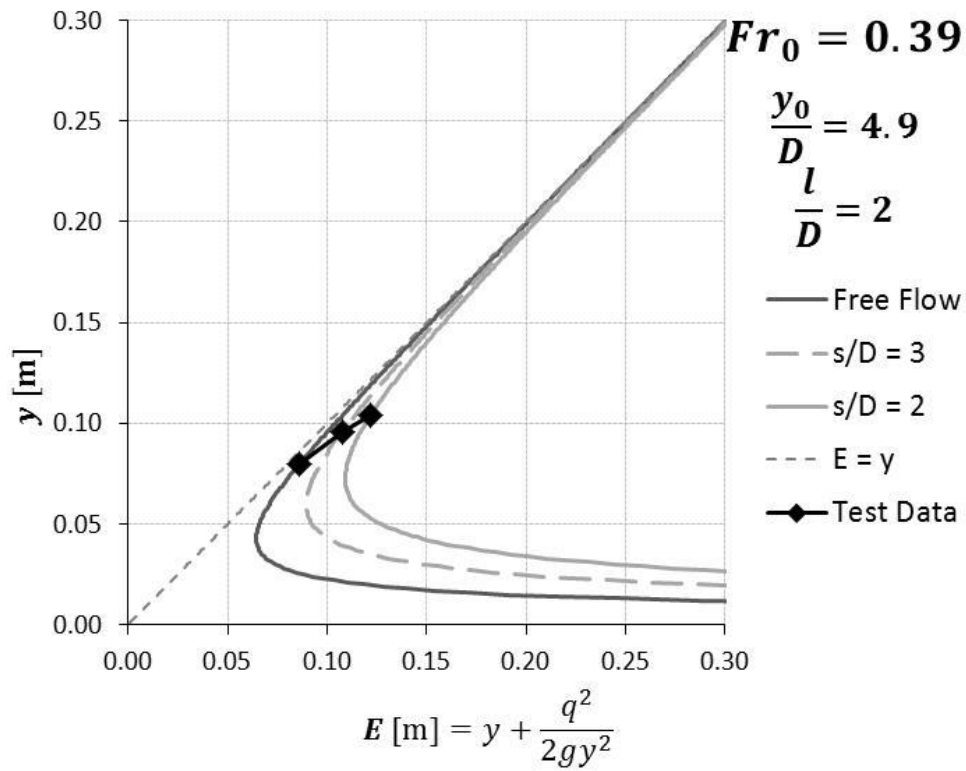
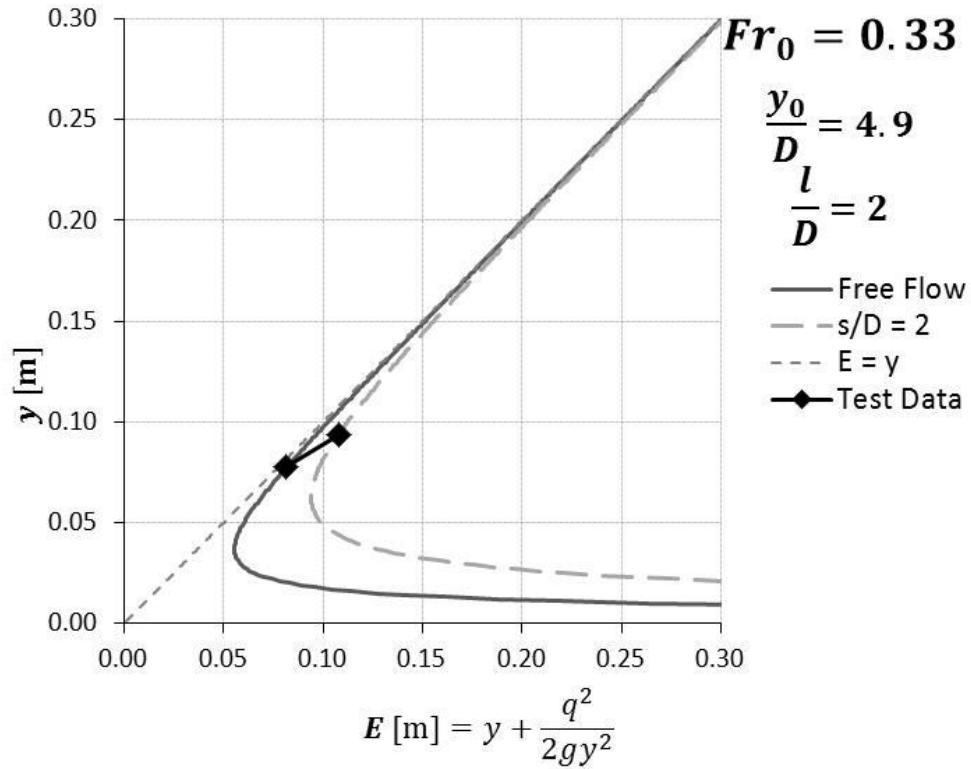


Figure 4-41: see caption below

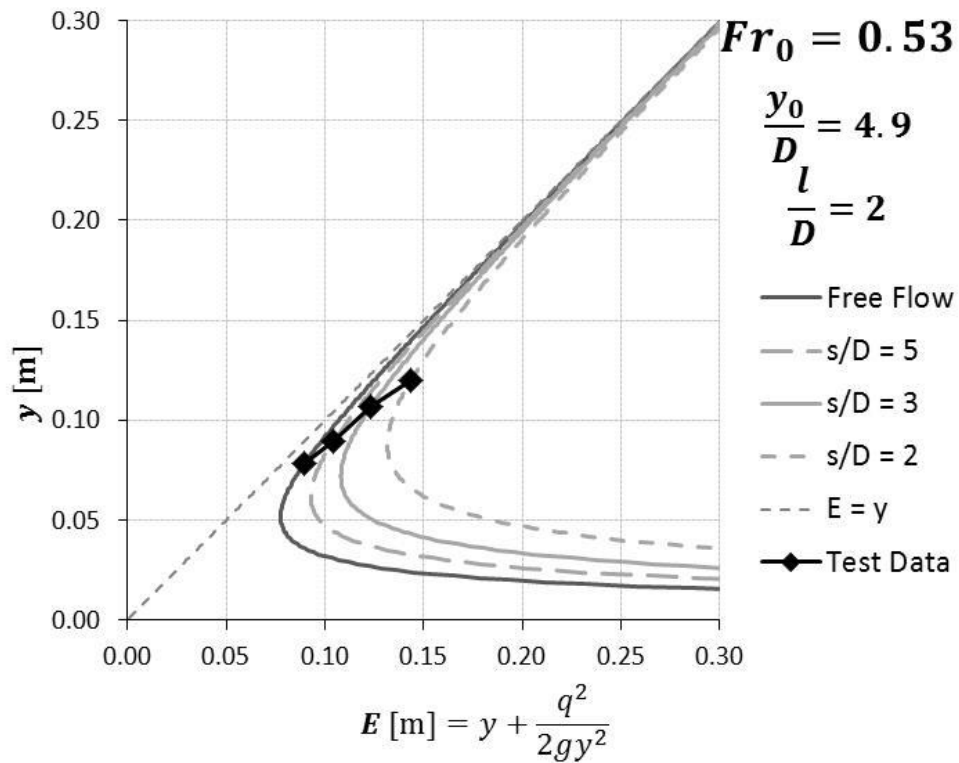
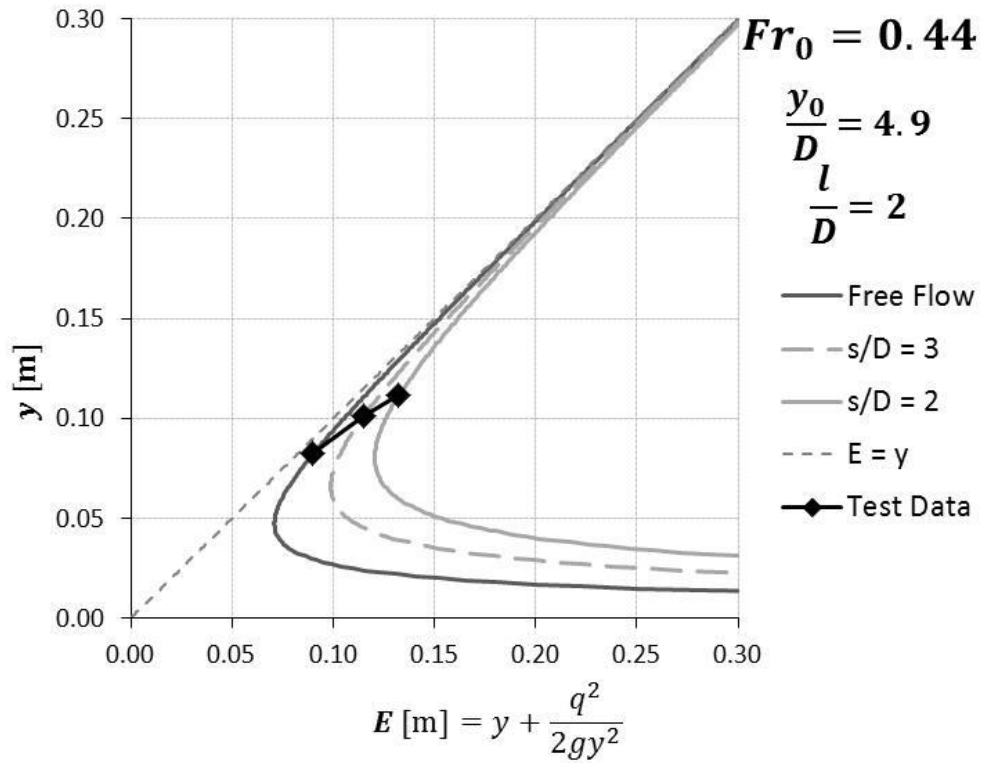


Figure 4-41: Specific energy diagram for double-row baffle-post structure at various l/D spacing. The y_0/D value, l/D spacing and D remained constant.

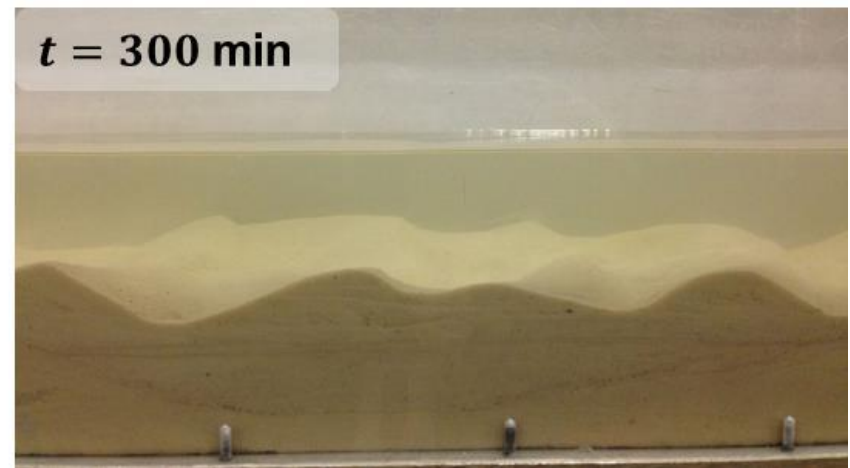
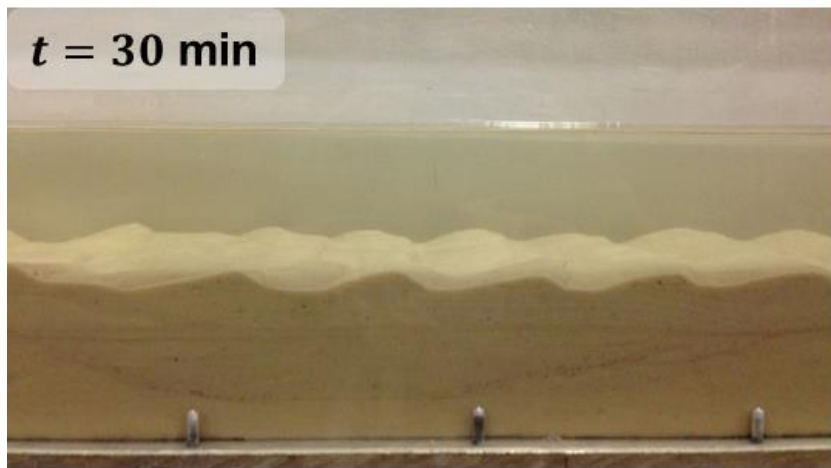
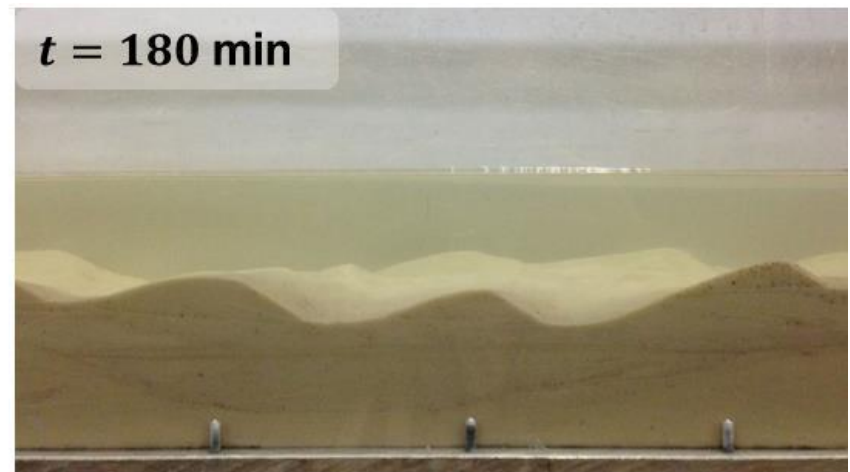
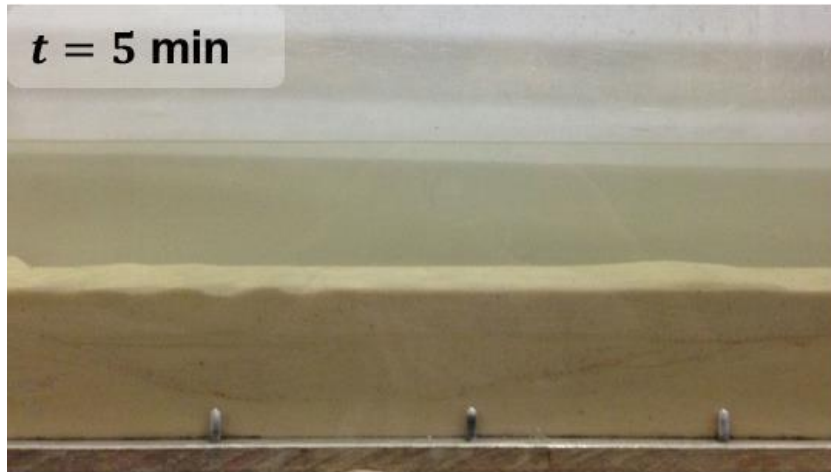


Figure 4-42: Experimental photographs for free flow conditions

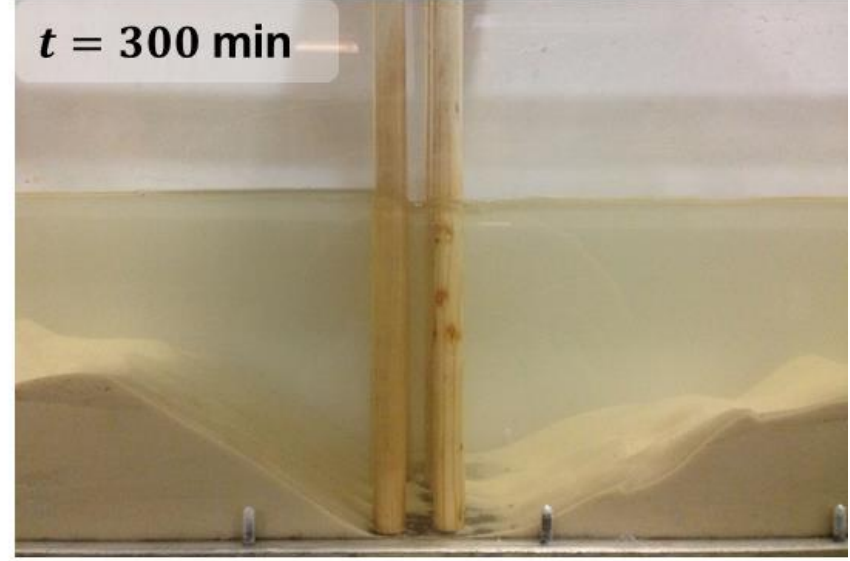
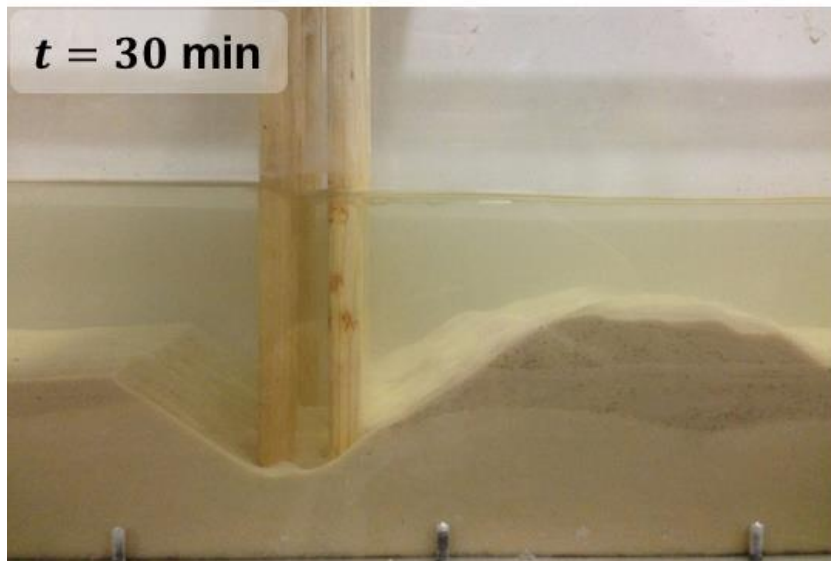
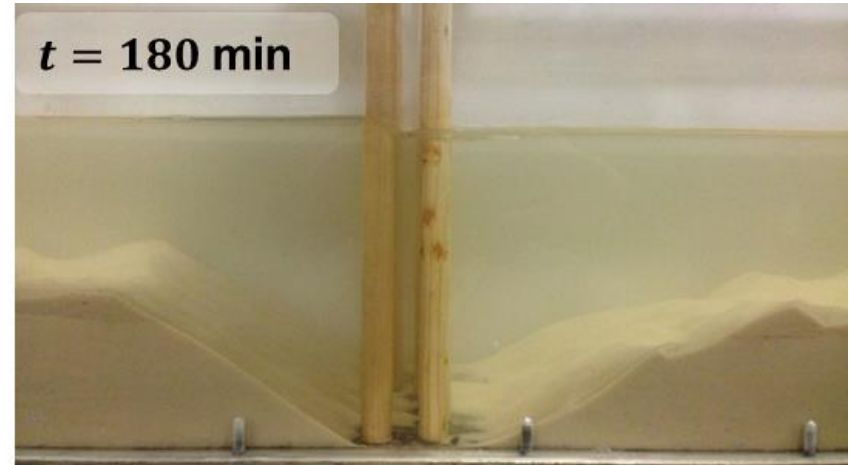
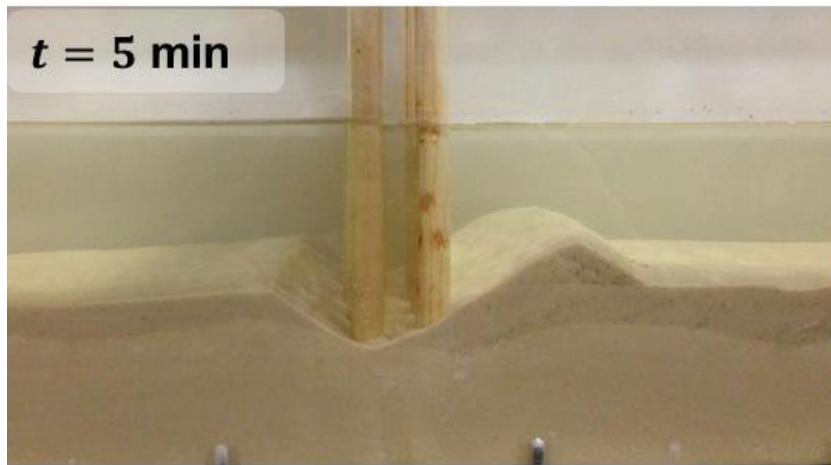


Figure 4-43: Experimental photographs for retarded flow conditions with no armoring at the base of the structure

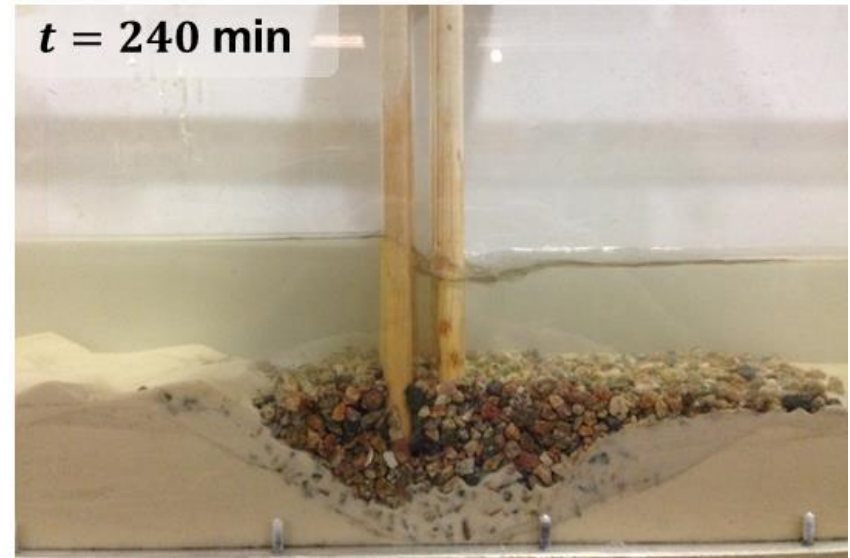
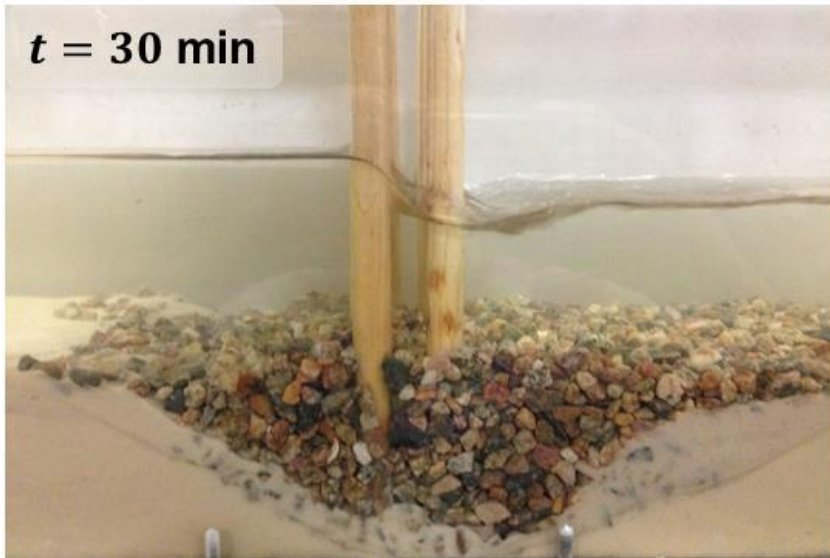
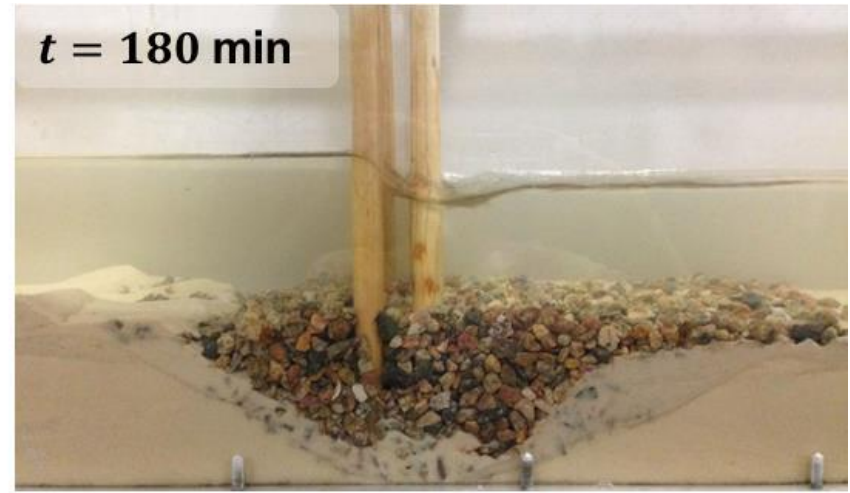
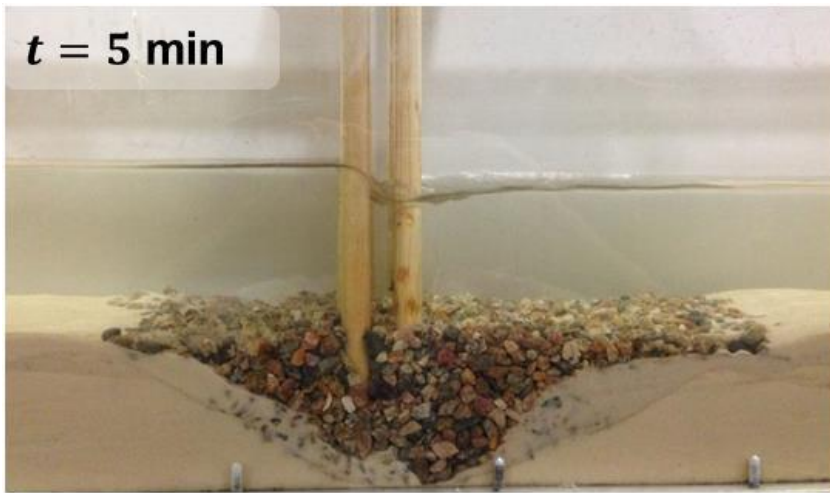


Figure 4-44: Experimental photographs for retarded flow conditions with armor at the base of the structure

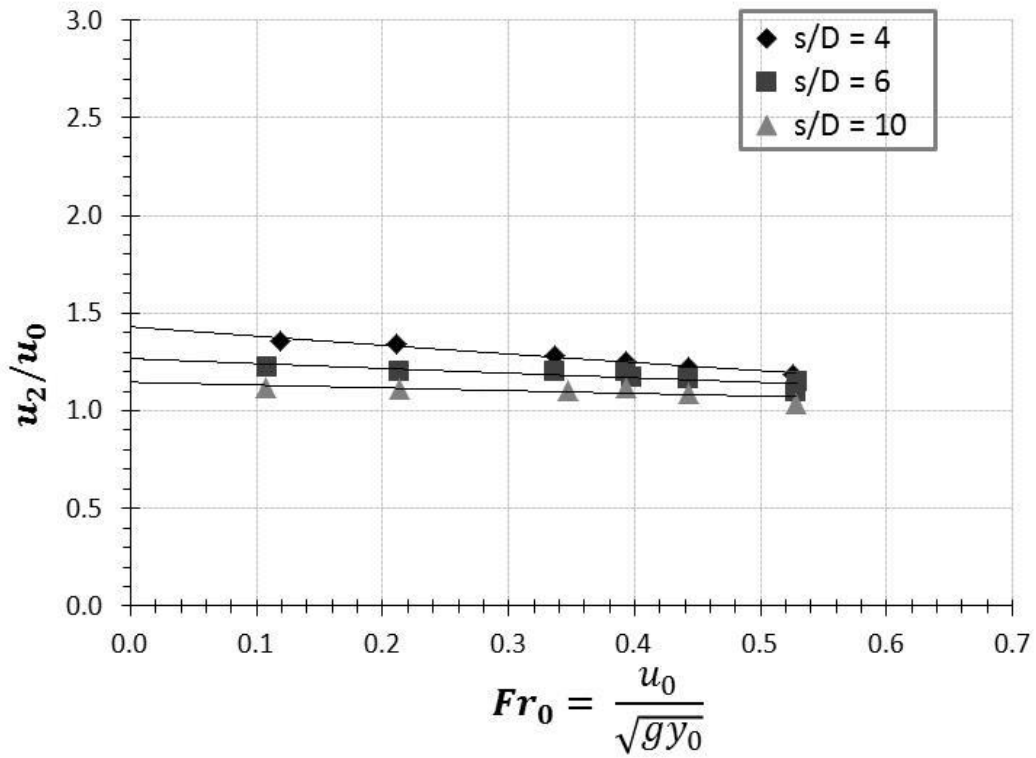
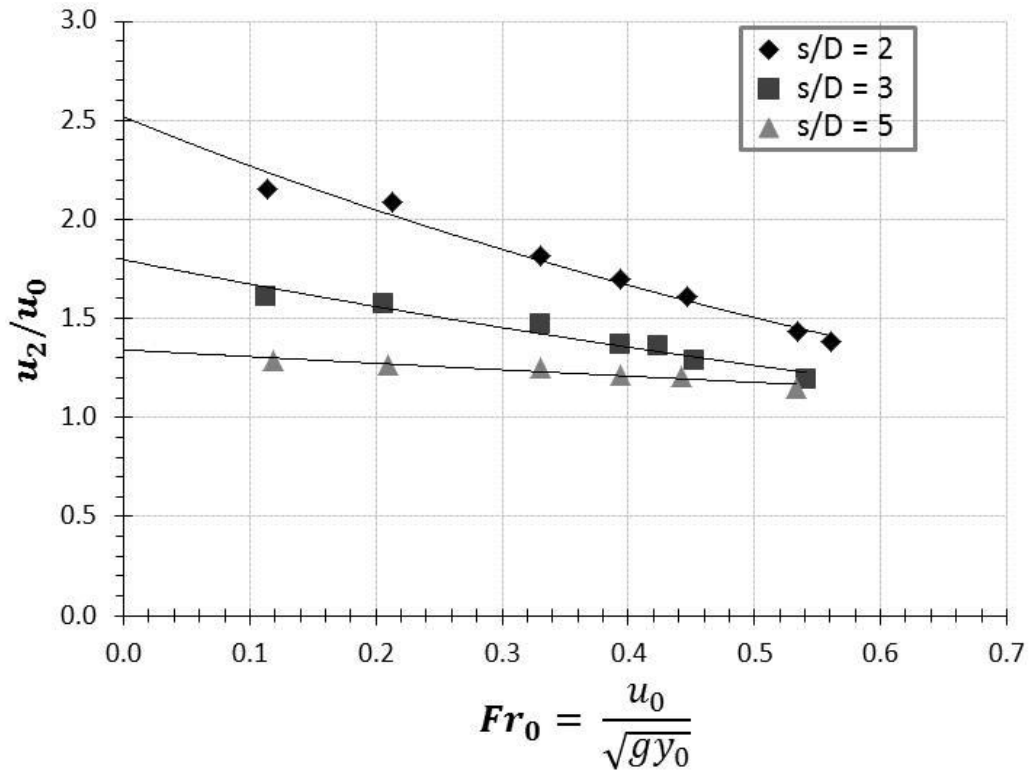


Figure 4-45: u_2/u_0 for double-row structure varying l/D spacing at $y_0 = 0.08$ m.

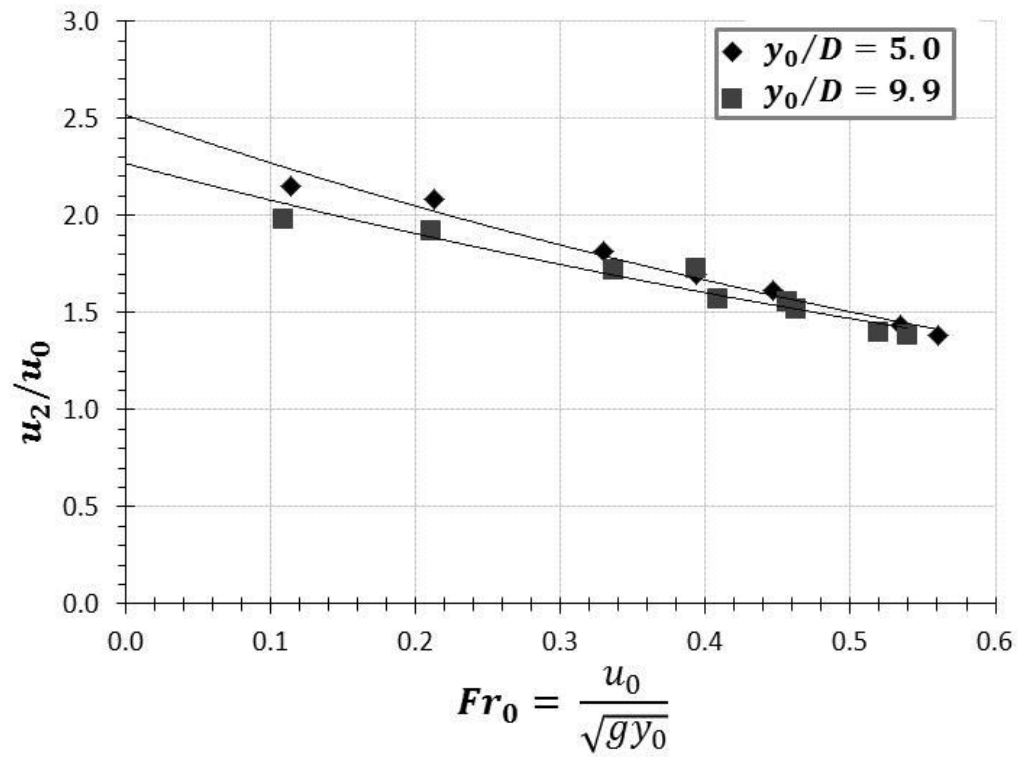
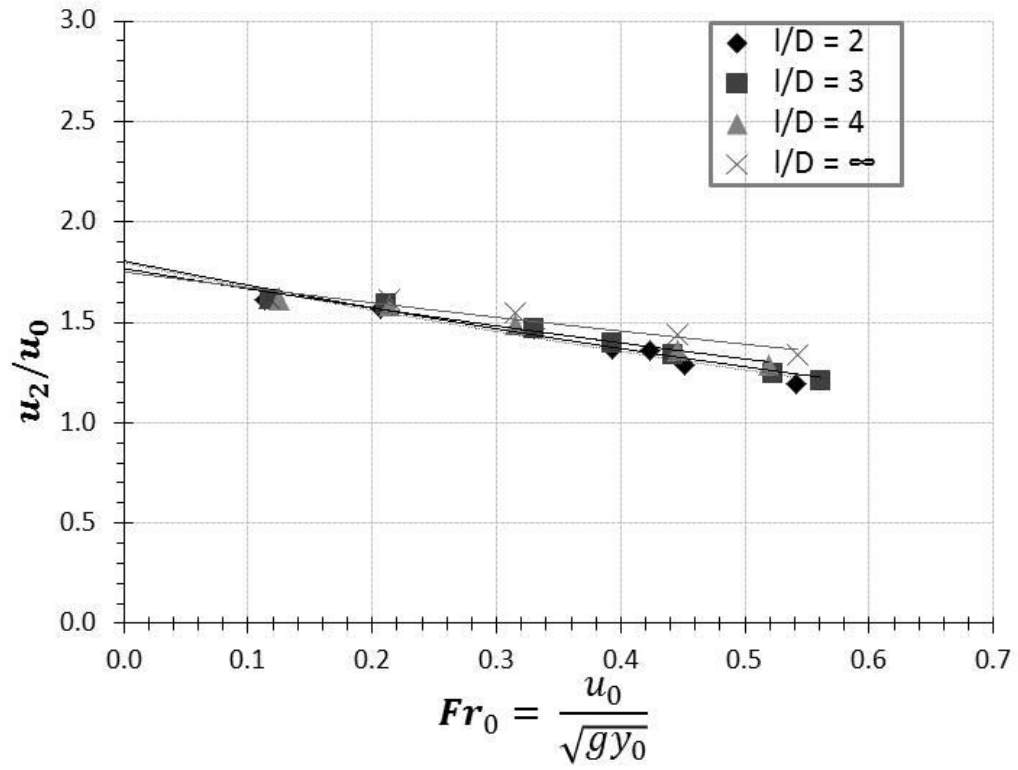


Figure 4-46: u_2/u_0 for double-row structure at $y_0 = 0.08$ m. The top graph varies l/D spacing. The bottom graph varies D .

5.0 Conclusions & Recommendations

5.1. Overview

This study sought to determine the hydraulic performance of baffle-post structures, which constrict, deepen and slow approach flows, and thereby reduce their capacity to transport bed sediment. The hydraulic performance of such structures can be formulated in terms of headloss and discharge coefficients, although the practical use of such coefficients is significantly decreased by their variation with approach flow conditions. More practical empirical relationships can be defined for the flow depth increase created by the use of baffle-post structures.

The program of experiments conducted for this study examined the performance of seventeen baffle-post configurations. Seven configurations consisted of single-row structures, where the lateral spacing of the baffle posts was varied. Ten configurations included two rows of baffle posts, where both lateral and streamwise spacing was altered as well as the baffle post diameter. Experiments were conducted in steady, uniform flow conditions in a rectangular re-circulating open channel flume.

From the collected data for the single row baffle-post structures, the headloss coefficient curve was plotted for multiple relative lateral spacing and multiple relative depths, all at two different Froude numbers: $Fr_0 = 0.15$ and $Fr_0 = 0.45$. Furthermore, the concept of choked flow conditions was explored to determine if the structure contracted the stream width past the critical value. The collected data for the double row of baffle-post structures provided information to develop headloss coefficient curves for multiple lateral spacing, streamwise spacing, and varying post diameters. These curves were plotted over varying Froude numbers at three relative depths.

Of immediate practical use for using baffle-post structures are empirical curves indicating the flow depth increase produced by baffle-post structures. For several geometric configurations of baffle-post structure, and varying approach flow Froude number, these data relate increased flow depth to initial (pre-structure) flow depth.

5.2. Conclusions

The literature on hydraulic structures contains few articles about baffle-post structures. The closest structures are closely spaced bridge piers (e.g., as shown in Figure 1-3) and trashracks used to screen debris and biota from entering water intake conduits. This study, therefore, is a substantial contribution to the broad field of hydraulic structures. Insights from the study have relevance for flow through rows of trees on floodplains, but this applicability was not pursued in depth.

The conclusions stemming from this study are presented in three groups:

- 1) The overall functioning of baffle-post structures;
- 2) Single-row, baffle-post structures; and,
- 3) Double-row, baffle-post structures.

5.2.1. General Conclusions

- 1) Headloss and discharge coefficients vary with approach flow conditions, making them cumbersome and less effective parameters for use in characterizing the hydraulic performance of baffle-post structures. However, semi-empirical trends for the relative depth parameter, y_1/y_0 offer a useful means for describing the performance of baffle-post structures.
- 2) The presence of a baffle-post structure created a M_1 gradually varied flow profile extending upstream of the structure, and thereby complicating the use of headloss and discharge coefficients. The flow accelerated through the structure and continued to accelerate a short

distance downstream of the structure, reaching a point of minimum flow depth, or maximum flow velocity. Finally, the flow either gradually or rapidly increased in depth.

- 3) The headloss coefficient increased as Fr_0 increased due to the increase in magnitude and extent of interaction of flow vortices generated at the structures.
- 4) For both the single- and double-row structures, the effective opening width, B_{eff} , associated with the lateral spacing parameter, s/D , was the most dominant geometric parameter influencing C'_L . C'_L increased as post decreased and flow blockage increased.
- 5) The relative depth of approach flow, y_0/D , had relatively negligible impact on C'_L above a certain depth. Below that depth ($y_0/D = 3.0$ for $Fr_0 < 0.3$ and $y_0/D = 5.0$ for $Fr_0 > 0.3$ in this study), C'_L increased because the turbulence generated by the posts interacted to a greater extent and impinged more on the channel bed.
- 6) The bedforms upstream of the structure decreased in size with distance closer to the baffle-post structure, reflecting the reduction in sediment transport rates upstream of the structure.
- 7) Baffle-post structures could potentially pose difficulties for fish and other aquatic life passage due to the possible confined space and higher flow velocities associated with such structures. Relative increases in velocity through the structure must be considered for the species of concern (e.g., trout or salmon) for a specific project.

5.2.2. Single-Row Baffle-Post Structures

- 1) The lateral spacing of posts, expressed as the parameter s/D , had the largest influence on the C'_L values, especially for tighter lateral spacing. Higher post density produced higher blockage ratios, thus higher flow resistance and energy dissipation. Furthermore, smaller flow openings allowed flow vortices to develop in closer proximity, making them more likely to interfere with one another, increasing the flow turbulence. As s/D decreased, C'_L values increased.

- 2) At $Fr_0 = 0.15$, C'_L had an inverse relationship with relative depth due to the vertical location of the downflow and horseshoe vortices in comparison with the channel bottom. At $Fr_0 = 0.45$ vortices are stronger and cover a larger spatial extents. Therefore, they are likely interacting with the bottom at all y_0/D values, resulting in a less defined relationship between C'_L and y_0/D .
- 3) The headloss parameter C'_L had a direct relationship with Fr_0 , which reflects the increased magnitude of the depth increase parameter and flow turbulence caused by the flow vortices generated by the structures.

5.2.3. Double-Row Baffle-Post Structures

- 1) As for single-row baffle-post structures, the lateral spacing (or effective width) parameter, s/D , had the largest influence on the hydraulic performance of the structure. This conclusion is assumed to be primarily due to the increased flow resistance and interaction of flow vortices.
- 2) Relative streamwise spacing, as expressed by the parameter l/D , had a relatively minor influence on values of C'_L .
- 3) As mentioned in Section 5.2.1, C'_L increased as Fr_0 increased, largely due to the increase in flow turbulence dissipation of energy that occurred with higher flow velocities and shallower flow depths.
- 4) For similar blockage ratios and effective widths, baffle post diameter had minimal impacts on C'_L values, especially at low values of Fr_0 .
- 5) At relative depths greater than 3.0 for low Fr_0 values and 5.0 for $Fr_0 > 0.3$, the relative depth had negligible impacts on C'_L .
- 6) Finally, choked flow conditions occurred for $s/D = 2$ starting at $Fr_0 = 0.33$. As the Froude number increased, the increase in specific energy needed to pass the discharge doubled at $Fr_0 = 0.53$. Again, at higher Froude numbers, the smallest effective width experienced the

largest increase in upstream energy relative to free flow conditions. The increase in specific energy and flow depth formed a linear relationship in the E-y plane with the four flow conditions.

5.3. Recommendations for Future Research

The primary purpose of this study was to determine the hydraulic performance of baffle-post structures, especially the extent to which they retarded approach flows. After the first set of experiments, the complexity of the structure became increasingly apparent. Therefore, future research is necessary to fully understand the impacts these structures may have on the hydraulics, geomorphology, and ecology of a river.

5.3.1. Future Research in Hydraulic Performance

This study focused on the development of a baffle-post structures with as many as two rows, smooth cylindrical posts, and initial Froude numbers between 0.10 and as high as 0.58. Investigation of the impact of the roughness of the posts should be made to determine if the tree post will influence the energy dissipation through the structure. Should the structure be installed over a large extent, stripping the tree post and smaller branches could be very costly; therefore, their effect on the hydraulic performance must be studied.

Furthermore, only uniform cylindrical baffle posts were analyzed in this study. Cylinders were chosen to simulate tree trunks, and it is unlikely that uniform diameter tree trunks can be found at a project site. Therefore, additional tests studying the impacts of variable diameter within a single structure are recommended.

While tree trunks have a relatively small upfront cost, they may require replacement and maintenance, especially in rivers with highly variable flow stages. Therefore, other materials and shapes may be more cost effective and should be tested.

In addition, only seventeen configurations were experimented upon, each of those configurations with one (or two) straight row(s) of baffles. To fully understand the hydraulic performance of the structure, staggered, diagonal, and perhaps random configurations should also be tested.

Finally, experiments were conducted with initial Froude numbers varying between 0.10 and 0.58, all of which are within the region of subcritical flow. Supercritical flow does not occur often over large spatial extents in nature. However, the author recommends testing the structure in supercritical flow conditions to determine if the headloss coefficient curve deviates when $Fr_0 > 1.0$.

5.3.2. Future Research in Sediment Transport

The primary purpose of the structure is to retain sediment upstream of the structure. However, due to time constraints, very little testing was performed to determine the effects of the structure on sediment transport. Therefore, future work is necessary to quantify the effects of the structure configurations on sediment transport.

As the primary sediment of concern is the bedload, tests must be performed to precisely quantify the portion of the volume of sediment bedload retained upstream of the structure. Furthermore, the study should also include the minimum bedload diameter retained by the structure, to determine its applicability to specific projects.

Secondly, passing the washload through the structure is instrumental in maintaining connectivity within the river reach. Future work could include quantifying the volume of washload retained by the structure as well as the amount passed through the structure. Furthermore, information on the maximum diameter of washload particles passed would be instructive.

Finally, the hydraulic test results showed an acceleration of flow directly downstream of the structure. To prevent local scour and degradation of the structural integrity of the baffle posts, protection is likely

needed. To minimize construction costs and local impact, research regarding the downstream scour hole will be necessary to determine the magnitude and extent of the scour protection.

5.3.3. Future Research for Scaling

Finally, future research should include similar testing at larger scales. This study was performed in a 0.20 m flume, using a 19.2 geometric ratio. To confirm these results are valid at a larger scale, 1:1 scale tests are recommended to be performed in a hydraulic laboratory with full control over the hydraulic and sediment loading. Should all results be confirmed to be accurate, testing the structure in the field would be appropriate.

6.0 References

- Abbe, T. B., & Montgomery, D. R. (1996). Large Woody Debris Jams, Channel Hydraulics and Habitat Formation in Large Rivers. *Regulated Rivers*, 12(23), 201-221.
- Acheson, A. (1968). *River Control and Drainage in New Zealand* (First ed.). Wellington, New Zealand: Ministry of Works.
- Bell, M. C. (1986). *Fisheries Handbook of Engineering Requirements and Biological Criteria*. Fish Passage Development and Evaluation Program, U.S. Army Corps of Engineers, Portland, OR.
- Bokaian, A., & Geoola, F. (1984). Wake-induced galloping of two interfering circular cylinders. *J. Fluid Mech.*, 146, 383-415.
- Daily, J., & Harleman, D. (1966). *Fluid Dynamics*. Reading, MA: Addison-Wesley.
- Discharge Coefficient* - *Wikipedia*. (2014, August 28). Retrieved February 2015, from Wikipedia: http://en.wikipedia.org/wiki/Discharge_coefficient
- El-Alfy, K. (2009). Backwater rise due to flow constriction by bridge piers. *Thirteenth International Water Technology Convergence*, (pp. 1295-1313). Hurghada, Egypt.
- Henderson, F. (1966). *Open channel flow*. New York, NY: Macmillan Publishing Co., Inc.
- Hotchkiss, R. H., & Frei, C. M. (2007). *Design for fish passage at roadway-stream crossings: synthesis report*. Federal Highway Administration, U.S. Department of Transportation. McLean, Virginia: Office of Infrastructure Research and Development.

- Jain, S. C. (2001). *Open-Channel Flow*. New York, NY: John Wiley & Sons, Inc.
- Julien, P. (2010). *Erosion and Sedimentation* (2nd ed.). New York: Cambridge Univ. Press.
- Julien, P. Y. (2002). *River mechanics*. New York: Cambridge University Press.
- Li, R.-M., & Shen, H. W. (1973). Effect of Tall Vegetation on Flow and Sediment. *Journal of the Hydraulics Division*, 99(5), 793-814.
- Luo, S. C., Gan, T. L., & Chew, Y. T. (1996). Uniform flow past one (or two in tandem) finite length circular cylinder(s). *Journal of Wind Engineering and Industrial Aerodynamics*, 59, 69-93.
- Maddock, I. (1999). The Importance of Physical Habitat Assessment for Evaluating River Health. *Freshwater Biology*, 41, 373-391.
- Melville, B. W., & Coleman, S. E. (2000). *Bridge scour*. Water Resources Publication.
- Simons, D., & Senturk, F. (1977). *Sediment Transport Technology*. Littleton, CO: Water Resources Pub., 1977, revised, 1992.
- Stone, B. S. (2002). Hydraulic Resistance of Flow in Channels with Cylindrical Roughness. *Journal of Hydraulic Engineering*, 128(5), 500-506.
- Tsikata, J., Tachie, M., & Katopodis, C. (2014). Open channel turbulent flow through bar racks. *Journal of Hydraulic Research*, 52(5), 630-643.
- Wilkerson, G. (2007). Flow through trapezoidal and rectangular channels with rigid cylinders. *Journal of Hydraulic Engineering*, 133(5), 521-533.
- Wohl, E. (2014). *Rivers in the landscape: science and management*. West Sussex, UK: John Wiley & Sons, Ltd.

Wong, M., & Parker, G. (2006). Reanalysis and correction of bed-load relation of Meyer-Peter and Muller using their own database. *Journal of Hydraulic Engineering*, 132(11), 1159-1168.

Appendix A – Measured Data

The following tables provide the data measurements taken during this experiment. Please note that all x values are streamwise distances, where $x = 0$ is at the upstream edge of the structure. The structure was placed 3.8m from the inlet for the hydraulic performance experiments and 7.79m from the inlet for the sediment transport experiments.

Table A-1: Measured data for hydraulic performance experiments for single-row baffle-post structures at $Fr_0 = 0.15$

Structure Geometry				Open Channel			GVF with Baffle-Post Structure				
s/D	n	D (cm)	s (cm)	Q (cfs)	Slope	y_0 (cm)	$y_{x=-0.28\text{ m}}$ (cm)	y_1 (cm)	y_{min} (cm)	x at y_{min} (cm)	
1.5	8	1.5875	2.3813	0.020	0	3.30	4.90	4.85	N.R.	N.R.	
2	7	1.5875	3.1750	0.020	0	3.25	4.30	4.35	1.20	4.35	
3	5	1.5875	4.7625	0.020	0	3.25	3.80	3.80	1.40	6.15	
3	4	1.5875	6.3500	0.020	0	3.15	3.60	3.60	1.70	5.30	
5	3	1.5875	7.9375	0.020	0	3.15	3.40	3.50	2.10	2.50	
6.0	2	1.5875	9.5250	0.020	0	3.25	3.40	3.40	2.20	2.50	
6.4	1	1.5875	10.160	0.020	0	3.35	3.40	3.30	2.50	2.20	
1.5	8	1.5875	2.3813	0.033	0	4.50	5.40	5.40	2.60	3.80	
2	7	1.5875	3.1750	0.033	0	4.55	5.10	5.20	3.00	3.30	
3	5	1.5875	4.7625	0.033	0	4.55	4.80	4.80	3.50	3.10	
3	4	1.5875	6.3500	0.033	0	4.35	4.55	4.60	3.60	2.80	
5	3	1.5875	7.9375	0.033	0	4.50	4.55	4.60	3.80	4.10	
6.0	2	1.5875	9.5250	0.033	0	4.35	4.40	4.40	3.90	2.50	
6.4	1	1.5875	10.160	0.033	0	4.30	4.35	4.35	4.20	1.50	
1.5	8	1.5875	2.3813	0.070	0	7.80	8.15	8.15	7.00	2.40	
2	7	1.5875	3.1750	0.075	0	7.80	8.10	8.10	7.10	2.10	
3	5	1.5875	4.7625	0.070	0	7.80	7.90	7.90	7.60		
3	4	1.5875	6.3500	0.075	0	7.60	7.65	7.65	7.40	N/A ¹	
5	3	1.5875	7.9375	0.070	0	7.75	7.80	7.80	7.70		
6.4	1	1.5875	9.5250	0.075	0	7.85	7.90	7.90			

¹Measurements were < 1.0 cm

Table A-2: Measured data for hydraulic performance experiments for single-row baffle-post structures at $Fr_0 = 0.45$

Structure Geometry				Open Channel			GVF with Baffle-Post Structure			
s/D	n	D (cm)	s (cm)	Q (cfs)	Slope	y_0 (cm)	$y_{x=-0.28\text{ m}}$ (cm)	y_1 (cm)	y_{min} (cm)	x at y_{min} (cm)
1.5	8	1.5875	2.3813	0.060	0	3.35	5.20	5.20	1.10	10.90
2	7	1.5875	3.1750	0.060	0	3.30	4.60	4.65	1.40	11.90
3	5	1.5875	4.7625	0.060	0	3.25	4.05	4.15	1.05	6.60
4	4	1.5875	6.3500	0.060	0	3.30	3.80	3.80	2.20	6.25
5	3	1.5875	7.9375	0.060	0	3.30	3.60	3.60	2.20	5.75
6.0	2	1.5875	9.5250	0.060	0	3.30	3.50	3.50	2.20	2.60
6.4	1	1.5875	10.160	0.060	0	3.30	3.35	3.35	2.30	2.85
1.5	8	1.5875	2.3813	0.110	0	4.95	6.55	6.60	2.80	4.80
2	7	1.5875	3.1750	0.110	0	4.85	5.80	5.90	2.70	4.10
3	5	1.5875	4.7625	0.110	0	4.85	5.40	5.50	2.90	3.90
3	4	1.5875	6.3500	0.110	0	4.85	5.20	5.15	3.20	5.00
5	3	1.5875	7.9375	0.110	0	4.85	5.00	5.00	3.50	2.90
6.0	2	1.5875	9.5250	0.110	0	4.85	5.05	5.20	3.70	4.25
6.4	1	1.5875	10.160	0.110	0	4.75	4.85	4.85	4.20	2.40
1.5	8	1.5875	2.3813	0.225	0.0003	7.70	11.05	11.10	3.10	13.10
2	7	1.5875	3.1750	0.225	0.0003	7.75	9.85	10.05	4.80	7.80
3	5	1.5875	4.7625	0.225	0.0003	7.75	8.85	9.10	5.10	7.10
4	4	1.5875	6.3500	0.225	0.0003	7.75	8.45	8.60	5.50	7.30
5	3	1.5875	7.9375	0.225	0.0003	7.75	8.20	8.35	6.30	6.00
6.0	2	1.5875	9.5250	0.225	0.0003	7.75	8.05	8.05	6.40	4.80
6.4	1	1.5875	10.160	0.225	0.0003	7.70	7.80	7.80	6.60	4.60
1.5	8	1.5875	2.3813	0.330	0	10.05	14.25	14.50	3.80	19.95
2	7	1.5875	3.1750	0.330	0	10.05	12.65	12.95	6.70	8.70
3	5	1.5875	4.7625	0.330	0	10.05	11.40	11.70	7.10	8.35
4	4	1.5875	6.3500	0.330	0	10.20	11.00	11.25	7.90	9.20
5	3	1.5875	7.9375	0.330	0	10.05	10.55	10.60	8.10	9.50
6.0	2	1.5875	9.5250	0.330	0	10.20	10.65	10.65	9.00	6.20
6.4	1	1.5875	10.160	0.330	0	10.20	10.55	10.55	9.40	5.20

Table A-3: Measured data for hydraulic performance experiments for single-row baffle-post structures at $y_0 = 0.08$ m

Structure Geometry				Open Channel			GVF with Baffle-Post Structure			
s/D	n	D (cm)	s (cm)	Q (cfs)	Slope	y_0 (cm)	$y_{x=-0.28\text{ m}}$ (cm)	y_1 (cm)	y_{min} (cm)	x at y_{min} (cm)
2	7	1.5875	3.1750	0.087	0	8.00	8.40	8.60	7.40	2.20
2	7	1.5875	3.1750	0.115	0	7.90	8.30	8.60	6.70	2.70
2	7	1.5875	3.1750	0.128	0	7.90	8.60	8.90	6.40	3.40
2	7	1.5875	3.1750	0.157	0	8.05	8.75	9.00	6.60	3.65
2	7	1.5875	3.1750	0.193	0	8.00	9.00	9.20	6.50	4.00
2	7	1.5875	3.1750	0.230	0	8.10	9.05	9.20	6.00	4.40
2	7	1.5875	3.1750	0.270	0	8.00	9.20	9.40	5.70	4.50
2	7	1.5875	3.1750	0.320	0	8.00	9.35	9.70	5.50	5.00
3	5	1.5875	4.7625	0.087	0	7.80	7.90	8.10	7.20	2.90
3	5	1.5875	4.7625	0.115	0	7.90	8.10	8.25	7.10	2.80
3	5	1.5875	4.7625	0.157	0	8.00	8.35	8.60	7.20	2.90
3	5	1.5875	4.7625	0.195	0	8.00	8.50	8.65	6.90	3.80
3	5	1.5875	4.7625	0.230	0	8.00	8.45	8.70	7.10	3.80
3	5	1.5875	4.7625	0.270	0	8.10	8.75	8.90	6.80	3.70
3	5	1.5875	4.7625	0.320	0	8.05	8.65	8.80	6.30	4.60
3	5	1.5875	4.7625	0.325	0	7.90	8.55	8.80	6.10	4.00
5	3	1.5875	7.9375	0.087	0	8.10	8.10	8.30	N/A	N/A
5	3	1.5875	7.9375	0.115	0	7.75	7.90	8.05	7.30	3.70
5	3	1.5875	7.9375	0.157	0	8.05	8.10	8.35		
5	3	1.5875	7.9375	0.195	0	8.00	8.15	8.35	7.50	3.60
5	3	1.5875	7.9375	0.230	0	8.20	8.40	8.55	7.50	4.30
5	3	1.5875	7.9375	0.270	0	8.00	8.20	8.30		
5	3	1.5875	7.9375	0.320	0	8.15	8.40	8.55	7.10	3.20
5	3	1.5875	7.9375	0.325	0	8.05	8.35	8.60	6.90	5.25

Table A-4: Measured data for hydraulic performance experiments for single-row baffle-post structures at $y_0 = 0.15$ m

Structure Geometry				Open Channel			GVF with Baffle-Post Structure				
s/D	n	D (cm)	s (cm)	Q (cfs)	Slope	y_0 (cm)	$y_{x=-0.28\text{ m}}$ (cm)	y_1 (cm)	y_{min} (cm)	x at y_{min} (cm)	
2	7	1.5875	3.1750	0.195	0	15.00	15.25	15.45	14.30	2.30	
2	7	1.5875	3.1750	0.357	0	15.30	15.80	16.00	14.70	2.00	
2	7	1.5875	3.1750	0.470	0	15.00	15.55	15.75	13.70	2.80	
2	7	1.5875	3.1750	0.610	0	15.00	15.75	16.00	13.20	3.60	
2	7	1.5875	3.1750	0.760	0	15.05	15.95	16.15	13.10	3.20	
3	5	1.5875	4.7625	0.195	0	15.00	15.05	15.25	14.80	2.25	
3	5	1.5875	4.7625	0.357	0	15.30	15.65	15.85	15.00	2.50	
3	5	1.5875	4.7625	0.470	0	15.00	15.25	15.40	14.30	3.70	
3	5	1.5875	4.7625	0.610	0	14.95	15.40	15.55	13.90	2.70	
3	5	1.5875	4.7625	0.760	0	15.05	15.55	15.75	13.60	3.70	
5	3	1.5875	7.9375	0.195	0	15.00	15.05	15.20	14.90	N/A	
5	3	1.5875	7.9375	0.355	0	15.40	15.45	15.60	15.20	3.00	
5	3	1.5875	7.9375	0.470	0	15.00	15.10	15.25	14.70	N/A	
5	3	1.5875	7.9375	0.610	0	14.95	15.15	15.30	14.50	N/A	
5	3	1.5875	7.9375	0.760	0	15.05	15.20	15.45	14.10	2.70	

Table A-5: Measured data for hydraulic performance experiments for single-row baffle-post structures at $y_0 = 0.20$ m

Structure Geometry				Open Channel			GVF with Baffle-Post Structure				
s/D	n	D (cm)	s (cm)	Q (cfs)	Slope	y_0 (cm)	$y_{x=-0.28\text{ m}}$ (cm)	y_1 (cm)	y_{min} (cm)	x at y_{min} (cm)	
2	7	1.5875	3.1750	0.175	0	19.85	19.90	20.05	19.80	N/A	
2	7	1.5875	3.1750	0.410	0	20.25	20.55	20.70	19.50	2.10	
2	7	1.5875	3.1750	0.630	0	19.60	19.95	20.15	18.60	2.90	
2	7	1.5875	3.1750	0.890	0	19.95	20.40	20.70	18.20	3.00	
2	7	1.5875	3.1750	1.150	0	20.30	21.10	21.30	18.40	3.35	
3	5	1.5875	4.7625	0.172	0	19.70	19.75	19.90	19.75	N/A	
3	5	1.5875	4.7625	0.410	0	20.25	20.35	20.50	19.90	2.40	
3	5	1.5875	4.7625	0.630	0	19.60	19.80	19.95			
3	5	1.5875	4.7625	0.890	0	19.90	20.20	20.35	19.00	2.40	
3	5	1.5875	4.7625	1.150	0	20.30	20.60	20.80	19.00	2.90	
5	3	1.5875	7.9375	0.172	0	19.70	19.70	19.85	19.90	N/A	
5	3	1.5875	7.9375	0.410	0	20.25	20.30	20.45			
5	3	1.5875	7.9375	0.630	0	19.60	19.75	19.85	19.40	N/A	
5	3	1.5875	7.9375	0.890	0	19.90	20.00	20.20	19.40	N/A	
5	3	1.5875	7.9375	1.150	0	20.30	20.40	20.65	19.40	2.55	

Table A-6: Measured data for hydraulic performance experiments for double-row baffle-post structures at $y_0 = 0.08$ m

Structure Geometry				Open Channel			GVF with Baffle-Post Structure				
No.	D (cm)	s (cm)	l (cm)	Q (cfs)	Slope	y_0 (cm)	$y_{x=-0.28\text{ m}}$ (cm)	y_1 (cm)	y_{min} (cm)	x at y_{min} (cm)	
16-2-2	1.5875	3.1750	3.1750	0.055	0	7.95	8.10	8.15	7.30	5.50	
16-2-2	1.5875	3.1750	3.1750	0.103	0	7.75	8.15	8.20	7.30	1.20	
16-2-2	1.5875	3.1750	3.1750	0.160	0	7.75	9.25	9.40	5.40	6.25	
16-2-2	1.5875	3.1750	3.1750	0.200	0	8.00	10.10	10.40	6.10	2.00	
16-2-2	1.5875	3.1750	3.1750	0.232	0.0003	8.15	11.10	11.15	5.00	9.50	
16-2-2	1.5875	3.1750	3.1750	0.265	0.0007	7.80	11.80	12.00	3.50	30.00	
16-2-2	1.5875	3.1750	3.1750	0.295	0.001	8.15	12.60	13.00	3.80	35.50	
16-3-2	1.5875	4.7625	3.1750	0.055	0	7.95	8.00	8.10	7.50	6.00	
16-3-2	1.5875	4.7625	3.1750	0.103	0	7.90	8.10	8.25	7.60	1.80	
16-3-2	1.5875	4.7625	3.1750	0.160	0	7.75	8.60	8.65	5.70	5.80	
16-3-2	1.5875	4.7625	3.1750	0.200	0	8.00	9.20	9.60	6.70	3.50	
16-3-2	1.5875	4.7625	3.1750	0.232	0.0003	8.40	10.05	10.15	6.60	4.40	
16-3-2	1.5875	4.7625	3.1750	0.232	0.0003	8.05	9.90	10.25	5.20	10.80	
16-3-2	1.5875	4.7625	3.1750	0.265	0.0007	7.80	10.45	10.70	4.00	19.50	
16-3-3	1.5875	4.7625	3.1750	0.057	0	7.80	7.85	7.95	7.50	7.00	
16-3-3	1.5875	4.7625	4.7625	0.105	0	7.80	8.00	8.05	7.80	1.60	
16-3-3	1.5875	4.7625	4.7625	0.160	0	7.75	8.45	8.65	6.40	6.90	
16-3-3	1.5875	4.7625	4.7625	0.200	0	8.00	9.10	9.40	7.40	4.00	
16-3-3	1.5875	4.7625	4.7625	0.230	0.0003	8.15	9.75	10.00	5.70	8.00	
16-3-3	1.5875	4.7625	4.7625	0.265	0.0007	7.95	10.30	10.50	4.50	23.50	
16-3-3	1.5875	4.7625	4.7625	0.295	0.001	8.15	10.75	11.10	4.30	15.70	
16-3-4	1.5875	4.7625	4.7625	0.060	0	7.75	7.80	7.90	7.40	8.90	
16-3-4	1.5875	4.7625	6.3500	0.105	0	7.95	8.15	8.25	7.40	8.50	
16-3-4	1.5875	4.7625	6.3500	0.160	0	8.00	8.65	8.80	6.90	8.80	
16-3-4	1.5875	4.7625	6.3500	0.230	0.0003	8.05	9.60	9.70	6.30	12.40	
16-3-4	1.5875	4.7625	6.3500	0.265	0.0007	8.00	10.00	10.20	3.70	27.00	
16-3-∞	1.5875	4.7625	∞	0.055	0	7.65	7.70	7.75	7.50	2.50	
16-3-∞	1.5875	4.7625	∞	0.105	0	7.95	8.05	8.10	7.30	2.30	
16-3-∞	1.5875	4.7625	∞	0.160	0	8.00	8.35	8.50	6.70	2.80	
16-3-∞	1.5875	4.7625	∞	0.230	0.0003	8.05	9.05	9.20	5.70	6.90	
16-3-∞	1.5875	4.7625	∞	0.265	0.0007	7.75	9.40	9.50	5.10	12.75	
16-5-2	1.5875	7.9375	3.1750	0.055	0	7.70	7.75	7.80	7.70	6.30	
16-5-2	1.5875	7.9375	3.1750	0.105	0	7.85	8.05	8.10	8.00	1.00	
16-5-2	1.5875	7.9375	3.1750	0.160	0	7.75	8.00	8.10	6.70	4.20	
16-5-2	1.5875	7.9375	3.1750	0.200	0	8.00	8.30	8.60	6.90	N/A	
16-5-2	1.5875	7.9375	3.1750	0.230	0.0003	8.15	8.65	8.80	6.00	7.40	
16-5-2	1.5875	7.9375	3.1750	0.265	0.0007	7.85	8.75	8.95	4.00	17.50	

Table A-7: Measured data for hydraulic performance experiments for double-row baffle-post structures at $y_0 = 0.08$ m

No.	Structure Geometry			Open Channel			GVF with Baffle-Post Structure			
	D (cm)	s (cm)	l (cm)	Q (cfs)	Slope	y_0 (cm)	$y_{x=-0.28\text{ m}}$ (cm)	y_1 (cm)	y_{min} (cm)	x at y_{min} (cm)
8-2-2	0.7938	1.5875	1.5875	0.055	0	7.70	7.85	7.90	7.10	3.00
8-2-2	0.7938	1.5875	1.5875	0.105	0	7.80	8.20	8.25	7.50	N/A
8-2-2	0.7938	1.5875	1.5875	0.160	0	7.65	8.95	9.05	6.20	4.50
8-2-2	0.7938	1.5875	1.5875	0.200	0	7.80	9.90	10.10	5.20	6.75
8-2-2	0.7938	1.5875	1.5875	0.230	0.0003	7.90	10.45	10.60	3.40	10.30
8-2-2	0.7938	1.5875	1.5875	0.265	0.0007	8.00	11.45	11.65	3.80	39.50
8-2-2	0.7938	1.5875	1.5875	0.265	0.0007	7.75	11.35	11.40	3.50	31.20
8-4-4	0.7938	3.1750	3.1750	0.055	0	7.70	7.75	7.80	7.40	3.50
8-4-4	0.7938	3.1750	3.1750	0.105	0	7.80	7.85	8.00	7.40	1.20
8-4-4	0.7938	3.1750	3.1750	0.160	0	7.65	8.05	8.20	6.60	3.90
8-4-4	0.7938	3.1750	3.1750	0.200	0	8.00	8.60	8.80	7.20	2.30
8-4-4	0.7938	3.1750	3.1750	0.230	0.0003	8.15	9.05	9.15	6.50	7.30
8-4-4	0.7938	3.1750	3.1750	0.270	0.0007	8.00	9.45		6.10	10.50
8-6-4	0.7938	4.7625	3.1750	0.050	0	7.55	7.60	7.65		
8-6-4	0.7938	4.7625	3.1750	0.105	0	7.75	7.80	8.00	7.80	N/A
8-6-4	0.7938	4.7625	3.1750	0.160	0	7.65	7.80	7.90	6.90	4.25
8-6-4	0.7938	4.7625	3.1750	0.200	0	7.90	8.30	8.40	6.90	5.25
8-6-4	0.7938	4.7625	3.1750	0.230	0.0003	8.15	8.55	8.70	6.70	6.20
8-6-4	0.7938	4.7625	3.1750	0.270	0.0007	8.00	8.95	9.05	6.25	10.00
8-10-4	0.7938	7.9375	3.1750	0.050	0	7.55	7.60	7.65		
8-10-4	0.7938	7.9375	3.1750	0.105	0	7.75	7.80	7.90	7.90	N/A
8-10-4	0.7938	7.9375	3.1750	0.160	0	7.50	7.65	7.70	7.00	3.90
8-10-4	0.7938	7.9375	3.1750	0.200	0	8.00	8.10	8.10	7.10	0.00
8-10-4	0.7938	7.9375	3.1750	0.230	0.0003	8.15	8.35	8.45		
8-10-4	0.7938	7.9375	3.1750	0.265	0.0007	7.90	8.45	8.60	6.70	9.00

Table A-8: Measured data for hydraulic performance experiments for double-row baffle-post structures at $y_0 = 0.15$ m

Structure Geometry				Open Channel			GVF with Baffle-Post Structure				
No.	D (cm)	s (cm)	l (cm)	Q (cfs)	Slope	y_0 (cm)	$y_{x=-0.28\text{ m}}$ (cm)	y_1 (cm)	y_{min} (cm)	x at y_{min} (cm)	
16-2-2	1.5875	3.1750	3.1750	0.125	0	14.50	14.70	14.75	14.10	5.40	
16-2-2	1.5875	3.1750	3.1750	0.230	0	14.85	15.50	15.70	13.20	5.20	
16-2-2	1.5875	3.1750	3.1750	0.350	0	14.65	17.00	17.20	12.50	6.40	
16-2-2	1.5875	3.1750	3.1750	0.350	0	14.90	16.95	17.20	12.30	6.10	
16-2-2	1.5875	3.1750	3.1750	0.500	0.0005	15.00	18.90	19.20	10.30	11.50	
16-2-2	1.5875	3.1750	3.1750	0.640	0.001	14.80	21.30	21.60	7.00	43.00	
16-2-2	1.5875	3.1750	3.1750	0.800	0.001	16.00	24.30	25.00	8.50	30.30	
16-3-2	1.5875	4.7625	3.1750	0.125	0	14.40	14.55	14.60	14.20	5.25	
16-3-2	1.5875	4.7625	3.1750	0.230	0	14.55	15.20	15.25	13.50	5.20	
16-3-2	1.5875	4.7625	3.1750	0.350	0	14.80	16.05	16.25	12.20	6.50	
16-3-2	1.5875	4.7625	3.1750	0.500	0.0005	15.00	17.40	17.60	11.10	11.60	
16-3-2	1.5875	4.7625	3.1750	0.640	0.001	14.20	18.50	18.80	7.30	35.30	
16-3-2	1.5875	4.7625	3.1750	0.800	0.001	13.70	20.80	21.80	8.50	39.70	
16-3-3	1.5875	4.7625	4.7625	0.125	0	14.40	14.55	14.60			
16-3-3	1.5875	4.7625	4.7625	0.230	0	14.55	15.00	15.10	13.60	7.05	
16-3-3	1.5875	4.7625	4.7625	0.350	0	14.80	15.80	16.00	12.90	7.00	
16-3-3	1.5875	4.7625	4.7625	0.500	0.0005	15.00	17.05	17.50	11.60	13.20	
16-3-3	1.5875	4.7625	4.7625	0.640	0.001	14.60	18.00	18.50	7.60	31.10	
16-3-4	1.5875	4.7625	6.3500	0.125	0	14.40	14.50	14.55	14.10	8.50	
16-3-4	1.5875	4.7625	6.3500	0.230	0	14.55	14.95	15.05	13.90	7.70	
16-3-4	1.5875	4.7625	6.3500	0.350	0	14.70	15.70	15.90	13.50	8.90	
16-3-4	1.5875	4.7625	6.3500	0.500	0.0005	15.00	16.80	17.20			
16-3-4	1.5875	4.7625	6.3500	0.640	0.001	14.40	17.70	18.20	7.60	35.10	
16-3-∞	1.5875	4.7625	∞	0.125	0	14.40	14.45	14.50	14.30	2.30	
16-3-∞	1.5875	4.7625	∞	0.230	0	14.55	14.75	14.90	13.70	2.30	
16-3-∞	1.5875	4.7625	∞	0.350	0	14.70	15.25	15.40	12.60	3.30	
16-3-∞	1.5875	4.7625	∞	0.500	0.0005	14.80	16.00	16.40	11.40	8.60	
16-3-∞	1.5875	4.7625	∞	0.640	0.001	14.10	16.90	17.70	11.20	14.80	
16-5-2	1.5875	7.9375	3.1750	0.125	0	14.60	14.70	14.80	14.40	6.30	
16-5-2	1.5875	7.9375	3.1750	0.230	0	14.50	14.75	14.80	14.20	5.80	
16-5-2	1.5875	7.9375	3.1750	0.350	0	14.65	15.15	15.20	13.50	6.60	
16-5-2	1.5875	7.9375	3.1750	0.500	0.0005	14.80	15.80	15.90	12.10	10.80	
16-5-2	1.5875	7.9375	3.1750	0.635	0.001	14.50	16.60	17.00	11.50	14.90	

Table A-9: Measured data for hydraulic performance experiments for double-row baffle-post structures at $y_0 = 0.15$ m

Structure Geometry				Open Channel			GVF with Baffle-Post Structure			
No.	D (cm)	s (cm)	l (cm)	Q (cfs)	Slope	y_0 (cm)	$y_{x=-0.28\text{ m}}$ (cm)	y_1 (cm)	y_{min} (cm)	x at y_{min} (cm)
8-2-2	0.7938	1.5875	1.5875	0.125	0	14.60	14.75	14.85	14.20	2.9
8-2-2	0.7938	1.5875	1.5875	0.230	0	14.70	15.35	15.50	13.40	3.3
8-2-2	0.7938	1.5875	1.5875	0.350	0	14.70	16.60	16.80	12.90	6.9
8-2-2	0.7938	1.5875	1.5875	0.500	0.0005	14.70	18.20	18.60	11.30	10.5
8-2-2	0.7938	1.5875	1.5875	0.635	0.001	14.50	19.90	20.50	7.00	46.5
8-4-4	0.7938	3.1750	3.1750	0.125	0	14.60	14.65	14.70	14.50	3.7
8-4-4	0.7938	3.1750	3.1750	0.230	0	14.70	14.85	15.00	14.10	4.1
8-4-4	0.7938	3.1750	3.1750	0.350	0	14.70	15.35	15.50	13.30	5.25
8-4-4	0.7938	3.1750	3.1750	0.500	0.0005	14.80	16.20	16.40	12.80	9.5
8-4-4	0.7938	3.1750	3.1750	0.640	0.001	14.30	17.20	17.60	12.40	17
8-6-4	0.7938	4.7625	3.1750	0.125	0	14.55	14.60	14.60	14.50	4.5
8-6-4	0.7938	4.7625	3.1750	0.230	0	14.60	14.70	14.85	14.10	4.5
8-6-4	0.7938	4.7625	3.1750	0.350	0	14.70	14.95	15.05	13.40	5.25
8-6-4	0.7938	4.7625	3.1750	0.500	0.0005	14.80	15.60	15.80	12.30	17
8-6-4	0.7938	4.7625	3.1750	0.635	0.001	14.50	16.30	16.80	13.30	14.2
8-10-4	0.7938	7.9375	3.1750	0.125	0	14.55	14.60	14.60	14.60	N/A
8-10-4	0.7938	7.9375	3.1750	0.230	0	14.60	14.65	14.70	14.30	3.7
8-10-4	0.7938	7.9375	3.1750	0.350	0	14.60	14.75	14.80	13.60	6
8-10-4	0.7938	7.9375	3.1750	0.500	0.0005	14.80	15.30	15.50		
8-10-4	0.7938	7.9375	3.1750	0.640	0.001	14.60	16.10	16.40	14.30	11.4

Table A-10: Measured data for hydraulic performance experiments for double-row baffle-post structures at $y_0 = 0.20$ m

Structure Geometry				Open Channel			GVF with Baffle-Post Structure				
No.	D (cm)	s (cm)	l (cm)	Q (cfs)	Slope	y_0 (cm)	$y_{x=-0.28\text{ m}}$ (cm)	y_1 (cm)	y_{min} (cm)	x at y_{min} (cm)	
16-2-2	1.5875	3.1750	3.1750	0.197	0	20.05	20.35	20.45	19.40	5.20	
16-2-2	1.5875	3.1750	3.1750	0.355	0	19.80	21.00	21.25	18.60	1.50	
16-2-2	1.5875	3.1750	3.1750	0.505	0	19.80	22.50	22.75	18.50	3.50	
16-2-2	1.5875	3.1750	3.1750	0.635	0.0005	19.80	23.70	24.00	16.30	10.60	
16-2-2	1.5875	3.1750	3.1750	0.815	0.001	19.60	25.70	26.20	14.50	14.50	
16-3-2	1.5875	4.7625	3.1750	0.197	0	20.05	20.15	20.15	19.50	5.70	
16-3-2	1.5875	4.7625	3.1750	0.355	0	19.60	20.25	20.45	19.00	5.00	
16-3-2	1.5875	4.7625	3.1750	0.505	0	19.80	21.05	21.25	18.30	4.30	
16-3-2	1.5875	4.7625	3.1750	0.635	0.0005	19.80	22.20	22.40	16.30	10.40	
16-3-2	1.5875	4.7625	3.1750	0.815	0.001	19.60	23.40	23.70	15.40	15.80	
16-3-3	1.5875	4.7625	4.7625	0.197	0	19.95	20.05	20.15	19.50	7.20	
16-3-3	1.5875	4.7625	4.7625	0.355	0	19.60	20.10	20.30	19.25	2.00	
16-3-3	1.5875	4.7625	4.7625	0.505	0	19.80	20.95	21.25	19.00	5.50	
16-3-3	1.5875	4.7625	4.7625	0.635	0.0005	19.80	21.80	22.10	16.50	9.40	
16-3-3	1.5875	4.7625	4.7625	0.815	0.001	19.60	22.80	23.30	14.70	16.50	
16-3-4	1.5875	4.7625	6.3500	0.195	0	19.85	19.95	20.00	19.20	8.50	
16-3-4	1.5875	4.7625	6.3500	0.197	0	19.95	20.00	20.10	19.60	8.50	
16-3-4	1.5875	4.7625	6.3500	0.355	0	19.60	20.05	20.25	19.30	1.50	
16-3-4	1.5875	4.7625	6.3500	0.505	0	19.80	20.95	21.10	19.00	5.00	
16-3-4	1.5875	4.7625	6.3500	0.640	0.0005	19.60	21.70	21.90	16.70	12.50	
16-3-4	1.5875	4.7625	6.3500	0.815	0.001	19.60	22.80	23.30	16.30	18.20	
16-3-∞	1.5875	4.7625	∞	0.197	0	19.85	19.95	20.00	19.70	2.60	
16-3-∞	1.5875	4.7625	∞	0.355	0	19.50	19.80	19.90	19.50	3.00	
16-3-∞	1.5875	4.7625	∞	0.505	0	19.80	20.40	20.45	17.80	2.00	
16-3-∞	1.5875	4.7625	∞	0.640	0.0005	19.60	20.70	20.90	16.20	8.00	
16-3-∞	1.5875	4.7625	∞	0.815	0.001	19.40	21.50	22.00	15.00	14.50	
16-5-2	1.5875	7.9375	3.1750	0.197	0	19.80	19.85	19.90	19.70	6.50	
16-5-2	1.5875	7.9375	3.1750	0.355	0	19.50	19.75	19.85	19.50	N/A	
16-5-2	1.5875	7.9375	3.1750	0.505	0	19.80	20.20	20.25	19.00	N/A	
16-5-2	1.5875	7.9375	3.1750	0.640	0.0005	19.60	20.50	20.70	17.00	8.80	
16-5-2	1.5875	7.9375	3.1750	0.810	0.001	19.40	21.00	21.30	16.30	14.90	

Table A-11: Measured data for hydraulic performance experiments for double-row baffle-post structures at $y_0 = 0.20$ m

Structure Geometry				Open Channel			GVF with Baffle-Post Structure			
No.	D (cm)	s (cm)	l (cm)	Q (cfs)	Slope	y_0 (cm)	$y_{x=-0.28\text{ m}}$ (cm)	y_1 (cm)	y_{min} (cm)	x at y_{min} (cm)
8-2-2	0.7938	1.5875	1.5875	0.195	0	20.05	20.20	20.20	19.30	2.90
8-2-2	0.7938	1.5875	1.5875	0.355	0	19.50	20.55	20.75	18.30	2.50
8-2-2	0.7938	1.5875	1.5875	0.505	0	19.75	22.00	22.25	18.00	6.50
8-2-2	0.7938	1.5875	1.5875	0.640	0.0005	19.60	23.00	23.30	16.00	10.70
8-2-2	0.7938	1.5875	1.5875	0.805	0.001	19.30	24.80	25.20	13.70	17.60
8-4-4	0.7938	3.1750	3.1750	0.195	0	19.90	20.00	20.10	19.70	4.00
8-4-4	0.7938	3.1750	3.1750	0.355	0	19.50	19.85	19.95	19.30	N/A
8-4-4	0.7938	3.1750	3.1750	0.505	0	19.75	20.40	20.50	19.10	4.50
8-4-4	0.7938	3.1750	3.1750	0.640	0.0005	19.60	21.00	21.20	17.50	9.50
8-4-4	0.7938	3.1750	3.1750	0.805	0.001	19.30	21.50	21.80	16.50	15.50
8-6-4	0.7938	4.7625	3.1750	0.195	0	19.90	20.00	20.50	19.80	4.50
8-6-4	0.7938	4.7625	3.1750	0.355	0	19.50	19.65	19.75	19.50	2.50
8-6-4	0.7938	4.7625	3.1750	0.505	0	19.75	20.00	20.15	19.50	5.50
8-6-4	0.7938	4.7625	3.1750	0.640	0.0005	19.60	20.30	20.50	18.00	9.50
8-6-4	0.7938	4.7625	3.1750	0.805	0.001	19.30	20.70	20.90		
8-6-4	0.7938	4.7625	3.1750	0.805	0.001	18.90	20.60	20.80	17.50	13.80
8-10-4	0.7938	7.9375	3.1750	0.195	0	19.85	19.90	19.95	19.85	
8-10-4	0.7938	7.9375	3.1750	0.350	0	19.75	19.80	19.85	19.00	5.60
8-10-4	0.7938	7.9375	3.1750	0.355	0	19.50	19.45	19.55	19.40	N/A
8-10-4	0.7938	7.9375	3.1750	0.505	0	19.75	19.95	20.00	19.30	N/A
8-10-4	0.7938	7.9375	3.1750	0.640	0.0005	19.60	20.00	20.20	18.50	7.60
8-10-4	0.7938	7.9375	3.1750	0.805	0.001	18.90	20.40	20.70	18.20	10.00

Table A-12: Measured flow and sand depth data for sediment transport experiments for free-flow conditions

t (min)	Q (cfs)	y_0 (cm)	$d_{x=-4.8m}$ (cm)	d_0 (cm)	$d_{x=2.0m}$ (cm)
0			9.0	9.0	9.0
5	0.175	17.5	9.5	8.0	8.8
13	0.173	17.9	9.6	8.5	9
17	0.185	17.2	10.1	9.2	8.4
30	0.183	16.6	10.7	8.8	8.1
45	0.177	17.0	9.2	9.0	8.4
60	0.173	16.7	9.6	8.8	8.5
90	0.170	16.4	9.7	8.2	9.8
120	0.165	16.1	9.6	7.4	10.3
180	0.155	16.3	8.9	9.0	9.4
240	0.155	16.3	10.2	9.0	9.1
300	0.150	16.3	9.6	9.9	10.5

Table A-13: Measured ripple amplitude, A , and wavelength, λ , for sediment transport experiments for free-flow conditions

t (min)	$A_{x=-4.8m}$ (cm)	$\lambda_{x=-4.8m}$ (cm)	A_0 (cm)	λ_0 (cm)	$A_{x=2.0m}$ (cm)	$\lambda_{x=2.0m}$ (cm)
0						
5						
13						
17	1.3	10.0	2.1	10	1.7	11
30	1.3	8.7	1.3	8.5	1.3	17
45	1.3	11.3	1.2	9.7	2.4	15
60	0.9	13.0	1.7	9.5	2.4	13.4
90	1.6	13.8	1.5	15.4	1.5	20
120	2.1	17.0	2.5	24	2.8	21
180	1.2	13.2	1.8	13.8	2.5	24
240	2.9	13.7	4.2	17	4.2	21
300	2.7	18.0	3	18	2.2	22

Table A-14: Measured flow data for sediment transport experiments for retarded flow due to double-row baffle-post structures without armoring

t (min)	Q (cfs)	y_1 (cm)	y_{min} (cm)	x at y_{min} (cm)
0	0.025	17.4	17.1	5.2
4	0.025	17.1	16.8	5.5
42	0.170	18.0	16.8	5.5
65	0.160	18.4	17.5	5.5
122	0.165	18.0	17.4	5.2
180	0.155	17.5	16.6	5.2
243	0.170	18.2	17.6	5.3
300	0.160	17.9	17.1	5.3
Free Flow	0.160	17.4		

Table A-15: Measured sand depth and ripple amplitude, A , data for sediment transport experiments for retarded flow due to double-row baffle-post structures without armoring

t (min)	$d_{x=-4.8m}$ (cm)	d_1 (cm)	$d_{x=2.0m}$ (cm)	$A_{x=-4.8m}$ (cm)	$A_{x=-0.3m}$ (cm)	$A_{x=2.0m}$ (cm)
0	9.0	9.0	9.0			
4	9.0	9.0	8.7			
42	9.1	3.9	8.7			
65	9.0	2.4	9.0			
122	10.0	1.8	10.8			
180	10.0	1.7				
243	10.6	2.0	11.0	1.8	3.7	2.2
300	9.5	1.8				
Free Flow						

Table A-16: Measured flow and sand depth data for sediment transport experiments for retarded flow due to double-row baffle-post structures with armoring

t (min)	Q (cfs)	y_1 (cm)	y_{min} (cm)	x at y_{min} (cm)	$d_{x=-4.8m}$ (cm)	$d_{x=-0.3m}$ (cm)	$d_{x=2.0m}$ (cm)
10	0.18	18.0	14.5	6.1	9.0	9.2	8.5
20	0.177	17.7	14.2	6.2	9.2	9.2	9.5
30	0.177	17.7	14.3	6.2	9.2	9.2	8.2
45	0.172	17.5	14.3	6.3	9.8	8.5	8.0
60	0.168	17.9	15.2	5.9	11.1	9.1	8.5
90	0.165	17.7	14.9	6.0	10.3	9.1	8.9
120	0.157	17.5	14.7	6.0	10.0	9.5	7.0
180	0.157	17.6	14.7	6.0	11.5	9.3	9.5
240	0.151	17.3	14.0	6.4	10.7	8.4	9.0
327	0.158	17.7	14.8	6.5	12.5	9.6	7.4
Free-Flow	0.156	16.6					

Table A-17: Measured ripple amplitude, A , and wavelength, λ , data for sediment transport experiments for retarded flow due to double-row baffle-post structures with armoring

t (min)	$A_{x=-4.8m}$ (cm)	$\lambda_{x=-4.8m}$ (cm)	$A_{x=-0.3m}$ (cm)	$\lambda_{x=-0.3m}$ (cm)	$A_{x=2.0m}$ (cm)	$\lambda_{x=2.0m}$ (cm)
10						
20						
30						
45	1.3	8.0			3.1	16.0
60	1.2	9.0	1.3	11.0	1.6	12.5
90	1.4	12.0	1.1	9.3	2.9	24
120	4.4	9.5	1.6	12.0	2.5	26.5
180	2.5	25.0	2.0	14.0	2.3	26
240	6.4	28.0	1.4	11.7	2.5	18

327	6.3	31.5	1.2	13.0	3.1	18
Free-Flow						